Joanna Krzemień

The role of Amot and Amotl1 in the central nervous system

PhD thesis
Completed in the Laboratory of Synaptogenesis
of the Nencki Institute of Experimental Biology
Polish Academy of Sciences

SUPERVISOR:
Dr. hab. Tomasz J. Prószyński
Auxiliary supervisor: Dr. Paweł Boguszewski

Warsaw, Poland 2020

Part of the results in this doctoral thesis have been published in
PLOS Biology, 2019, 17(5):e3000252

Amot and Yap1 regulate neuronal dendritic tree complexity and locomotor coordination in mice

Katarzyna O. Rojek*, Joanna Krzemień*, Hubert Doleżyczek, Paweł M. Boguszewski, Leszek Kaczmarek, Witold Konopka, Marcin Rylski, Jacek Jaworski, Lars Holmgren and Tomasz J. Prószyński

*** - co-first authors**

This work was supported by the National Science Centre Research Grants:
2012/05/E/NZ3/00487 – OPUS (TJP)
2019/33/B/NZ3/02528 – OPUS (TJP)

I would like to thank:

My PhD supervisor, Dr. hab. Tomasz Prószyński for providing me the opportunity to work in his laboratory and for valuable supervision and disscussions that enabled for my scientific and personal development.

Professor Leszek Kaczmarek and Dr. Paweł Boguszewski for their support

All of my collegues from the Laboratory of Synaptogenesis for great work atmosphere, as well as scientific and personal suport: Kasia Rojek, Marta Gawor, Krzysztof Bernadzki, Marcin Pęziński, Agata Błażewicz, Agata Litwinowicz, Paloma Alvarez-Suarez, Bhola Shankar Pradhan, Teresa De Cicco

Kasia Rojek for great cooperation, valuable scientific disscusions, support in tough times when working on our manuscript revisions which enabled to complete our joined research project. You are the best team partner I could imagine!

Marta Gawor for her calm and warm attitude, as well as patience in every difficult situation

Krzysztof Bernadzki and Marcin Pęziński for their smile and their endless words of support

Paweł Niewiadomski for giving me the faith in my future carrier

My best friend Karolina Rogala. You helped me went through the most difficult personal and scientific times and thanks to you I was able to complete this journay and get ready to the new life chapter. You are my only one soul mate.

Finally, I would like to thank my family:

My Mom for being involved in every step of that journay and for her unlimited faith in me,

My Dad for a strong attitude who didn't let me give up, constantly saying: "I am sure you will make it"

My sisters, Karolina, Agnieszka and Kasia for a support in the worst moments, for laugh and for creating a piece of mind atmosphere whenever I felt overloaded.

My great dogs, Leyla and Nelson, who were the only withenneses of the hours I have spent at days and nights writing this thesis, and that I could wear a smile they gave me consnatly.

I dedicate this thesis to Teresa and Wiesław, my parents,
I love you

TABLE OF CONTENTS

ABBREVIATIONS

ABBREVIATIONS	DESCRIPTION
Amot	Angiomotin
Amotl1	Angiomotin like 1
Amotl2	Angiomotin like 2
AAV	Adeno-associated virus
BP	Base pairs
CB	Calbindin
CNS	Central nervous system
DMSO	Dimethyl sulfoxide
DTT	dithiothreitol
EDTA	Ethylenediaminetetraacetic acid
F	Forward
GLU	Glutamate
GLN	Glutamine
kDa	kilodalton
KO	Knock-out
Map2	Microtubule associated protein 2
Mm	Mus musculus
NAA	N-Acetyl Aspartate
NAAG	N-Acetylaspartylglutamic acid
NeuN	Neuronal nuclei
NP- 40	Tergitol-type nonyl phenoxypolyethoxylethanol
P	Postnatal days
PAGE	Polyacrylamide gel electrophoresis
PBS	Phosphate buffered sakine
PCR	Polymerase chain reaction
PFA	Paraformaldehyde
PSD	Post-synaptic density
R	Reverse
RIPA	Radioimmunoprecipitation assay
RT	Room temperature
SD	Standard deviation
SDS	Sodium dodecyl sulfate
SEM	Standard error of the mean
Syn	Synaptophysin 1
TEA	Tris-acetate-EDTA
TBS	Tris-buffered saline
TBST	Tris-buffered saline and tween
WB	Western blot
WT	Wild type
Yap1	Yes-associated protein 1

ABSTRACT

Neurons are highly specialized cells that consist of three morphologically and functionally distinct compartments: cell body that contains the nucleus, long axonal protrusion extending from the cell body, and multiple shorter projections called dendrites. The complex tree-like structure of dendritic arbors, that comprises thousands of contact points between cells termed synapses, allows for receiving information from other neurons, which can be further transmitted through axons to destination cells. Hence, the proper formation and maintenance of extensively branched dendritic tree and multiple synapses are crucial for assembly of functional neuronal network. Abnormalities in the dendritic tree architecture are often associated with numerous neurological and psychiatric disorders like Down's syndrome, epilepsy, Autism spectrum disorders, or Schizophrenia.

The majority of mechanisms involved in neuronal morphogenesis have been studied on cultured neuronal cells, which provide a relatively simple system to study major cellular processes. However, the main disadvantage of the *in vitro* methods, is the lack of the external cues that come from surrounding environment in living organism. Therefore, it is of great importance to investigate the underpinnings of dendrite organization and to search for novel molecular players involved in neuronal morphogenesis in *in vivo* studies.

The Angiomotin (Amot) protein together with the closely related Angiomotin-like 1 (Amotl1) and Angiomotin-like 2 (Amotl2) constitute a family of the Angiomotin scaffold proteins that regulate the actin cytoskeleton, adhesion, and play role in the Hippo signaling pathway. However, their function in the central nervous system is widely unknown. A recent *in vitro* study has demonstrated that Amot localizes to synaptic compartments in mature hippocampal neurons where it regulates the organization of the postsynaptic machinery. Our laboratory has identified Amot as a novel mediator of dendritic tree morphogenesis in cultured hippocampal neurons and we showed that its function depends on the interaction with the Hippo pathway transcriptional coactivator, Yap1.

The main objective of my research was to investigate the Angiomotins role in the brain organization and mouse behavior. I have focused my studies on two members of the Angiomotin family of proteins, Amot and Amotl1. To investigate the Amot function in the mouse brain I have generated mice with neuron-specific depletion of Amot protein. Additionally, as we have demonstrated that Yap1 interacts with Amot in cultured hippocampal

neurons and plays a critical role in dendritic morphogenesis, I have generated Yap1 neuronal knockout mice. My experiments reveled that both proteins localize to synaptic compartments in the hippocampal pyramidal neurons and cerebellar Purkinje cells *in vivo.* Importantly, Amot or Yap1 depletion led to a similar phenotype of abnormal cerebellar morphology in mice that showed decreased thickness of the molecular layer, but not the granular and Purkinje cell layers. The cerebellar molecular layer is filled with Purkinje cells dendritic trees. Therefore, I analyzed the structure of the individual Amot or Yap1-depleted Purkinje neurons in the brain and I found abnormalities in the development of dendritic tree arbors in these cells. Moreover, I have showed that Amot or Yap1-depleted mice exhibit impairments in locomotor coordination.

The second aim of my thesis was to unravel the potential function of Amotl1 protein in the organization and function of the mouse brain. Firstly, I have generated a novel Amotl1 knockout mouse line. My histochemical experiments and magnetic resonance imaging (MRI; conducted in collaboration with Small Animal Magnetic Resonance Imaging Laboratory, Mossakowski Medical Research Centre, Warsaw, Poland)-based analysis of Amotl1-depleted brains revealed a significant increase in the volume of lateral ventricles and cerebral cortex. Moreover, I have found that Amotl1 mutant mice do not show impairments in motor coordination. Instead, they exhibited hyperactivity, reduced anxiety, and alterations in their social behavior. Strikingly, I observed episodes of backward walking and increased circling behavior in these mice that have been previously described as potential symptoms of hallucinations in rodents. Lastly, the spectroscopic analysis of brain metabolites demonstrated increased ratio of N-Acetylaspartylglutamic acid (NAAG) to N-Acetyl Aspartate (NAA) and higher level of Glutamine (Gln) in the Amotl1 depleted brains. Increased volume of lateral ventricles together with the abnormal NAAG/NAA and Gln levels have been associated with schizophrenia both in humans and mouse models of the disease.

STRESZCZENIE

Neurony są wysoce wyspecjalizowanymi komórkami układu nerwowego, które zbudowane są z trzech odrębnych morfologicznie oraz funkcjonalnie części: ciała komórki, które zawiera jądro komórkowe, długiej wypustki cytoplazmatycznej zwanej aksonem oraz wielu krótszych i rozgałęzionych wypustek - dendrytów. Złożona, drzewiasta struktura dendrytów neuronu umożliwia wytworzenie pomiędzy sąsiadującymi komórkami licznych punktów kontaktowych, zwanych synapsami. Synapsy zlokalizowane na dendrytach umożliwiają odbieranie informacji od sąsiadujących komórek, która następnie przekazywana jest wzdłuż aksonu do kolejnych neuronów lub komórek docelowych. Z tego względu prawidłowa struktura rozgałęzionego drzewa dendrytycznego jest kluczowa dla przekazywania informacji pomiędzy komórkami i utrzymania funkcjonalnych sieci neuronalnych. Nieprawidłowości w architekturze drzewa dendrytycznego są często związane z zaburzeniami neurologicznymi i psychiatrycznymi, takimi jak zespół Downa, padaczka, zaburzeniami ze spektrum autyzmu lub schizofrenii.

Większość mechanizmów zaangażowanych w morfogenezę drzewa dendrytycznego odkryto w badaniach *in vitro* prowadzonych przy użyciu hodowanych neuronów. Głównym ograniczeniem tej metody jest brak zewnętrznych sygnałów pochodzących z otaczającego środowiska w organizmie, które mogą mieć znaczący wpływ na rozwój drzewa dendrytycznego. Z tego powodu ważne jest badanie molekularnych podstaw organizacji dendrytów *in vivo*.

Białko Angiomotyna (Amot) wraz z blisko spokrewnionymi białkami Amotl1 i Amotl2 stanowią rodzinę białek rusztowania zwaną Angiomotyny, które regulują cytoszkielet aktynowy, adhezję komórkową i odgrywają ważną rolę w regulacji ścieżki sygnałowej Hippo. Funkcja Angiomotyn w ośrodkowym układzie nerwowym pozostaje słabo poznana. Ostatnie badania z wykorzystaniem metody *in vitro* wykazały, że Amot jest zlokalizowany na synapsach w dojrzałych neuronach hipokampalnych, gdzie reguluje organizację maszynerii postsynaptycznej. Dodatkowo, badania prowadzone przez naszą pracownię pokazały, że białko Amot reguluje morfogenezę drzewa dendrytycznego w hodowanych neuronach hipokampalnych. Funkcja Amot w tym procesie zależy od interakcji z wpół-aktywatorem transkrypcji zależnej od ścieżki Hippo, białkiem Yap1.

Głównym celem mojej rozprawy było zbadanie roli białek Amot i Amotl1 w organizacji mózgu i zachowaniu myszy. W celu zbadania roli białka Amot w ośrodkowym układzie nerwowym, wygenerowałam myszy z niedoborem białka Amot specyficznie w neuronach. Mając na uwadze ważną rolę interakcji białka Amot i Yap1 w morfogenezie hodowanych neuronów hipokampalnych, równocześnie prowadziłam badania z wykorzystaniem myszy pozbawionych ekspresji białka Yap1 w neuronach. Wyniki moich doświadczeń wykazały, że oba białka zlokalizowane są na synapsach neuronów piramidalnych hipokampa i komórek Purkinjego w móżdżku. Myszy pozbawione białka Amot lub Yap1 w neuronach wykazywały nieprawidłową, zmniejszoną strukturę móżdżka, który charakteryzował się zredukowaniem grubości warstwy molekularnej kory móżdżkowej. Warstwa molekularna wypełniona jest drzewami dendrytycznymi komórek Purkinjego. Analiza struktury pojedynczych komórek Purkinje pozbawionych ekspresji białka Amot lub Yap1 w mózgu myszy wykazała liczne nieprawidłowości morfologii drzew dendrytycznych w tych komórkach. Ponadto wykazałam, że myszy pozbawione białka Amot lub Yap1 prezentowały upośledzenie koordynacji ruchowej.

Kolejnym celem mojej pracy było zbadanie funkcji białka Amotl1 w organizacji i funkcji mózgu. W tym celu stworzyłam myszy z nokautem białka Amotl1. Moje eksperymenty histochemiczne i analiza mózgu w oparciu o rezonans magnetyczny (MRI) ujawniły wzrost objętości komór bocznych mózgu i kory mózgowej. Wykazałam, że myszy pozbawione ekspresji Amotl1 nie prezentują upośledzenia koordynacji ruchowej, natomiast charakteryzowały się innymi licznymi zaburzeniami behawioralnymi, takimi jak nadpobudliwość ruchowa, zmniejszony poziom lęku oraz upośledzenie zachowań społecznych. Zaobserwowałam także, że zaburzona ekspresja białka Amotl1 prowadzi do epizodów poruszania się w tył myszy oraz wzrostu częstotliwości kręcenia się wokół własnej osi. Wcześniejsze badania sugerują, że takie zachowania mogą być objawem halucynacji u gryzoni. Analiza spektroskopowa metabolitów mózgu wykazała zwiększony stosunek kwasu N-acetyloaspartyloglutaminowego (NAAG) do asparaginianu N-acetylowego (NAA) i wyższy poziom glutaminy (Gln) w mózgach myszy z nokautem białka Amotl1. Zwiększona objętość komór bocznych mózgu, a także nieprawidłowy poziom metabolitów NAAG/NAA i Gln są rozpoznawane jako morfologiczne i molekularne cechy rozwoju schizofrenii zarówno u ludzi, jak i w mysich modelach tej choroby.

1 Introduction

How do individuals recognize each other? Why organisms intuitively avoid the subject heading toward them? Why we prefer certain types of food? What causes people's feelings or emotions? Searching for answers to questions regarding control of motor functions, learning abilities and emotions is one of the main interest of neuroscience. The brain is considered a command center and its proper development, organization and function not only impacts individual's actions and emotions but also influences the activity of other body parts.

1.1 The brain organization

The central nervous system consists of the spinal cord and the brain, the most complex organ in human body. It creates our thoughts, actions, decisions, emotions and is responsible for our voluntary movements and unconditional motor reflexes. The brain is composed of neurons, glial cells and blood vessels. Although it represents only 2 percentage of our body mass, human brain distinguish us from other organisms due to the evolution of extraordinary cognitive abilities over close relatives (Heyes et al., 2012 [83]; MacLean et al., 2016 [124]).

The brain is composed of structurally and functionally specialized areas and its three main structural divisions are the cerebrum, cerebellum and brain stem (Fig. 1). The cerebrum is the largest part of a brain that consist of two C-shaped left and right hemispheres, connected with a thick track of nerve fibers called corpus callosum, found exclusively in mammals (Suárez et al., 2014 [196]). Although both hemispheres are generally equal in size, the brain-mapping techniques provided insights into their structural and functional asymmetry (Toga and Thompson, 2003 [206]). Functionally, left side mostly controls all the logical tasks, preprocess social emotions and is responsible for our written and spoken language skills, whereas the right hemisphere finds its role in managing emotional expression, artistic and creative awareness, face recognition as well as facial expression and body posture (Priyanka et al., 2016 [160]). Another structural division of the brain to consider are four distinct parts of the cerebral cortex that show diversity in functions. First, the frontal lobe which is involved in motor function and integrates learning, creative and reasoning abilities into the goal oriented decisions making behavior (Collins et al., 2012 [42]). Additionally, it became widely recognized as important brain region for a speech production due to identification of Broca's area,

however there is an ongoing debate over its precise role in language production (Broca et al., 1861 [28]; Rorden et al., 2008 [173]). Second, the temporal lobe carries the language comprehension Wernicke's area and is implicated in multiple cognitive domains such as vision, audition, memory (Bajada et al., 2017 [16]). Third, the cortical region that integrates several modules of somatosensory, visual and auditory cues is called the parietal lobe. Last but not least, the occipital lobe is strongly implicated in vision functions due to receiving information from sensory receptors located on the eye retinas (Aversi-Ferreira et al., 2010 [14]; Ogawa et al., 2014 [151]).

The main brain area that is recognized for its impact on an individual's motor coordination is the cerebellum (Thach et al., 1992 [201]). This unique structure, that contains about 50 percentage of total number of neurons in the adult brain, is among the first brain areas to begin neuronal differentiation and while reaching its state of maturity as one of the latest (Wang et al., 2001 [216]). In fact, the cerebellum controls wide range and different levels of motor functions, such as oculomotor activity, motor speech, grip forces, voluntary limb movements or sensorimotor synchronization (Manto et al., 2012 [127]). Moreover, due to a number of neuroimaging studies, there is a clear evidence of the cerebellar involvement in the cognitive associative, emotional and motor learning (Stoodley et al., 2012 [195]; Buckner et al., 2013 [29]; Timmann et al., 2010 [205]).

Underneath the cerebral cortex and in front of the cerebellar structure, the thalamic, hypothalamic, hippocampal brain structures and amygdala regions are located (Fig. 1). Altogether, these areas compose the brain unique functional complex called the limbic system, however individually have different identity in brain functioning. While the hippocampus is greatly related to our memory and learning abilities, amygdala processes the aggressive emotions, fear and social behavior, the thalamus is considered as a central brain station that mediates sensory signals between cortical and cerebellar areas and plays role in sleep regulation, arousal, and primary sensory processing (Lisman et al., 2017 [117]; Cardinal et al., 2002 [35]; Davis et al., 2001 [48]; Fama et al., 2015 [59]).

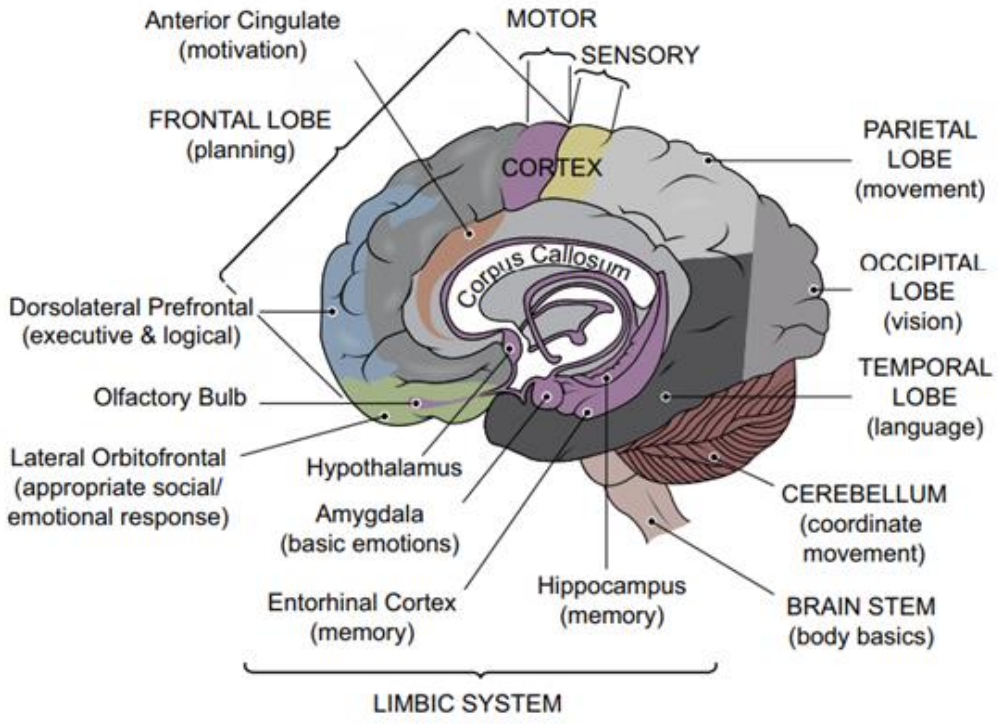

Fig.1. Major brain structures and functions. Different structures and highlighted with different colors. Cerebral lobes are shown in different shades of grey color, while the limbic system is colored light violet. (https://www.brainwaves.com/).

In order to ensure the proper brain function, all of the above mentioned brain structures require nutrient supplementation and metabolic waste removal. The brain ventricular system, that develops from a single cavity inside the neural tube, provides that important brain circulation through the flow of cerebrospinal fluid (CSF) (Nieuwenhuys et al., 2008 [144]). Opposite to the all abovementioned brain structures, that brain areas are not densely packed with cells. On the contrary, the ventricular system is comprised of four interconnected fluid-filled lumen called third, fourth, and two of lateral ventricles located in each of the brain hemispheres. About 75 percentage of the CSF is produced and secreted by choroid plexuses structure located inside the lateral ventricles, while the residual part contributes from ependymal cells extracellular fluid (ECF) and altogether constitute about 140 ml total CSF volume (Edsbagge et al., 2004 [53]; Perez-Figares et al., 2001 [158]; Weller et al., 2009 [220]). A great part of CSF is distributed to the subarachnoid spaces providing mechanical brain protection inside the human skull. The CSF remarkable function as a brain cleaner and feeder. Moreover, since early twentieth century scientists have proposed a possible role of CSF in sending different molecules to distant brain parts (Cushing et al., 1910 [45]; Nicholson et al., 1999 [143]).

Over time, several studies have proved this theory and showed that numerous neuropeptides are synthesizes by the choroid plexus structure, actively secreted to the CSF and thought its flow can influence appropriate receptors in distant brain areas (Nilsson et al., 1992 [145]; Skipor et al., 2008 [186]).

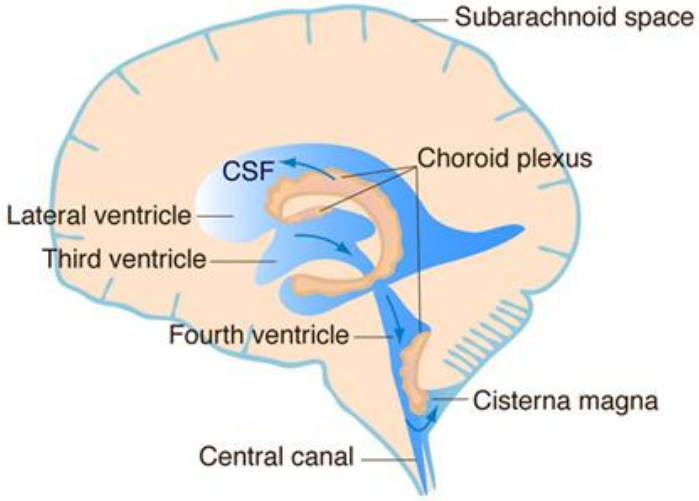

Fig. 2. The organization of human brain ventricular system. Ventricular system is composed of four interconnected cavities: two lateral ventricles, a third and fourth ventricles connected to the central spinal canal. All are filled with a cerebrospinal fluid (CSF), produced by the choroid plexus structure that additionally fills the brain subarachnoid space (Lehtinen et al., 2013).

Summing up, the human brain is composed of numerous diverse structures that are specialized in distinct brain functions. However, these areas simultaneously cooperate with each other to provide proper functioning of the whole organ. The basic cellular components of the brain that provide communication between diverse brain structures are called neurons.

1.1.1 Brain connectivity – neurons, dendritic tree, and synapses

The human brain contains around 100 billion of neurons, and similar number of glial cells (von Bartheld et al., 2016 [214]). Neurons are among the most highly polarized cells within our body with structurally and functionally distinct compartments. There are many types of neurons in our body that differ in structure, physiology, and their molecular components and, therefore could have different characteristics (Fig. 3). However, a standard neuron has long projection

called axon, the cell body that contains cell nucleus, and numbers of processes named dendrites (Fig. 4).

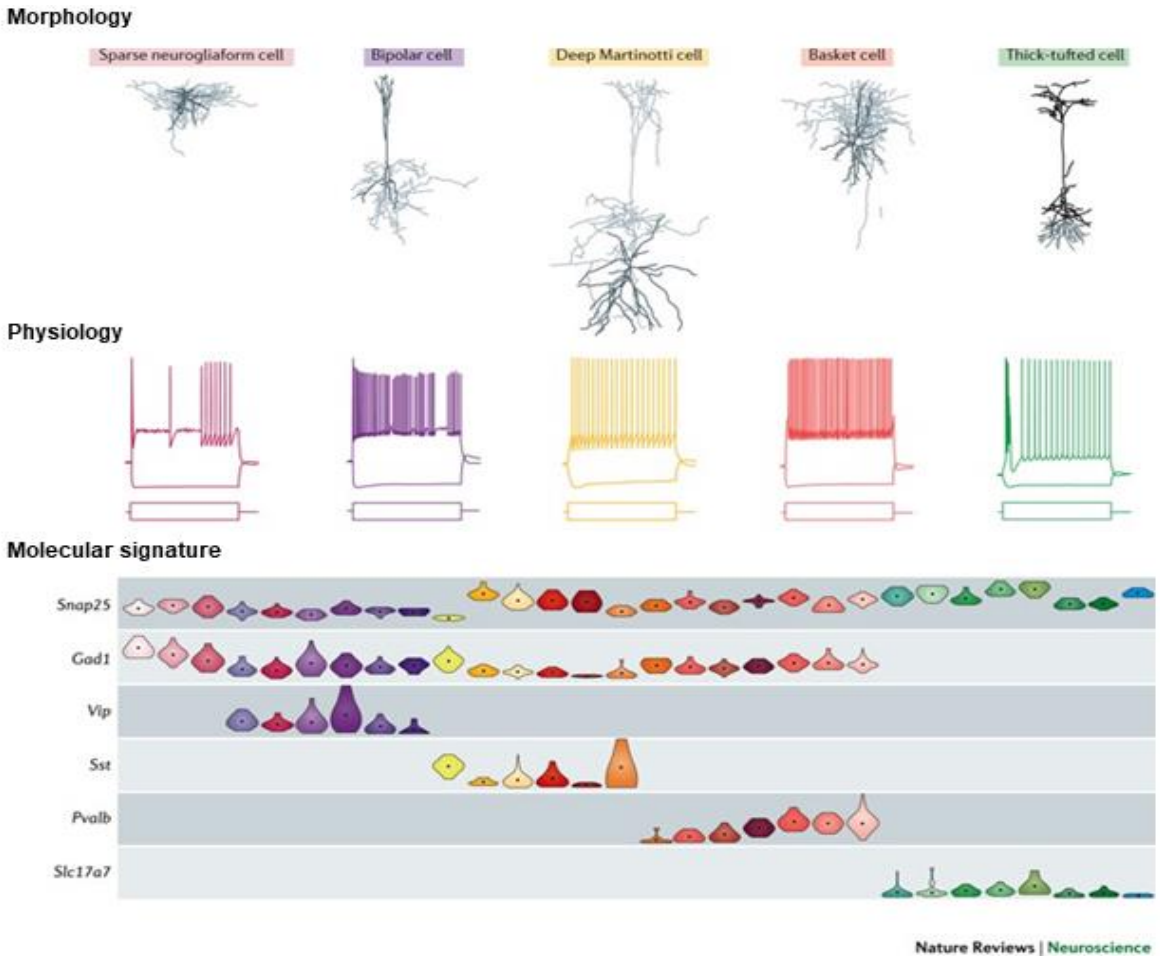

Fig. 3. The criteria of neuronal diversity. The upper panel shows representative subclasses of different cortical neurons. Dark grey color represents their axons, whereas light grey shows dendrites. Middle panel points different electrophysiological responses of the above cells. The lowest panel indicate the molecular signatures for these cells. The high of violin-shaped plots indicate the range of expression level, width- the proportion of cells expressing similar level of the gene. For the whole graph one color represents data for a particular neuronal subclass (Zeng and Sanes, 2017, modified).

The major role of these cells is to receive, modulate, integrate, and transmit electrical and chemical signals from and toward the neighboring cells. The dendrites of a presynaptic neuron receive and collect the input information from surrounding cells, which is further transmitted along the axon. On its terminals axon releases signaling molecules (neurotransmitters) that interact with receptors on postsynaptic cells at tiny contact points, termed postsynaptic

density (Ovsepian et al., 2017 [154]). Moreover, great number of nerve axon fibers are emulated by glial processes, which form a membranous sheath around axons, called myelin (Berret et al., 2016 [23]; Sherman and Brophy, 2005 [182]).

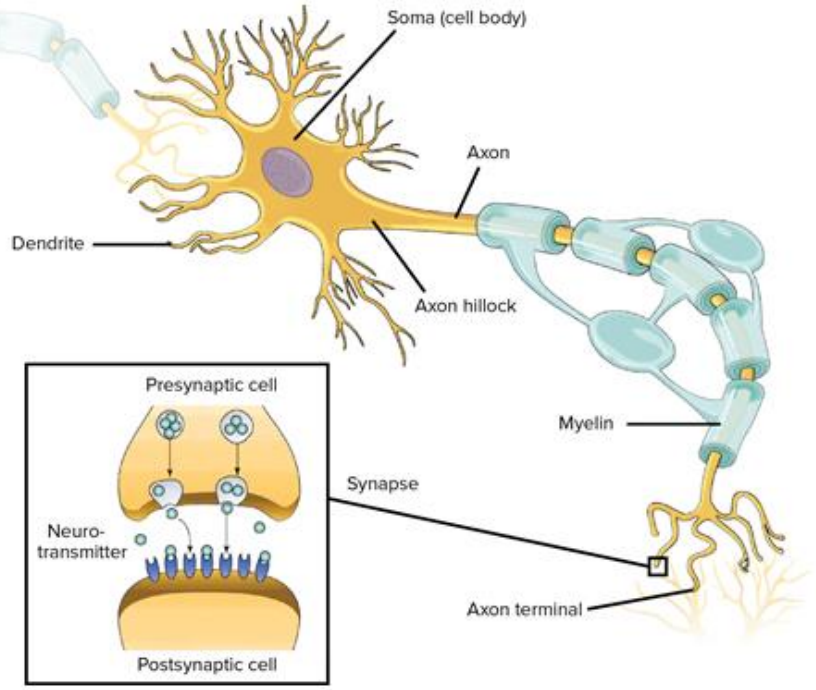

Fig. 4. Graphical representation of a typical neuron structure. Each neuronal cell contains branched dendrites, cell body and long axon which send signal to another cells via synapses. Boxed image present the synaptic organization that contains pre- and postsynaptic neurons (OpenStax College, Biology (CC BY 3.0); modified).

The amount of information that neuron receives through the synapses is determined by the complexity of dendritic arbors that all together form a tree-like structure. The dendritic tree architecture and synapse distribution correlate with a cell local functions and critically affect border neuronal networks (Jan et al., 2003 [108]; Ascoli et al., 1999 [13]; Gao et al., 2007 [66]). As evidenced by time-lapse microscopy, dendritic arbors remain highly dynamic structure constantly forming new connections in response to the information received by postsynaptic signaling (Cline et al., 2001 [41]; Dailey and Smith, 1996 [47]). Thus, it is crucial for the whole brain function to develop, maintain and control the proper organization of dendritic field on a single cell level. That complex process is highly orchestrated by both, extrinsic and intrinsic molecular mechanisms (Arikkath et al., 2012 [9]). Decades of research on the neuronal dendritic morphogenesis revealed hundreds of molecular factors that implicate dendrites growth,

branching, complexity or polarity. That neuronal features are influenced by different extracellular cues, such as neurotrophins, extracellular guidance factors or cell adhesion molecules. For example, it has been reported that a number of secreted factors, such as the brain-derived neurotrophic factor (BDNF) or Wnt family glycoproteins promote dendrite formation and complexity (Horch and Katz, 2002 [87]; Rosso et al, 2005 [174]). On the other hand, Cadherin-catenin cell adhesion complex and both secreted and transmembrane semaphorins promote dendritic branching and control dendrite bifurcations respectively (Arikkath et al., 2008 [8]; Nakamura et al., 2009 [141]). However, the intrinsic genetic program of dendrites formation may occur independently of extracellular cues. Likewise, there is a broad number of studies that identified cellular molecular players involved in dendrites organization, like signaling molecules (Cysteine rich protein 1, Serine/Threonine Kinase 25, Calcium/calmodulin—dependent protein kinases), regulators of the cytoskeleton (Rac/Rho/Cdc4 small GTP binding proteins) and several transcription factors (Nf-κB, cyclin amp response element-binding (CREB), Neurogenin2) (Ma et al., 2011 [123]; Matsuki et al., 2010 [129]; Puram et al., 2011 [163]; Luo et al., 2002 [121]; Leemhuis et al., 2004 [112]; Gutierrez et al., 2005 [75]; Redmond et al., 2002 [171]; Hand et al., 2005 [80]). Last but not least, the interesting group of dendritic tree regulators constitutes of synaptic scaffold proteins. An important examples from that group are postsynaptic density proteins 95 (PSD95) and Erbin, a member of the leucine-rich repeat and PDZ domain (LAP) family, which concentrates at synapses in mature neurons. These proteins have been recently reported to affect a dendritic tree architecture (Charych et al., 2006 [39]; Arikkath et al., 2008 [8]). Although the hundreds of factors regulating dendritic tree morphology have been already identified, we are still far from understanding how neurons develop their shape.

Summing up, the human brain shows multiple levels of organization that altogether form a complex structure which controls all basic vital functions and regulates individuals behavior. The brain organization begins at molecular level and specific genes expression, that impact synapses neurotransmission and neuronal organization, thus enabling for creation of local microcircuits between cells in particular brain areas. Lastly, the local neuronal microcircuits form large scale networks that connect and communicate different brain structures, providing in summary different behavioral outcome (Fig. 5). For that reason, any disturbances at the

genomic level could result in neurodevelopmental, neurodegenerative and neuropsychiatric disorders.

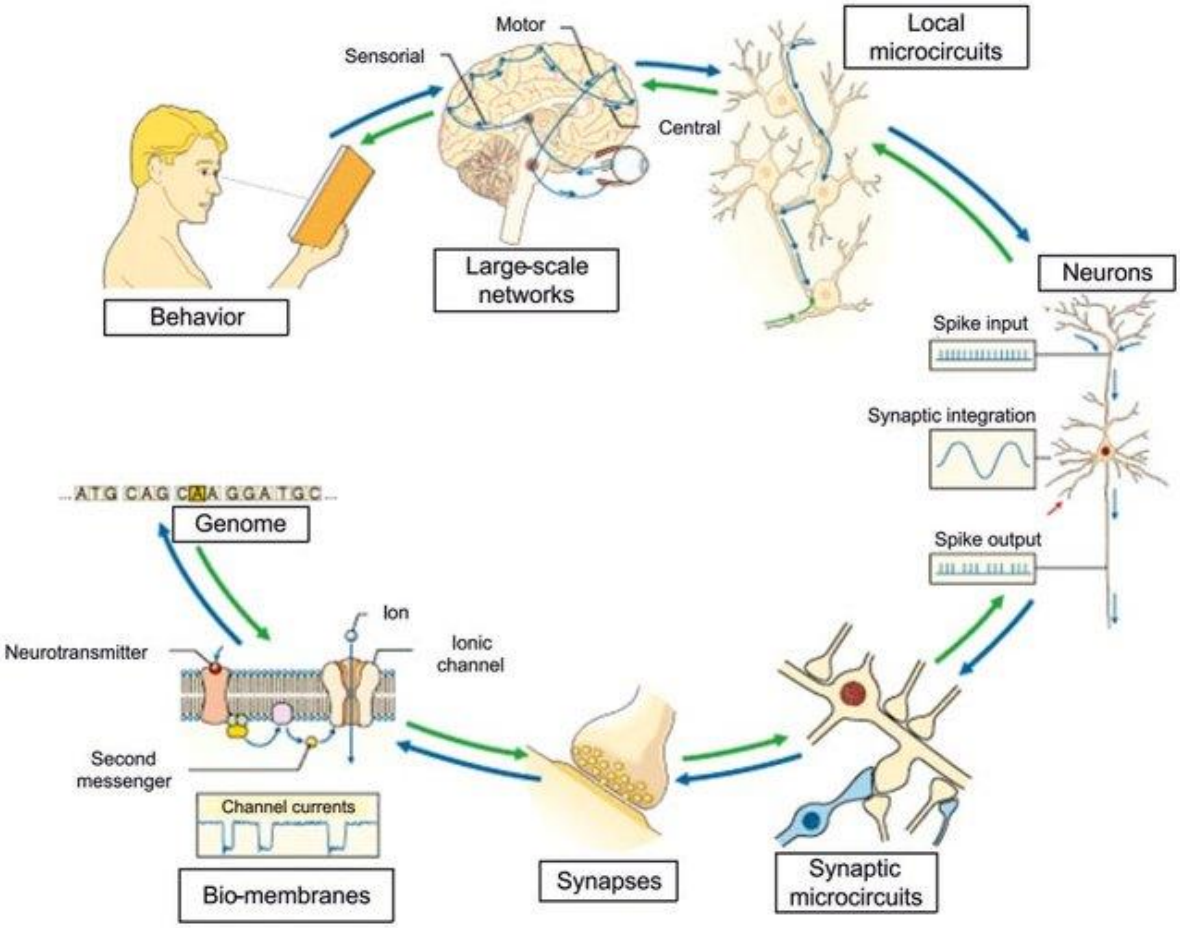

Fig. 5. A multilevel organization of the brain. The brain organization starts at genomic level and any disturbances on the molecular level can affect synaptic function. Further it influences synaptic connections, neuronal organization and functioning of the neighboring neurons microcircuits. Lastly, it all impacts large scale neuronal networks that connects different brain areas and shows the outcome in individual's behavior. Moreover, our action and external environment can also have an impact at all levels of the brain organization and function (D'Angelo and Wheeler-Kingshott, 2017).

1.1.2 Abnormalities in dendritic tree organization and brain disorders

Inappropriate dendritic morphogenesis has been reported in variety of neurological disorders. These impairments are often characterized by altered dendritic development and branching,

abnormal dendritic spine density and morphology or synapse loss. In consequence, all of these abnormalities can affect dendritic trees functional capabilities and thus, influence local microcircuits and large-scale neuronal networks. Changes in dendritic architecture and therefore miscommunication between neurons have been found in neurodevelopmental and neuropsychiatric disorders, such as Rett syndrome, Autism Spectrum Disorders (ASDs), Down syndrome (DS), Alzheimer's disease (AD), Fragile X syndrome (FXS), Schizophrenia and anxiety disorders or depression (Kaufmann et al., 2000 [97]; Eiland and McEwen, 2012 [54]; Soetanto et al., 2010 [191]) (Fig. 6).

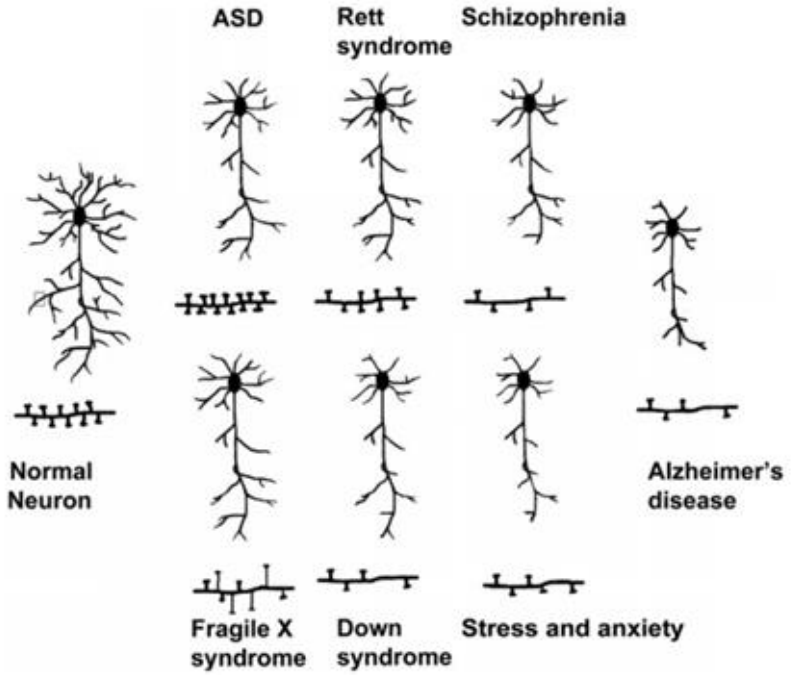

Fig. 6. Schematic representation of neurons morphological abnormalities found in numerous neuropsychiatric disorders. Neurons of Autism Spectrum Disorders (ASD) patients show increased number of dendritic spines and decreased dendrite branching (CA1 and CA4 hippocampal subfields). In Rett syndrome impaired dendritic branching is found in motor and frontal cortex. Schizophrenia diagnosed patients show reduced dendritic branching and spine density in hippocampal CA3 region. In Alzheimer's disease CA1 hippocampal neurons have shorter dendritic length of basal and apical dendrites and reduced number of dendritic spines. Studies on the brains from Fragile X syndrome diagnosed individuals report high density of long, fillopodia-like shaped immature dendritic spines and aberrant dendritic morphology. Remarkable reduction in dendrite length, dendritic tree organization and spine density are found in the adult Down syndrome (DS) patients. Chronic stress and anxiety cause decreased spine density and shorter dendrites in CA3 hippocampal neurons in human subjects (Kulkarni and Firestein, 2012).

A great number of neuroimaging and molecular studies indicated numerous neuropathologies associated with intellectual impairments observed for these heterogenic disorders, which often share some similarities, whereas from the other hand differ significantly. For example, the Rett syndrome shows loss of neuronal cells and functional impairments particularly in the cortical area that result in reduction of brain size (Jellinger et al., 1986 [94]). Deeper analysis of the patient's brain cortex revealed reduced size of pyramidal neurons dendritic trees and impaired arborization found in the frontal and temporal cortical lobes (Armstrong et al., 1995 [10]; Armstrong at al., 2000 [11]). Molecular studies indicated its major cause, the loss of function mutations in methyl DNA-binding factor (MeCP2) that affect insulin-like growth factor (IGF) gene expression and represses BDNF transcription involved in dendrite morphogenesis (Itoh at al., 2007 [104]; Giacometti et al., 2007 [67]; Gonzales and LaSalle, 2010 [72]; Zhou et al., 2006 [242]). The Autism spectrum disorder's individuals, that share variety of social, cognitive, perceptional and motor skill impairments, showed increase in volume of limbic system components, the hippocampus and amygdala (Muhle et al., 2004 [140]; Rapin, 1997 [167]; Schumann et al., 2004 [180]). On the cellular level, the ASD patients brains have abnormal dendritic branching pattern in the hippocampal subregions and increased spine density found for cortical neurons (Raymond et al., 1996 [169]; Hutsler et al., 2010 [92]). Genetic and biochemical studies of ASD's patients pointed out the importance of the MET gene and hepatocyte growth factor (HGF) in development of the disease, as they regulate dendritic organization and are downregulated in patients brain tissue (Gutierrez at al., 2004 [74]; Campbell, 2007 [31]). Another studies revealed that the group of postsynaptic adhesion molecules, neuroligins 3 and 4, are mutated in ASD subjects and, although their role in dendritic growth and arborization is unclear, they may influence synaptic abnormalities found in patients (Jamain et al., 2003 [107]; Zhang et al., 2009 [232]). Recently, the association between mutations in synaptic adhesion and scaffolding molecules and the Autism Spectrum Disorders have been reported (Südhof, 2008 [197]). Similarly to Rett syndrome, the brain size reduction is also observed in Down Syndrome young patients (DS), a disease caused by an extra copy of 21 chromosome. Brain structural abnormalities found in DS patients include reduced cerebral, cerebellar and hippocampal volumes (Golden et al., 1994 [71]; Raz et al., 1995 [170]). Moreover, a remarkable shrinkage of dendritic length accompanied with decreased spine density has been observed (Becker et al., 1991 [19]; Takashima et al., 1989 [199]). One of the proteins that is associated with the mental retardation seen in DS individuals is the cell adhesion molecule DSCAM. Although its function

in brain is not fully understood, it plays significant role in inhibition of dendrite branching and synaptogenesis, and importantly, that gene was found to be overexpressed in DS patient's (Benavides-Piccione et al., 2004 [21]; Alves-Sampaio et al., 2010 [6]). Lastly, brans of schizophrenia diagnosed patients, often show reduced cerebral cortical tissue and increased lateral ventricles (Harvey et al., 1993 [81]; Zipursky et al., 1992 [244]; Wright, 2000 [226]; Jaaro-Peled et al., 2010 [105]). On the cellular level, there was, however, no report on cell loss contribution to the phenotype, instead there are several studies showing impaired dendritic arborization and decrease in dendritic spine density in the prefrontal cortex brain area and CA3 hippocampal area (Broadbelt et al., 2002 [27]; Glantz and Lewis, 2000 [69]; Kolomeets et al., 2007 [110]). The molecular studies on schizophrenic individual's brains revealed misregulation of number of genes involved in dendritogenesis and synaptic function. Decreased immunoreactivity for microtubule-associated protein-2 dendritic marker, reduced synaptophysin or drebrin synaptic proteins expression and loss of the N-methyl-D-aspartate glutamate receptor (NMDA) NR1, NR2 subunits have been frequently observed (Glantz and Lewis, 1997 [70]; Hill et al., 2006 [84]; Weickert et al., 2013 [219]). Another line of evidence underlying the crucial role of proper dendritic tree organization comes from studies on neurological conditions causing motor function disabilities. The brain part that is involved in motor control is the cerebellum. The whole cerebellar input comes from the mossy fibers and climbing fibers (Fig. 7). The mossy fibers innervate neurons in the cerebellar nuclei and granule cells located in the cerebellar cortex, whereas the climbing fibers transmit signals that comes from the spinal cord to the cerebellar nuclei and Purkinje neurons. The cerebellar GABAergic Purkinje cells form one of the most complex dendritic arbors among other neurons, and provide the sole output from the cerebellar cortex. Their aberrant activity could lead to ataxias or cerebellar-induced dystonia's. The loss of distal Purkinje neurons dendrites has been observed in human hereditary ataxic condition (Koeppen at al., 1991 [109]). More recently, Louis and his colleagues have reported a regressive changes in cerebellar Purkinje cell dendritic architecture for patients diagnosed with essential tremor disorder (Louis et al., 2014 [120]).

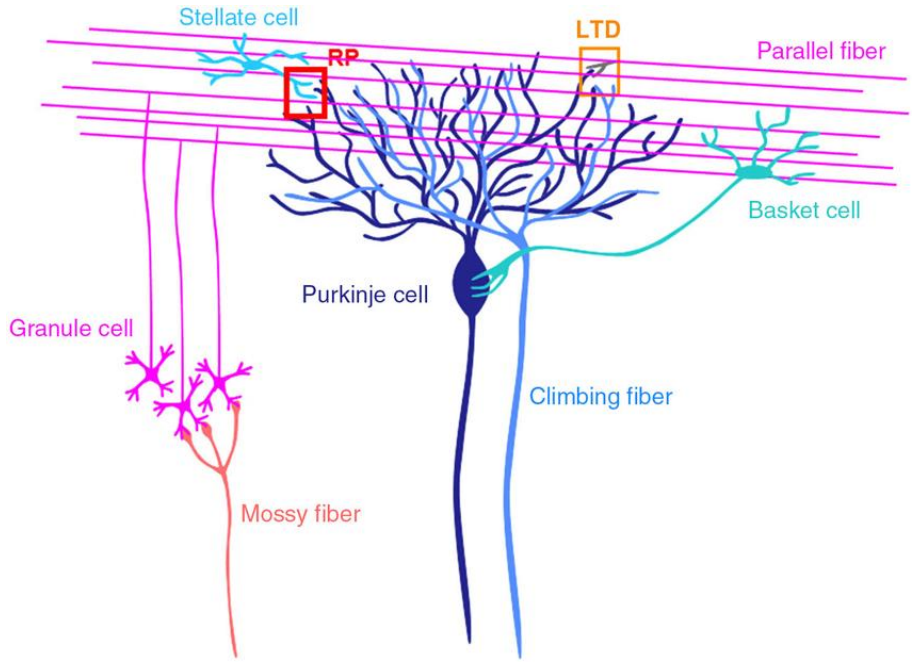

Fig. 7. The schematic graph of neuronal circuits formed in cerebellar cortex. The mossy fibers extend from brainstem and connect to the granule cell, which further send their axonal projections to molecular layer and therefore communicate with stellate cells, Purkinje cells and basket cells. The climbing fiber coming from spinal cord form numerous synapses on Purkinje cells. Long-term depression (LTD), a type of neuronal plasticity can occur at excitatory parallel fiber-Purkinje cell synapses, whereas rebound potentiation (RP) appear at inhibitory GABAergic synapses formed between stellate and Purkinje cells.

Although each of the above mentioned neuropathological conditions is characterized by its own set of symptoms, they show consistency in the dendritic tree structure impairments. Thus, knowing that dendritic abnormalities widely underlie cognitive and motor dysfunctions in human, it is of a great importance to understand the molecular mechanisms causing dendrites impairments and to identify new factors involved in neuronal morphogenesis.

1.2 The Angiomotins

1.2.1 Discovery and structural characteristic of Angiomotins

The Angiomotin 80 kDa protein (Amot p80) was originally identified by Troyanovsky et. al in 2001 in yeast two-hybrid screening for Angiostatin-binding proteins, known inhibitor of angiogenesis and tumor growth (Troyanovsky et al., 2001 [207]). The authors indicated that Amot localizes to the leading edge of endothelial migrating cells, where it overlaps with F-actin distribution and is implicated in the angiostatin inhibition of cellular migration and tube

formation processes. The mRNA expression analysis detected Amot synthesis in the heart, brain, liver, lung, kidney, pancreas, and placenta, indicating its broad expression. Due to Amot's anti-migratory functions in endothelial cells, the authors termed the protein Angiomotin. Nowadays, scientists are aware of a probable artifact of Amot p80-Angiostatin interaction identified with artificial yeast two-hybrid system, as both proteins localize to the different sides of the cell membrane. The intracellular Amot p80 protein lacks a signal peptide or the trans-membrane domain that could enable its binding to the secreted, extracellularly located Angiostatin (Bratt et al., 2003 [26]). Further investigations led to the discovery of two polypeptides with significant homology to Amot: Angiomotin-like 1 (initially named junction-enriched and –associated protein, JEAP) and Angiomotin-like 2 (Bratt et al., 2003 [26]; Nishimura et al., 2002 [146]). Altogether these evolutionary conserved proteins constitute a family of polypeptides called Motins or Angiomotins. Originally, the 98 kDa Angiomotin-like 1 (Amotl1) protein was termed JEAP due to its cellular distribution to tight-junctions (TJs) complexes of the exocrine gland cells, where it co-localizes with transmembrane occludin and peripheral membrane ZO-1 junctional enriched proteins (Nishimura et al., 2002 [146]). Similarly, the Amotl2 protein was initially found to overlap with another tight-junction protein, MAGI-1, and, therefore was given additional term as MAGI-1-associated coiled-coil tight junction protein (MASCOT) (Patrie et al., 2005 [156]). Further studies identified an additional Amot isoform of predicted 130kDa molecular weight (Amot p130) that results from alternative splicing between the exon 2 and 3 of Amot gene (Ernkvist et al., 2006 [55]).

The Angiomotin proteins (Amot, Amotl1, Amotl2) share structural similarities, they have N-terminal intrinsically disorders-domain (ID), prolin-rich site, centrally located coild-coil (CC) domain, and C-terminally located PDZ-binding motif (Fig. 8, Bratt et al., 2003 [26]). The N-terminal ID domain of Amot p130, Amotl1 and Amotl2 proteins contains the three L/P-PxY motifs, which mediate interactions with WW domain proteins, such as the Hippo pathway transcriptional coactivator Yap1 or the multiple factors of the neural-precursor cell-expressed developmentally downregulated 4 (Nedd4) ubiquitin E3 ligases family of proteins (Wang et al., 2011 [217]; Zhao et al., 2011 [235]; Chenji et al., 2012 [40]; Ray et al., 2019 [168]). All tree Angiomotins contain the F-actin binding region within the ID domain that comprises the phosphorylation site for the Hippo pathway core kinase LATS, which regulates Motins binding to actin fibers (Ernkvist et al., 2006 [55]; Mana-Capelli et al., 2014 [126]; Chan, 2013 [38]). The entire ID domain of

Amot is absent in p80 isoform of Amot. The proline-rich region enables for interaction with Src homology 3 (SH3) protein domains. The CC domain allows Angiomotins to self-associate forming homo-or hetero-dimers with other Angiomotin family members or bind to different CC domain-containing polypeptides like other components of the Hippo Pathway, the Moesin, ezrin, and radixin-like protein (Merlin) (Patrie et al., 2005 [156]; Yi et al., 2011 [230]; Li et al., 2015 [115]). The C-termini of all Angiomotins comprise PDZ-binding motifs that mediate interactions with the PDZ domains of other proteins, such as polarity proteins Patj and Par3 (Ernkvist et al., 2009 [57]; Wells et al., 2006 [221]). All Angiomotins, therefore, have multiple protein-protein binding domains that collectively coordinate spectrum of protein interactions.

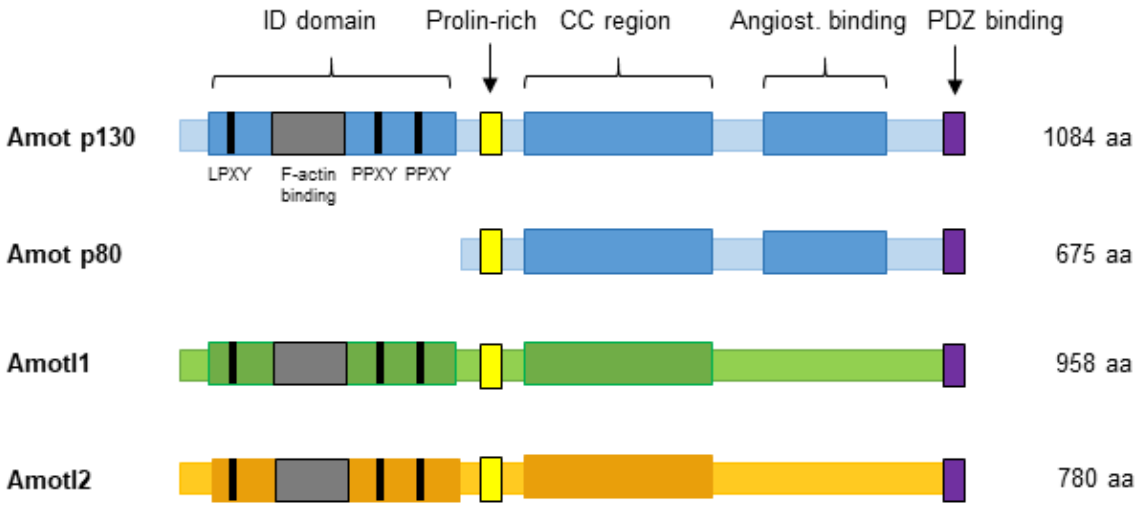

Fig. 8. Schematic representation of Angiomotins organization. Angiomotin family of proteins comprises of three structurally similar polypeptides: Amot, Amotl1 and Amotl2. Amot is expressed in two different isoforms, longer Amot p130 and shorter Amot p80, that lacks the entire N-terminal domain. The ID domain of Amot p130, Amotl1 and Amotl2 contains 3 similar motifs L-P/PXY (black line) that are the site of interaction with Yap1 transcriptional coactivator. Additionally, the ID domain contains a F-actin binding region, within which phosphorylation site for Lats kinases is located (red line). Proline-rich (yellow), the coil-coiled domain and PDZ-binding sites (violet) are present in all proteins of the family.

1.2.2 Angiomotins expression and function

1.2.2.1 Expression in tissue

There is an increasing interest in Motins in recent years, since over 150 scientific articles appeared from their initial identification. Although all Angiomotins share significant structural similarities, their expression pattern differs spatiotemporally and depends on the cellular and physiological contexts. Early northern blot analysis of Angiomotins mRNA expression revealed that all three proteins are widely expressed in different mouse tissues, however at different levels: Amot showed the highest expression in brains, skeletal muscles, and placentas, Amotl1 was found abundant in brain, heart, lung, skeletal muscle, kidney and uterus, whereas the highest transcript level of Amotl2 was detected in lung tissues (Bratt et al., 2003 [26]). Similarly, Motins analysis showed abundance mRNA expression across the human body, which was found at variable levels for analyzed tissues as presented in data generated by the Illumina human BodyMap 2.0 platform (Fig. 9, Moleirinho et al., 2014 [138]). Interestingly, the divergent protein expression of Amot isoforms was observed throughout the mouse development: Amot p80 was detectable from the early stages of embryogenesis, with no Amot p130 expression found during fetal development (Ernkvist et al., 2006 [55]). This is in consistency with the data obtained from a mouse retina tissue that showed increased Amot p80 protein expression in mouse at postanaday day 3 (P3), whereas Amot p130 was detectable at P7 the earliest and expressed exclusively in the retina of an adult mouse (Ernkvist et al., 2008 [56]). These differences in Angiomotins expression during the development and based on tissue-origin may indicate their potential diverse functions.

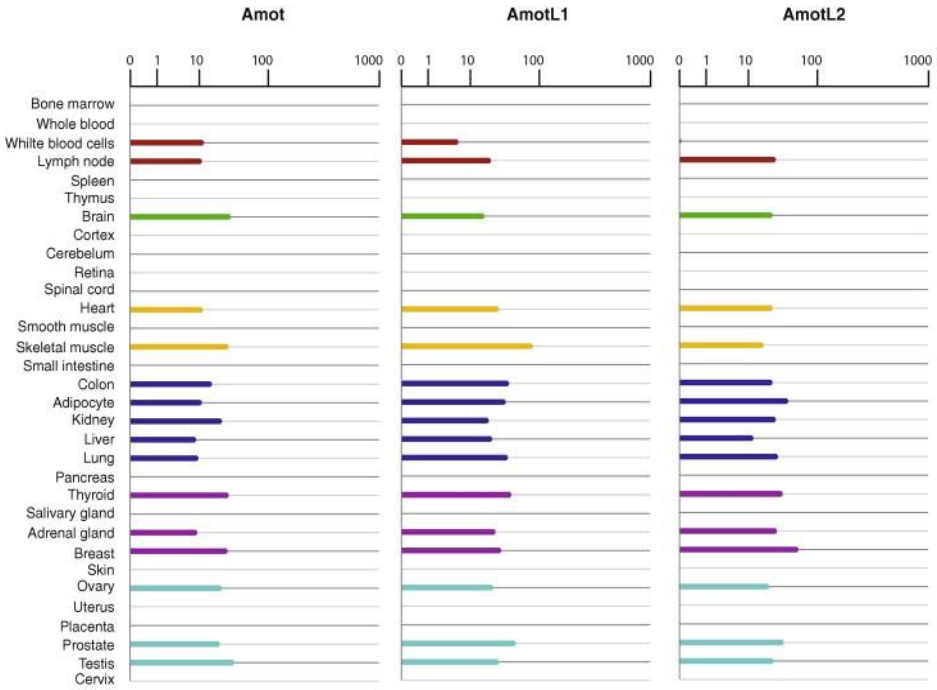

Fig. 9. Angiomotins mRNA expression in different human tissues. Samples were collected from 16 individuals and the expression data were obtained from the Illumina human BodyMap 2.0 platform. Amot expression is found the highest for testis, brain, thyroid and skeletal muscle; Amotl1 showed slightly higher values for skeletal muscle over the rest of tissues analyzed, whereas Amotl2 mRNA was highly detectable in breast lysates. Different colors represent tissue origin (red- immune system; green- nervous system, yellow- muscle tissues; navy- internal tissues; violet- secretory organs; blue- reproductive system). (Bratt et al., 2003).

1.2.2.2 Functions in embryogenesis

Angiomotins have important functions in various physiological and pathological processes, such as embryonic development, angiogenesis, the Hippo-signaling pathway regulation and carcinogenesis. Although some Angiomotins have overlapping functions, there are many evidence for exclusive properties of each Angiomotin. During early embryogenesis, Amot is phosphorylated by LATS1/2 kinases at the inner mass cells adherent junctions and therefore it regulates the Hippo-signaling pathway activity which is indispensable for proper development of the trophectoderm and the inner cell mass linage (Nishioka et al., 2009 [147]; Hirate et al., 2013 [85]; Hirate et al., 2014 [86]). Moreover, the Amot localization that is regulated by the Rho-associated kinase (Rock), impacts proper apical-basolateral polarization of outer cells (Mihajlović et al., 2016 [135]). Importantly, at the post implantation developmental stages Amot knockout mice display embryonic lethality due to defects in endoderm cell migration and severe intersomitic vascular insufficiency together with dilated vessels in the brain

(Shimono et al., 2003 [183]; Aase et al., 2007 [1]). It has been found that these processes are governed by Amot interactions with Patj polarity and RhoA GTPase exchange factor Syx proteins that control local GTPase activity necessary for growth-factor mediated cell migration (Ernkvist et al., 2009 [57]). Interestingly, the Lars Holmgren group have documented the Amotl1 function in regulation of vascular endothelial cell migration. They proposed that, similarly to Amot, Amotl1 controls cellular polarity via the interactions with Patj and RhoGEF Syx proteins (Zheng et al., 2009 [239]). The authors showed that silencing Amotl1 in zebrafish also resulted in vascular embryogenic deficiency. However, Amot and Amotl1 knockdown differed in the spreading phenotype of the intersegmental vessels horizontal tip cells and authors provide the explanation for possible diverse spatiotemporal expression of both proteins. Simultaneously, another group have shown that Amotl1 interacts with Amot p80 and induces remodeling of actin cytoskeleton via binding to F-actin fibers that could also have probable effect on the cell migration and blood vessel formation (Gagné et al., 2009 [65]). Lastly, the Amotl2 protein was shown to regulate embryonic cell movements due to its interaction with non-receptor tyrosine kinase Src and actin fibers organization. It inhibits the Wnt/β-catenin signaling by interacting to and trapping the β-catenin protein in zebrafish embryos (Huang et al., 2007 [89]; Li et al., 2012 [116]). Thus, although all of the Angiomotins play important role in the embryonic development, their function appears slightly different probably due to difference in spatiotemporal expression and interacting partners.

1.2.2.3 Molecular functions in the Hippo pathway regulation

One of the most recognizable functions of all Angiomotins is the regulation of the Hippo-signaling pathway in diverse cells and conditions. In general the Hippo pathway controls the organ size and stem maintenance due to regulation of cellular proliferation and apoptosis (Zhao et al., 2011 [235]). It is composed of the core kinase cascades Mst1/2 and Lats1/2 that regulate the function and cellular localization of transcriptional co-activator Yap1 and Taz, downstream effectors of the Hippo-signaling pathway (Zhao et al., 2010 [234]; Zhao et al., 2007 [237]). Unphosphorylated Yap1 translocates to the cell nucleus where it binds to the DNA-binding TEA domain (TEAD) transcription factors and in result induces the expression of the Hippo pathway dependent genes, such as CTGF and c-Myc oncogenes (Vassilev et al., 2001 [212]; Zhao et al., 2010 [234]; Zhao et al., 2008 [238]). All Motins bind directly to Yap1 protein through their ID

domains and therefore, they have been recognized as novel components of the Hippo pathway (Zhao et al., 2011 [235]; Huang et al., 2018 [90]). However, similarly to other molecular functions of Motins they regulate the Hippo-signaling pathway in different manner depending on the cell context (Fig. 10). In the TJs of epithelial cells Amot can interact with Merlin, an upstream regulator of Hippo-pathway, preventing its auto inhibition, thus enabling for binding to Lats1/2 and activation of the pathway (Li et al., 2015 [115]). Interestingly, in Madin-Darby Canine Kidney cells (MDCK) or HEK-293 cells Amot inhibits the Yap1-dependent transcription, whereas in pathological conditions, such as breast cancer cells it promotes Yap1 translocation to the nucleus and TEAD-dependent gene transcription (Chan et. al, 2011 [37]; Lv et al., 2015 [122]). In addition, the Amotl1 was also shown to negatively regulate Yap1 nuclear localization in HEK293 cells, therefore restricting its pro-apoptotic function (Oka et al. 2012 [152]). This year Zhou and colleagues proved Amotl1 pro-oncogenic function in gastric carcinogenesis (Zhou et al., 2020 [241]). Amotl1 and Yap1 interaction prevents both factors from NEDD4 E3 ubiquitin-mediated degradation and thus promotes Yap1 nuclear translocation (Skouloudaki et al., 2012 [187]; Zhou et al., 2020 [241]). Finally, all tree Angiomotins have been found to regulate the Hippo-dependent transcription by preventing Yap1 nuclear localization. In MDCK cells Amotl2 knockdown leads to decreased Yap1 TJs localization, its reduced phosphorylation and nuclear accumulation, thus presenting the link between Hippo pathway and cell contact inhibition (Zhao et al., 2011 [236]). Moreover, Amotl2 has been found to negatively regulate a tissue growth process in zebrafish mediated by crosstalk between Yap1 and Wnt/β-catenin effector Left1 and by mTOR (Agarwala et al., 2015 [3]). Importantly, it has been shown that Amotl2 repressive function on Yap1 can be attenuated by mechanistic target of rapamycin (mTOR) signaling mediated phosphorylation (Artinian et al., 2015 [12]). Last but not least, it has been shown that F-actin inhibits Amot-mediated cytoplasmic retention of Yap1 though competitive binding to Amot p130 (Mana-Capelli et al., 2014 [126]). From the other hand, it was found that Amot could bind both, actin fibers and Yap1, which occurs probably due to its oligomerization (Zhao et al., 2011 [235]). Nevertheless, this data provides important crosstalk between Motins and actin organization in Yap1 and Hippo-signaling pathway activity.

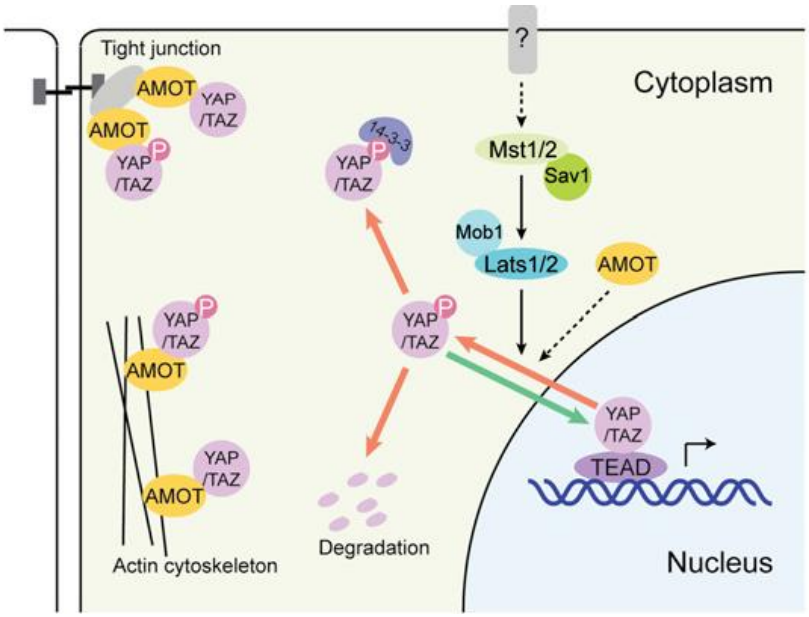

Fig. 10. Schematic diagram of Amot regulation of the Hippo-signaling pathway component, Yap1 cellular localization and function. Amot can inhibit Yap1/TAZ nuclear localization through its binding and localization to tight junctions or promote Yap1/TAZ phosphorylation by Lats 1/2 Hippo-signaling kinases.

1.2.2.4 Role in the cancer development

Although Angiomotins function in numerous cancer types development highly depends on the Hippo pathway regulation, it has been shown that they can act separately of Yap1 interaction. For example, in mouse liver Amotl2 directly associates and negatively regulates protein kinase B (AKT), thus Amotl2 downregulation in mouse liver and human liver cancers leads to AKT activation and hepatomegaly (Han et al., 2017 [78]). All Angiomotins are widely expressed in most types of tumors, however the Amot increased transcript expression in cancer samples was found exclusive over the other member of the family (Jiang et al., 2016 [95]). Thus, Amot is postulated to be useful prognostic marker for cancer disease and patient survival. Altogether, accumulating evidences provide insights into all Motins function in the Hippo pathway and carcinogenesis regulation, both as oncogenes and tumor suppressors. However, their relevant regulatory mechanisms are dependent on cell and physiological context and need further investigation. Last but not least, Angiomotins have been associated with the pathological processes underlying viral infections, such as releasing of HIV-1 from the human cells and

completing immature virion assembly, and promoting the cell egress of Ebola viral particles and therefore virus spreading. (Mercenne et al., 2015 [133]; Han et al., 2020 [79]).

1.2.2.5 Angiomotins function in the nervous system

Angiomotin protein family has been mostly studied in embryogenesis, angiogenesis and cancer development. Although all three Angiomotins are expressed in the mouse and human brain their function in the nervous system remained unknown (Troyanovsky et al., 2001 [207]; Bratt et al., 2003 [26]). The first insight into Angiomotins role in the nervous system came from a study on the neuromuscular junction (NMJ), a chemical synapse of the peripheral nervous system (PNS) that connects the motor neuron to a muscle fiber (Proszynski TJ, Sanes JR, 2013 [161]). The authors found that Amotl2 localizes to the postsynaptic membrane in cultured myotubes and *in vivo*. Moreover, Amotl2 depletion led to enlargement of synaptic podosomes which influence the postsynaptic composition and structure. It is worth attention that numerous protein are engaged in the NMJ organization simultaneously involved in the regulation of central nervous system (CNS) synapses. Thus, the initial studies on the Amotl2 function in synapse organization provided a starting point for broad research on Angiomotins role in the nervous system. Importantly, the genetic studies of the hippocampal neurons homeostatic scaling processes indicated Amot association to Autism and Amyotrophic Lateral Sclerosis (ALS) disorders (Schanzenbächer at al., 2016 [178]). During the time of my PhD studies, two groups have published first reports of their work on Angiomotins function in the CNS. Firstly, Wigerius and colleagues have demonstrated that Amot p130 is indispensable for dendritic spine stabilization in mature hippocampal neurons *in vitro* (Wigerius et al., 2018 [224]). Authors found that Amot p130 isoform, but not Amot p80, localizes to dendritic spines and its synaptic distribution is negatively regulated by phosphorylation through Lats kinase of the Hippo-pathway. Moreover, Amot p130 controls dendritic spine morphogenesis through coupling F-actin to postsynaptic scaffolds proteins, PSD95 and multi-PDZ damin protein 1 (MUPP1). In contrast to Amot p130, the shorter isoform of Amot that lacks the N-terminal domain (Amot p80) was distributed to somatodendritic compartments in cultured hippocampal neurons and was excluded in dendritic spines. Interestingly, both Amot isoforms were abundantly expressed in different structures of the rat brain. The second publication that appeared during my project implicates Amot in neuronal differentiation (Zaltsman et al.,

2019 [231]). Zaltsman and coworkers have found that Amot-Yap1 interaction increases during neural development in neural stem cells (NSCs). Furthermore, they showed that Amot p130 regulates Yap1 localization, leading to its nuclear exclusion during development. This involved a decrease in F-actin polymerization, and authors proposed Amot as a bridge between actin cytoskeleton organization and Yap1 subcellular localization during neural development. Simultaneously, they found Amotl1 and Amotl2 expression in NSCs, however at lower levels when compared to Amot. The most recent neuronal study of the Amot function has showed that it acts as intermediate signal transducer for NSCs that triggers the decision on neurogenesis in response to extracellular stiffness features (Kang et al., 2020 [96]). Therefore, Amot plays a critical role in NSCs mechanotransduction. Recent experiments in our laboratory revealed Amot's critical role in dendritic morphogenesis of cultured hippocampal neurons (Rojek, Krzemien et al., 2019 [172]). My colleague, Kasia Rojek has found that Amot function in developing neurons relay on its interaction with Yap1 and that both proteins localize to dendritic processes at early developmental stages, whereas both relocalize to synaptic compartments in mature cells. The knockdown experiments demonstrated that Amot and Yap1 are indispensable for proper dendritic growth and arborization (Fig. 11). Importantly, she showed that Amot and Yap1 role in dendritic organization does not depend on binding to TEAD transcription factors, thus does not affect the expression of the genes regulated by the canonical Hippo-signaling pathway. Instead, Amot and Yap1 affect phosphorylation of mTORC1 effector, S6 kinase and its target S6 ribosomal protein (Fig.12). This would suggest that Amot and Yap1 could regulate dendritic tree morphology through regulation of translation process. Interestingly, s6 ribosomal protein was shown previously to regulate dendritogenesis (Jaworski et al., 2005 [93]; Urbanska et al. 2012 [210]).

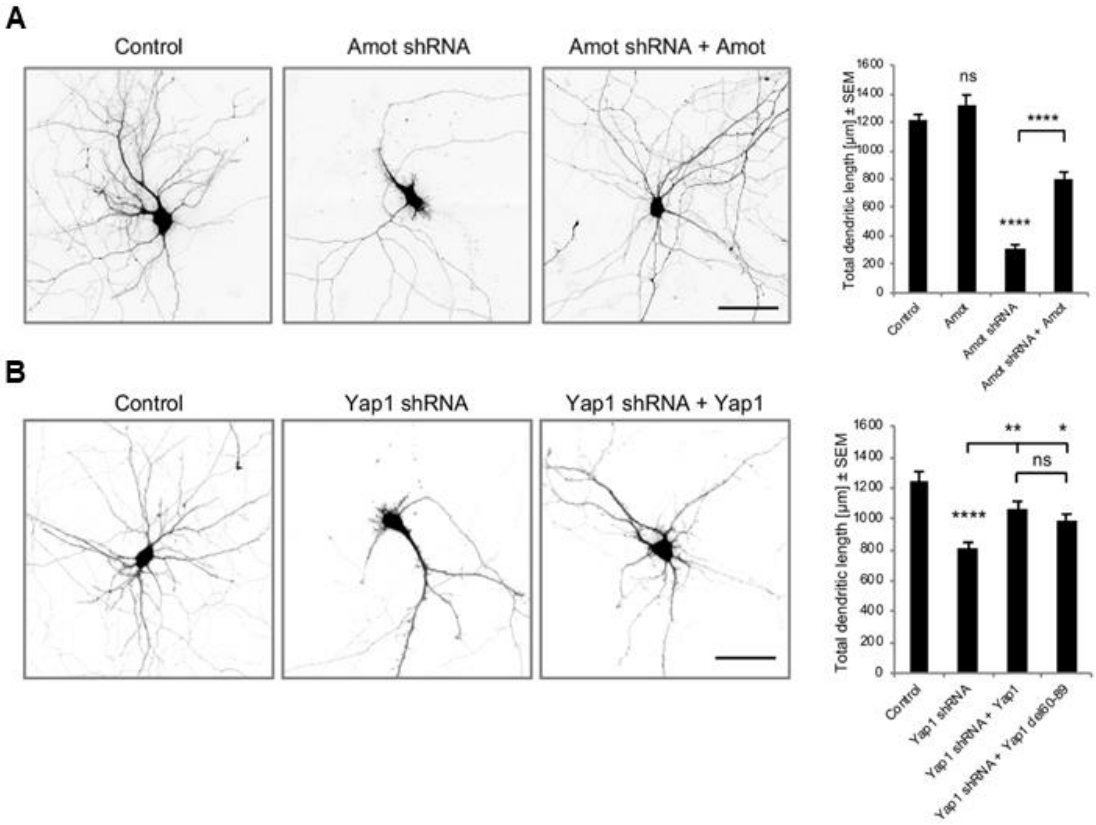

Fig. 11. Amot and Yap1 depletion in developing neuros affect dendritic growth. A) The images of the rat hippocampal neurons transfected with empty plasmid (control), the plasmid with Amot shRNA (Amot shRNA) or co-transfected with the Amot shRNA plasmid with a vector expressing wild type Amot (Amot shRNA + Amot). Amot knockdown specifically impairs dendrites development. Right graph represents the quantification of total dendritic length upon Amot knockdown and in the rescue experiments. Amot depleted neurons have significantly shorter dendrites. B) The photographs of the rat hippocampal neurons transfected with empty plasmid (control), the plasmid with Yap1 shRNA (Yap1 shRNA) or co-transfected with the Yap1 shRNA plasmid with a vector expressing wild type Yap1 (Yap1 shRNA + Yap1). Yap1 knockdown (Yap1 shRNA) impairs dendrites development. Right graph represents the quantification of total dendritic length upon Yap1 knockdown and in the rescue experiments. Yap1 depleted neurons have significantly shorter dendrites. Expression of the Yap1 mutant that is unable to bind the TEAD transcription factors (Yap1 del60-89) in Yap1 knockdown neurons also rescued observed phenotype to the level comparable to expression of wild-type Yap1. (Rojek et al., 2019).

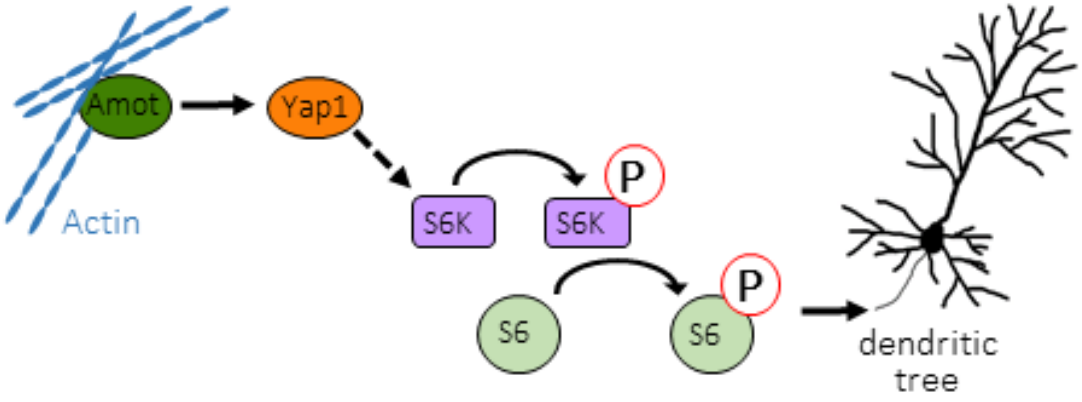

Fig. 12. Schematic representation of Amot and Yap1 function in dendritic organization. Amot interacts with Yap1 and regulates dendritic tree morphology through the regulation of S6 phosphorylation by S6K. (Rojek et al., 2019).

2 Aim of the study

An increasing number of studies highlights the important role of Amot in the proper neuronal organization and function. Studies on hippocampal cultured neurons reveled Amot's role in neural differentiation, dendrite organization in developing neurons, and dendritic spine stabilization in mature cells (Wigerius et al., 2018 [224]; Zaltsman et al., 2019 [231]; Kang et al., 2020 [96]; Rojek et al., 2019 [172]). Although the expression of other Angiomotins, Amotl1 and Amotl2, have been also found in the rodent and human brains, to date there is no report on their function in neurons. Moreover, the function of all three Angiomotins in the brain organization and behavior have never been studied. Thus, the main aim of my project was to investigate Angiomotins involvement in mouse brain organization and analyze potential behavioral abnormalities upon protein depletion. I have focused my studies on two proteins of the Angiomotin family, Amot and Amotl1, and known Amot neuronal interactor, Yap1. The specific aims included:

Aim 1: To analyze brain morphology of Amot and Yap1 neuronal-knockout mice

Aim 2: To study the behavior related to observed brain structural impairments in Amot and Yap1 mutants

Aim 3: To generate Amotl1 global knockout mouse line

Aim 4: To analyze brain structures in Amotl1 depleted mice

Aim 5: To study Amotl1 mutants brain function with behavioral assays

3 Materials and methods

3.1 Buffers

All of the buffers and the ingredients used for their preparation are listed in the table 1 below.

Table 1. List of homemade buffers used in the study

Name	Ingredients
Antifreeze solution	30% ethylene glycol, 15% sucrose and 0.05% sodium azide in PBS
Phosphate buffered saline (PBS)	137 mM NaCl, 2.7 mM KCl, 10 mM Na_2HPO_4; 1.8 mM KH_2PO_4, pH = 7.4
Radioimmunoprecipitation assay (RIPA) buffer	50 mM Tris-HCl [pH = 8.0], 150 mM NaCl, 2% Igepal CA-630 [NP-40], 0.25% sodium dodecyl sulfate [SDS], 1 mM NaF, and 1 mM dithiothreitol [DTT] supplemented with Mini Protease Inhibitors cocktail (Roche, Indianapolis, IN, USA; catalog no. 11873580001)
Sodium dodecyl sulfate polyacrylamide gel electrophoresis (SDS-PAGE) running buffer	25 mM Tris-HCl pH = 7.4, 192 mM glycine, 0.1% SDS, pH = 8.3
5 x Transfer buffer	1.5 M glycine, 1.5 M Tris-Base, 0.15% SDS; prepared before use in a 1:3:1 ratio (5 x transfer buffer : H_2O : ethanol)
Tris-acetate-EDTA (TAE) buffer	40 mM Tris (pH = 7.6), 20 mM acetic acid, 1 mM EDTA
Tris-buffered saline (TBS)	50 mM Tris-HCl pH = 7.5, 200 mM NaCl
Tris-buffered saline with Tween (TBST)	0.1% Tween-20 in 1 x TBS

3.2 Commercial kits

Throughout this study several commercially available kits that are listed in the table 2 were used (see below).

Table 2. List of commercial kits and medium used in the study

Name	Description	Supplier and catalog number
Clarity Western ECL Substrate	Kit for luminol-based detection of proteins in Western blotting (medium sensitivity)	Bio-Rad, Hercules, CA, USA; catalog no. 1705061
Immobilon Western Chemiluminescent HRP Substrate	Kit for luminol-based detection of proteins in Western blotting (high sensitivity)	Merk Millipore, Burlington, MA, USA; catalog no. WBKLS0500 Burlington, MA, USA;
Optimal Critical Temperature Medium (OCT)	Medium of watersoluble glycols for cryostat sectioning at temperatures below -10ºC	Leica Biosystems, Wetzlar, Germany; catalog no. 14020108926
SuperSignal™ West Femto Maximum Sensitivity Substrate	Kit for luminol-based detection of proteins in Western blotting (high sensitivity)	Thermo Fisher Scientific, Waltham, MA, USA, catalog no. 34096

3.3 Mouse strains and husbandry

All of the mice that were used for experiments were bred in a specific pathogen-free (SPF) animal facility at the Nencki Institute of Experimental Biology. Routine microbiome profiling and standard health screening of mice was performed by the animal facility four times a year. All mice were on a C57BL/6 genetic background which is the most common inbred strain used for basic and preclinical research. The experimental procedures were approved by the First Warsaw Local Ethics Committee for Animal Experimentation and the experiments were carried out in accordance with relevant guidelines and regulations.

3.3.1 Amot and Yap1 conditional knockout mice

Amot fl/fl mice were kindly provided by Lars Holmgren Laboratory (Karolinska Institute, Stockholm, Sweden). These animals have Amot alleles floxed (*fl*) with two loxP sites flanking critical 2nd exon of the gene (Fig. 15 in "Results" section). *Yap fl/fl* mice (*Yap1*$^{tm1.1Dupa}$/J) have been previously described (Zhang et al., 2010 [233]) and were purchased from the Jackson Laboratory (Bar Harbor, ME, USA; stock no. 027929). In these mice the first two exons of the Yap1 gene are surrounded by loxP sites (Fig. 15 in "Results" section). *Amot fl/fl* and *Yap1 fl/fl* mice were born at the expected Mendelian ratios and develop normally. *Amot fl/fl;Syn-Cre*

and *Yap1 fl/fl;Syn-Cre* neuron-specific knockout (KO) mice were generated by crossing *Amot fl/fl* or *Yap1 fl/fl* animals with *Synapsin1-Cre* mouse strain (*Syn-Cre*) obtained from the Jackson Laboratory (B6.Cg-Tg(Syn1-cre)671Jxm/J, stock no. 003966). These mice carry Cre recombinase under the control of a 4kb rat synapsin I promoter providing Cre activity in neuronal cells, including brain, spinal cord and dorsal root ganglia detectable from a mouse embryonic day E12.5 (Zhu et al., 2001 [243]).

3.3.2 Amotl1 knockout mice

Amotl1 fl/fl mice were a generous gift from Lars Holmgren Laboratory (Karolinska Institute, Stockholm, Sweden). In these mice two loxP sites flank exons 5 and 6 of Amotl1 gene which cause a frame shift resulting in premature stop codon at 300 amino acids upon recombination (Fig. 30 in "Results" section). Amotl1 systemic knockouts (*Amotl1 KO/KO*) were generated by crossing *Amotl1 fl/fl* mice with a *Cytomegalovirus-Cre* (*CMV-Cre*) transgenic animals obtained from the Jackson Laboratory (B6.C-Tg(CMV-cre)1Cgn/J, stock no. 006054). In this strain, the Cre recombinase gene was inserted under the control of human cytomegalovirus minimal promoter, which drives the expression in all tissues, including germline and allows for Cre activation during early embryonic development. In the next step of Amot1 knockout mouse line generation, *Amotl1 KO/KO;CMV-Cre* mice were crossed with the animals of the same genotype to eliminate *CMV-Cre* allele from the population (Fig. 30 in "Results" section). *Amotl1 KO/KO* mice were born at expected Mendelian ratios and they developed with no gross abnormalities. C57BL/6J wild-type (WT) animals were used as a "control" group for all experimental procedures comprising *Amotl1 KO/KO* mice.

3.3.3 STOP-tdTomato reporter mice

The *STOP-tdTomato* (*STOP-Tom*) mouse (Madisen et al., 2010 [125]) was a kind gift from Witold Konopka, Laboratory of Animal Models, Neurobiology Center, Nencki Institute of Experimental Biology. These knock-in animals carry the Gt(ROSA)26Sor locus with inserted STOP-of transcription sequence flanked by LoxP sites and placed between the promoter composed of cytomegalovirus, chicken beta-actin gene and rabbit beta-globin gene elements (CAG), and the red fluorescent protein (*tdTomato*) coding sequence (Madisen et al., 2010 [125]). Following Cre-mediated excision of the loxP-flanked STOP cassette, a robust expression of

tdTomato fluorescence occurs in all cells with Cre expression. These mice were used to confirm the activity and specificity of Cre recombinase in *Syn-Cre* and *CMV-Cre* mice as well as for visualization of single Purkinje cells morphology (see description in the 3.8 section).

3.4 Genotyping

All of the mice were genotyped at weaning. Additionally, animals used for the experiments were re-genotyped before each procedure. Polymerase chain reaction (PCR) conditions and sets of primers used for genotyping are provided in the table 3 and 4 below.

3.4.1 DNA extraction

Genomic DNA was extracted from the mice tail tips or brain homogenates using Chelex 100 (Sigma-Aldrich, St. Louis, MO, USA; catalog no. C7901). Briefly, a small tissue sample was placed into 200 µl of 10 % Chelex in water. Next, the samples were incubated in 95^{o}C for 20 min, centrifuged at 12 000 x g at RT for 10 min and the supernatant was collected for further genotyping reactions.

3.4.2 Polymerase chain reaction (PCR)

The isolated DNA supernatant was used as a template for the PCR. Basic components of PCR reaction included: 12,5 µl of a 2 x PCR Master Mix (Thermo Fisher Scientific, Waltham, MA, USA; catalog no. K0171) containing Taq polymerase (0,05 U/ µl, 0.4 mM of each dNTP and reaction buffer), 2 µl of the genomic DNA, 2,5 µl of each primer and Milli-Q (MQ) ultrapure water that filled up the reaction volume to 25 µl. Specific primers and genotyping reaction conditions for each gene are listed below (see table 3 and 4 respectively).

Table 3. Primers used for genotyping

Gene	Primer forward	Primer reverse
Amot WT and FL	5'-GATGGATGCTATGAGAAGGTG-3'	5'-GTAAGGATTACAGAGTCTGGG-3'
Amot KO	5'-ATAGCTAGTGAGCAGTAGCAG-3'	5'-GTAAGGATTACAGAGTCTGGG-3'

Amotl1 WT and FL	5'-AATGCTCCAGACTAGCTGCC-3'	5'-ATGCATCTGTAATCCCAGCTC-3'
Amotl1 KO	5'-GAACAAGACTCCACTTTCAGC-3'	5'-ATGCATCTGTAATCCCAGCTC-3'
Cre	5'-GCCTGCATTACCGGTCGATGCAACGA-3'	5'-GTGGCAGATGGCGCGGCAACACCATT-3'
Tomato WT	5'-AAGGGAGCTGCAGTGGAGTA-3'	5'-CCGAAAATCTGTGGGAAGTC-3'
Tomato knock-in	5'-GGCATTAAAGCAGCGTATCC-3'	5'-CTGTTCCTGTACGGCATGG-3'
Yap1 WT and FL	5'-CCATTTGTCCTCATCTCTTACTAAC-3'	5'-GATTGGGCACTGTCAATTAATGGGCTT-3'
Yap1 KO	5'-CCATTTGTCCTCATCTCTTACTAAC-3'	5'-CAGTCTGTAACAACCAGTCAGGGATAC-3'

Table 4. PCR cycling conditions

Gene	Cycling conditions	
Amot	**Temperature**	**Time**
	Step 1: 95ºC	3 min
	Step 2: 95ºC	30 sec
	Step 3: 59ºC	1 min
	Step 4: 72ºC	1 min
	Steps 2-4 repeated 34 times	
	Step 5: 72ºC	5 min
Amotl1	**Temperature**	**Time**
	Step 1: 95ºC	3 min
	Step 2: 95ºC	30 sec
	Step 3: 59ºC	1 min
	Step 4: 72ºC	1 min
	Steps 2-4 repeated 34 times	
	Step 5: 72ºC	5 min
Cre	**Temperature**	**Time**
	Step 1: 95ºC	3 min
	Step 2: 95ºC	30 sec
	Step 3: 59ºC	1 min
	Step 4: 72ºC	1 min
	Steps 2-4 repeated 34 times	
	Step 5: 72ºC	5 min
Tomato	**Temperature**	**Time**

	Step 1: 95ºC Step 2: 95ºC Step 3: 60ºC Step 4: 72ºC Steps 2-4 repeated 35 times Step 5: 72ºC	3 min 30 sec 30 sec 1 min 5 min
Yap1	**Temperature**	**Time**
	Step 1: 95ºC Step 2: 95ºC Step 3: 60ºC Step 4: 72ºC Steps 2-4 repeated 34 times Step 5: 72ºC	3 min 30 sec 30 sec 1 min 5 min

3.4.3 DNA electrophoresis

A PCR products were separated on 1% agarose gels (Bio standard Prona, catalog no. BS500) with 0.5 µg/mL ethidium bromide added in 1x TAE buffer. GeneRuler 1kb DNA Ladder (Thermo Fisher Scientific, Waltham, MA, USA; catalog no. 11551615) was used as a DNA size marker and 20µl of a PCR reactions contained 6x Loading Dye (Thermo Fisher Scientific, Waltham, MA, USA; catalog no. R0611) were loaded onto the gel. Electrophoresis was carried out in 1xTAE buffer at 80-120 Voltage current for 40 min. A DNA fragments were visualized on the gels under UV light and recognized by predicted PCR products size.

3.5 Anesthesia and euthanasia of mice

All animals used for brain harvesting and protein extraction procedures were anesthetized and euthanized by an isoflurane inhalation (Baxter Polska, Warsaw, Poland; Aerrane 100%, ATC N01AB06). Mice were exposed to 5% or greater isoflurane concentration for 3-5 min. One minute after animals breathing has stopped the surgical plane of anesthesia was confirmed firstly by loss of toe pinch reflexes and animals were intracardially perfused for the immunohistochemistry experiments. For the brain protein extraction procedures mice were subjected to isoflurane inhalation for 7-10min, loss of pedal withdrawal reflexes was confirmed and manual cervical dislocation and decapitation was performed.

3.6 Analysis of protein localization

3.6.1 Perfusion, brain harvesting and fixation

For the immunohistochemistry experiments mice were intracardially perfused. Briefly, animals were anesthetized induced with 5% isoflurane, a 25 gauge needle attached to a peristaltic pump (BT50S, 0,00011-190 ml/min; Aqua-Trend, Lodz, Poland) was inserted into a left ventricle of the mouse heart and an incision to animal's right atrium was made. The mice were transcardially perfused with an ice-cold 1x PBS for 2min, followed by perfusion with 4% PFA in PBS for 3-4 min at a flow rate of 5ml/min. A successful perfusion was confirmed by the body stiffness, the head was removed and the brain was dissected from the scull. Brains were post-fixed in 4% PFA in PBS overnight at 4^{o}C and cryoprotected with 30% sucrose solution in PBS at 4^{o}C for about 24 hours.

3.6.2 Cryostat sectioning

Cryosectioning of mice brain was performed to prepare brain slices for immunohistochemistry and confocal microscopy. First, tissue was completely embedded in the optimal critical temperature medium (OCT) (Leica Biosystems, Wetzlar, Germany; catalog no. 14020108926) on the metal chuck and frozen at -20^{o}C for 10min inside the cryostat devise (Leica 1950 Ag Protect; Leica Biosystems, Wetzlar, Germany). After the OCT compound turned white and the tissue block was properly frozen, the chuck was positioned in a cryostat for cutting and 40 µm coronal brain slices were obtained. For *in vivo* single Purkinje cell analysis the cerebellum was sectioned at 100 µm thickness. The brain slices were collected into antifreeze solution (30% ethylene glycol, 15% sucrose and 0.05% sodium azide in PBS) and kept at 4^{o}C for storage.

3.6.3 Immunohistochemistry

Brain slices were first washed with PBS three times for 5 min at room temperature (RT). After washes, a nonspecific staining was blocked with 10% bovine serum albumin (BSA) in PBS with 0.3% Triton X-100 for 1 hour at RT. Next, a primary antibody was diluted to appropriate concentration in the blocking buffer and incubated with tissue slices overnight at 4^{o}C. Unbound antibody was washed out three times for 10 min with PBS and Alexa Fluor-conjugated secondary antibody diluted in 0.3 % Triton X-100 in PBS was applied for 1 hour at

RT. Finally, slices were washed again with PBS and were placed onto the glass slides. Coverslips were mounted to glass slides by few drops of the Fluoromount Aqueous Mounting Medium (Sigma-Aldrich, St. Louis, MO, USA; catalog no. F4685) containing DAPI (AppliChem, Darmstadt, Germany; catalog no. A4099) and applied directly onto the brain slices to stain the cells nuclei. Primary and secondary antibodies used for the immunohistochemistry experiments are listed below (see Table 5).

Table 5. Antibodies used for immunohistochemistry

Name	Dilution	Supplier and catalog number
Primary antibodies		
anti-Amot	1:200	Aviva, San Diego, CA, USA; catalog no. ARP34661_P050
anti-Amotl1	1:200	Aviva, San Diego, CA, USA; catalog no. ARP42927_P050
anti-Calbindin	1:500	Synaptic Systems, Goettingen, Germany; catalog no. 214006
anti-Map2	1:1000	Sigma, St. Louis, MO, USA; catalog no. M1406
anti-NeuN	1:1000	Abcam, Cambridge, MA, USA; catalog no. ab177487
anti-Synaptophysin1	1:250	Synaptic Systems, Goettingen, Germany; catalog no. 101004
anti-VGAT	1:500	Synaptic Systems, Goettingen, Germany; catalog no. 131002
anti-VGLUT1	1:500	Synaptic Systems, Goettingen, Germany; catalog no. 135302
anti-VGLUT2	1:500	Synaptic Systems, Goettingen, Germany; catalog no. 135402
anti-Yap1	1:250	Aviva, San Diego, CA, USA; catalog no. ARP50530_P050
Secondary antibodies		
Goat anti rabbit IgG (H+L) conjugated with Alexa-Fluor-488	1:500	Thermo Fisher Scientific, Waltham, MA, USA; catalog no. A-11034
Goat anti rabbit IgG (H+L) conjugated with Alexa-Fluor-568	1:500	Thermo Fisher Scientific, Waltham, MA, USA; catalog no. A-11011

Goat anti mouse IgG (H+L) conjugated with Alexa-Fluor-568	1:500	Thermo Fisher Scientific, Waltham, MA, USA; catalog no. A-11004
Goat anti chicken IgY (H+L) conjugated with Alexa-Fluor-488	1:500	Thermo Fisher Scientific, Waltham, MA, USA; catalog no. A-11039
Goat anti chicken IgY (H+L) conjugated with Alexa-Fluor-647	1:500	Thermo Fisher Scientific, Waltham, MA, USA; catalog no. A-21449
Goat anti guinea pig IgG (H+L) conjugated with Alexa-Fluor-568	1:500	Thermo Fisher Scientific, Waltham, MA, USA; catalog no. A-11075
Goat anti guinea pig IgG (H+L) conjugated with Alexa-Fluor-647	1:500	Thermo Fisher Scientific, Waltham, MA, USA; catalog no. A-21450

3.7 Analysis of protein expression

3.7.1 Protein extraction from the brain tissue

Whole mouse brain or separated brain compartments were cut into smaller pieces with a sterile razorblade and lysed with an ice-cold radioimmunoprecipitation assay (RIPA) buffer (50mM Tris-HCl [pH = 8.0], 150 mM NaCl, 2% Igepal CA-630 NP-40, 0,25% sodium dodecyl sulfate [SDS], 1 mM dithiothreitol [DTT], 1 mM NaF) supplemented freshly with a Mini Protease Inhibitors cocktail (Roche, Indianapolis, IN, USA; catalog no. 11873580001). The amount of 50 mg of brain tissue were lysed in 100 µl of lysis buffer. Tissues were mechanically homogenized with Bio-Gen PRO200 Homogenizer (PRO Scientific, Oxford, CT, USA; catalog no. 01-01200), incubated on ice for 15 min, transferred into 2 ml microcentrifuge tubes and centrifuged for 30 min at 20 000 g at 4^{o}C. Finally, supernatant containing protein extracts was collected and kept at -20^{o}C for further analysis.

3.7.2 Samples preparation

Protein concentration and purity was determined by the NanoDrop 2000C spectrophotometer (Thermo Fisher Scientific, Waltham, MA, USA) absorbance at 280 nm (A280), and 50 µg of the protein was loaded into one well of polyacrylamide gel (see section 3.7.3 below). Before loading to the gels well, 2x Laemmli Sample Buffer (Bio-RAD, Hercules, CA, USA; catalog no.

1610737) containing 100 µM DTT was added to protein lysates and samples were boiled at 95°C for 10 min to denature and unfold proteins.

3.7.3 Sodium Dodecyl Sulfate Polyacrylamide Gel Electrophoresis (SDS-PAGE)

Proteins were separated based on their mass by sodium dodecyl sulfate-polyacrylamide gel electrophoresis (SDS-PAGE). 1 mm thick polyacrylamide gels were prepared freshly before the electrophoresis from 8% separating gel solution and poured on top with 4% stacking gel solution (see the table 6 for the gel composition). For gels preparation and samples electrophoresis Mini-PROTEAN Tetra cell (BIO-RAD, Hercules, CA, USA) equipment was used. The Color Prestained Protein Standard Ladder (New England BioLabs, Ipswich, MA, USA; catalog no. P7712S) was used as protein size reference. Samples were loaded onto the gel wells and electrophoresis was performed in 1 x SDS-PAGE buffer at 80-120 voltage.

Table 6. Polyacrylamide gel composition

	8% separating gel (ml)	4% stacking gel (ml)
Water	3,7	3,8
30% acrylamide	2,1	0,7
1,5 M Tris-HCl buffer pH=8,8	2	-
1,5 M Tris-HCl buffer pH=6,8	-	0,4
10% SDS	0,08	0,05
10% APS	0,08	0,05
TEMED	0,008	0,005

3.7.4 Western blotting

Proteins were transferred from acrylamide gels to nitrocellulose membranes (PALL, Port Washington, NY, USA; catalog no. 66485) using a Trans-Blot Turbo device (Bio-Rad, Hercules, CA, USA; catalog no. 1704270) for 7 minutes under 1,3 A, 25 V electric current. After transfer, membranes were rinsed briefly in distilled water and were blocked to prevent non-specific binding for 1 hour at RT with 10% nonfat milk in Tris-buffered saline with Tween solution

(TBST). After blocking, an appropriate concentration of primary antibody diluted in 5% nonfat milk in TBST was added to the membrane and incubated overnight at 4°C. The next day, membranes were washed three times with TBST for 10 min followed by 1 hour incubation with the appropriate horseradish peroxidase-conjugated (HRP) secondary antibody diluted in 5% milk in TBST at RT. All washes and incubations were performed with constant rocking. Membranes were then washed again in TBST and developed in chemiluminescent reagent Immobilon Western Chemiluminescent HRP Substrate (Merk Milipore, Burlington, MA, USA; catalog no. WBKLS0500). Membranes were exposed to autoradiography films that were developed in the medical film processor Fujifilm FPM 800A located in the dark room.

3.7.5 Antibodies used for western blotting experiments

All primary and secondary antibodies used for western blotting experiments are listed below.

Table 7. Antibodies used in western blot analysis

Name	Dilution	Supplier and catalog number
Primary antibodies		
anti-Amot	1:500	Gift from Lars Holmgren (Karolinska Institutet, Stockholm, Sweden)
anti-Amotl1	1:500	Gift from Lars Holmgren (Karolinska Institutet, Stockholm, Sweden)
anti-Yap1	1:1000	Sigma-Aldrich, St. Louis, MO, USA; catalog no. WH0010413M1
anti-α-Tubulin	1:10000	Abcam, Cambridge, MA, USA; catalog no. ab18251
Secondary antibodies		
Horseradish peroxidase-conjugated anti-mouse immunoglobulin G (IgG)	1:7500	Cell Signalling Technology, Danvers, MA, USA; catalog no. 7076
Horseradish peroxidase-conjugated anti-rabbit immunoglobulin G (IgG)	1:7500	Cell Signalling Technology, Danvers, MA, USA; catalog no. 7074

Horseradish peroxidase-conjugated anti-guinea pig immunoglobulin G (IgG)	1:7500	Abcam, Cambridge, MA, USA; catalog no. ab6908

3.8 Morphological analysis of single Purkinje cells *in vivo*

To analyze the morphology of single Purkinje cells *in vivo*, three transgenic mouse strains were used: *Amot fl/fl; STOP-Tom, Yap fl/fl; STOP-Tom*, and *STOP-Tom* (control). Serotype 8 adeno-associated virus (AAV8-Syn-Cre, SignaGen Laboratories, Rockville, MD, USA; catalog no. SL100883) that expressed Cre under the neuron-specific synapsin 1 promoter was injected into mouse cerebellum at postnatal day 0 (P0). At the same time, Cre activity in infected neurons enabled Cre-mediated induction of td-Tomato expression and visualization of Purkinje cells dendritic tree morphology. Viral injections described below (see section 3.8.2) were performed blind to genotype.

3.8.1 Induction of anesthesia

New born pups (P0) were placed separately on ice for up to 4 min to induce anesthesia by hypothermia. To avoid skin damage, pups were placed on a wet paper towel and then transferred to the ice bucket. Deep anesthesia was confirmed by lack of movement upon gentle squeezing of a paw.

3.8.2 Cerebellar AAV injection

Newborn pups were intracerebrally injected with of AAV8-Syn-Cre (2 µl, 1.7×10^9 viral genomes (VGs) in sterile PBS) using 10 µl syringe with a 32 G needle. Before each injection, skin on the head was sterilized with 70% ethanol. The needle was inserted free-hand down the lambda suture through the skin and skull. After virus administration, needle was left in the tissue for about 1 min to enable complete absorption of the liquid and then slowly withdrew. After completing injection mice pups were placed back onto the warming pad until its skin color turned to pink and pups began to move, and transferred to their mothers. Three weeks after viral infection, the animals were perfused as described above (see section 3.6.1), brains

were extracted, post-fixed, cryoprotected and sectioned into 100 µm coronal slides before the confocal microscopy.

3.9 Behavioral assessments

All behavioral experiments were performed on 3 month-old male mice that were habituated before each procedure.

3.9.1 Mice habituation

The animals were habituated to handling prior to each experiment and were taken to the behavioral examination room 1 h before the tests to allow their acclimatization.

3.9.2 Test for locomotor activity and coordination

3.9.2.1 Open Field test

Amot fl/fl; Syn-Cre, Yap fl/fl;Syn-Cre and *Amotl1 KO/KO* mice activity was tested in the Open Field. Animals mobility was monitored and recorded by an overhead video tracking system that was connected to EthoVision XT (Noldus Information Technology, Wageningen, the Netherlands). Briefly, each mouse was placed separately in the middle of a round Plexiglas box (64 cm diameter) enclosed by 30 cm high walls and monitored for 10 consecutive minutes. The arena was cleaned with 70% ethanol, dried and cleaned again with water to eliminate olfactory cues between each session. The videos were collected in a digital format and analyzed with EthoVision XT video tracking system to extract all possible behavioral data (distance traveled, speed, time spend immobile, time spend in the zone center).

3.9.2.2 Rotarod experiment

Amot fl/fl; Syn-Cre, Yap fl/fl;Syn-Cre, Amotl1 KO/KO and control mice *(Amot fl/fl, Yap fl/fl, WT)* were tested on a Rotarod to evaluate their motor performance and coordination. The apparatus consists of a horizontal, 30 mm diameter rod with knurled pattern of straight ridges on its surface that allow mice to grip it effectively. A computer-interfaced apparatus with a rod turning at accelerating speed from 4 to 40 rotations per minute over 240 second per trial

was used (TSE, Bad Homburg, Germany). Briefly, mice were placed on the rod that was elevated approximately 30 cm above the base of the apparatus. Rotations started 10-20s after animals were allowed to freely follow the rotating rod and the cumulative time the mouse maintained its balance on the platform prior to falling off was measured as latency to fall. Animals were tested over 3 to 5 constitutive days in three trials per day. Subjects were pre-trained (day 0) one day before the actual experiment.

3.9.2.3 Foot-fault test

The foot-fault task was used to confirm coordination and balance deficits of *Amot fl/fl; Syn-Cre* and *Yap fl/fl;Syn-Cre* mice. Animals were placed separately at the beginning of parallel stainless steel bars (12 mm diameter, 50 cm length, 15 mm apart) and allowed to freely move toward the shelter localized at the end of the runway. The shelter contained bedding from animals home cage. A total of three consecutive runs were recorded for each mouse. The average time to complete the trial as well as the average number of paw misplacements (footslips) were calculated for each animal. *Amot fl/fl* and *Yap fl/fl* mice served as a control animals for Amot knockouts (*Amot fl/fl;Syn-Cre)* and Yap1 knockouts *(Yap fl/fl;Syn-Cre)*, respectively.

3.9.2.4 CatWalk gait analysis

The CatWalk® 7.1 automated gait analysis system (Noldus Information Technology, Wageningen, the Netherlands) was used to assess additional locomotor defects of Amot and Yap knockout mice. The apparatus consist of a 1.3 m long runway made of glass plate placed horizontaly 1.5 m above the floor. Fluorescent tube mounted alongside the runway sent the light rays internally through a glass floor causing a brief reflection when the mouse stepped on the runway, thereby producing an image of a paw prints. Two walls located perpendicular to a plate made a corridor that directed an animal over the glass plate. Mice freely traverse the corridor to the shelter located at the end of the platform. The whole run of an animal is recorded by a high-speed camera beamed under the walkway and paw prints are labeled and processed by CatWalk 7.1 acquisition software. Mice were pretrained to run over the walkway the day before recording when three uninterrupted experimental runs were collected from

each animal. A wide number of the mouse locomotor parameters were obtained during each run: spatial parameters (stride length, base of support), temporal parameters (the run duration, stand and swing phase duration, average run speed) and coordination parameters (duty cycle and regularity index). Four transgenic strains of mice were used for these analysis: *Amot fl/fl;Syn-Cre, Yap fl/fl;Syn-Cre* and *Amot fl/fl* and *Yap fl/fl* as controls. A paw print designations and data analysis were performed in a blinded manner.

3.9.2.5 Footprint assay

Amotl1 KO/KO mice and control *WT* animals were subjected to footprint analysis of gait abnormalities. In this experiment mouse paws were coated with non-toxic water-based paints (blue for forepaws and red for hind-paws) to record their walking patterns during uninterrupted locomotion. Mice were allowed to walk across a white paper runway (50 cm long) from its beginning to the darkened box localized at the end of the corridor. To encourage the animal to walk continuously across the paper, a bright light illuminated the start point of the walkway. Each mouse received four consecutive runs and their walking pattern from hind-paws and forepaws was analyzed for stride length, stride width and front/hind footprint overlay (the distance between the center of front footprint and the center of hind footprint). Strides on the first and last 4 cm of the walkway were excluded resulting in at least 3 middle steps taken for all measurements.

3.9.2.6 Abnormal locomotor behavior analysis

The analysis of *Amotl1 KO/KO* mice spontaneous rotations presented as complete circular locomotor activity was videotaped as described in section 3.9.2.1 for all mice subjected to the Open Field experiment. A single rotation was scored by the EthoVision XT video tracking system each time when mouse completed continuous and at least 360 degrees circle locomotion in either clockwise or counterclockwise direction. An average number of both directions rotations per 10 min of the Open Field experiment was counted for each animal.

Mice backward walking was analyzed in Open Field videotapes and the Three-chamber sociability test (for description see section below 3.9.3.2). The percentage of animals that performed at least one backward walking episode was scored manually from videotapes, blinded to the animals genotype and separately for the Open Field and Three-chamber

(habituation and social preference phases) tests. Backward walking episode was scored when the mouse performed at least two step backward with all paws then.

3.9.3 Social behavior tests

3.9.3.1 Nest building behavior

Mice were housed in the group of two in their home cages and with ad libitum access to food and water. All cages were cleaned few days before the study. The day prior to testing, environmental enrichment was removed from cages two hours before the dark phase of lighting cycle began. Next, one piece of paper towel (20 cm x 19 cm) was placed in the cage corner as material for nests. Paper towel was selected from other nesting materials because of its facility to tear easily by an animal. Nesting material was carefully removed from the cage two days later and mice were given a score for the material used for nesting. For quantification, the whole peace of tissue was straighten, photographed and its perforated areas were analyzed manually using arbitrary threshold with Image J software.

3.9.3.2 Three-chamber social preference test

The test apparatus consisted of rectangular Plexiglas arena (63 cm length, 44 cm width, 25 cm height) divided into three interconnected equally sized compartments that were connected with small square doorways. The tested mouse was placed into the central area and allowed to freely explore the new environment for 5 min. After the habituation time animal was gently taken back to its home-cage while the two perforated cups (8 cm diameter, 9,5 cm height) were located to each side chamber. One wire cup was empty and served as a novel object for tested animal and another contained unfamiliar conspecific of the same genotype, sex and age-matched. All mice used as a social stimuli were exposed to the sham experimental procedure and placed once daily underneath the cup for 3 days ahead of testing to allow their habituation. For the 10 min of testing session experimental mouse was introduced again to the middle chamber of the apparatus and allowed to explore all three compartments that contained either the empty cup, the cup with stranger mouse or the empty chamber between them. All experiments were performed in a darkened lighting conditions (4-5 lux) and recorded by an overhead video camera. Time spent in each chamber was analyzed with

tracking system connected to EthoVision XT (Noldus Information Technology, Wageningen, the Netherlands). Moreover, a time spent sniffing each target (empty cup vs. cup with another mouse) was registered manually by blinded experimenter and "direct interest index" (%) was counted using following formula: S*100/E (S-time spent sniffing the cup; E-whole time spent in the chamber).

3.9.3.3 Eco-HAB social approach task

The Eco-HAB automated RFID (radio-frequency identification)-based system (Puścian et al., 2016 [164]; Nencki Institute of Experimental Biology, Warsaw, Poland) was used to assess different aspects of social impairments in *Amotl1 KO/KO* mice. Animals were subcutaneously injected with glass-covered microtransponders (9.5 mm length, 2.2 mm diameter) that emitted a unique identification code for each mouse. Mice were moved to the experimental room for their habituation to inverted light-dark cycle conditions (the light phase from 23:00 to 11:00). The group of 10 subjects were housed together about 1-2 weeks prior experiments and placed to the Eco-HAB apparatus consisted of four polycarbonate housing compartments (30 cm length, 30 cm width, 18 cm height) that were connected by a tube-shaped corridors made from Plexiglas (30 cm length, 36 mm inner diameter, 40 mm outer diameter) and ended with RFID antennas on both sides (see Fig. 41A in "Results" section). The Eco-HAB experimental protocol was divided into two steps. First, mice were subjected to adaptation phase when they could freely explore the testing apparatus for 72 hr. Next, the olfactory social stimuli (bedding from the cage of an unfamiliar mouse that were strain, sex and age-matched with tested group) and non-social scent (fresh bedding) were introduced to experimental animals. For the 24 hr of social preference testing phase, beddings were placed behind the rectangular perforated partitions (11.5 cm width, 15 cm height) of two opposite apparatus compartments and mice could freely explore both olfactory stimuli. Perforations were vertical, rectangular shaped, had soft edges, and began 1 cm above the bottom of the cage. The remaining two chambers contained unrestricted food and drinking water throughout whole test and provided shelters where mice could sleep and rest. During the test each animal could freely travel and select preferred compartments within available territory. The time that each animal has spent in each compartment was measured, and the social preference was scored as the ratio of time spent in proximity to the social stimuli vs non-social scent.

3.9.4 Tests for anxiety-like behavior

3.9.4.1 Marble-burying test

The marble-burying was conducted in polypropylene box (39 cm length, 28 cm width, 28 cm height) filled with 5cm depth of fresh bedding and fifteen clear glass marbles (2 cm diameter) evenly spaced in three columns on the surface of bedding (Fig. 36A in "Results" section). Animals were placed separately onto the central area of the box and allowed to freely explore the new environment. After 30 min of testing, mice were placed back to their home-cage and number of marbles that were buried to 2/3rd of their depth were counted manually. Whole experiments were videotaped by the overhead mounted camera and analyzed with the EthoVision XT tracking system (Noldus Information Technology, Wageningen, the Netherlands) for values of total distance moved and mean velocity of each animal. Additionally a self-grooming episodes and digging duration that represents mice repetitive behavior were scored manually from the recordings. Each mouse was given fresh bedding and marbles cleaned with 70% ethanol and water to eliminate any olfactory cues. All experiments were performed in a darkened lighting conditions (4-5 lux).

3.9.5 Repetitive behavior assessment

Animals were placed individually into a standard home-cage (43cm x 27,5cm) with a thin layer of bedding (1cm) to eliminate anxiety-like responses caused by neophobia and to prevent potentially competitive behaviors like digging. Experiment was started after 10 min of habituation followed by 10 min of experiment when the mouse was allowed to freely explore the cage. Cumulative time of spontaneous grooming all body parts was scored by observer with a stopwatch.

3.9.6 Olfactory behavioral test

Buried-food assay was employed to evaluate mice olfactory function. The day prior experiments animals were given 1 gram of their regular chow covered in peanut butter to recognize its odor as palatable stimulus and increase their motivation for seeking during testing. Experimental animals were food-deprived overnight prior to testing. On the day of

experiments, individual mice were placed in the center of a clean home cage with 4 cm depth of bedding. Olfactory stimulus (1 gram of peanut butter covered chow) was buried under the bedding in one of the cage corners chosen in a random fashion (Fig. 42A in "Results" section). Latency to find food was scored for each mouse by observer and was defined as the time that subject needed to uncover the pellet and lick it or grasp in their front paw. To prevent transmission of any additional olfactory cues each mouse was given new and autoclaved cage with fresh bedding. Moreover experimenter has changed the gloves after every session. All experiments were performed in a darkened lighting conditions (4-5 lux).

3.10 Magnetic Resonance Imaging of mice brain

Magnetic Resonance Imaging (MRI) of mice brains was performed with a Bruker 7T MRI BioSpec 70/30 tomograph (Bruker, Massachusetts, USA) with Avance III console (Small Animal Magnetic Resonance Imaging Laboratory, Mossakowski Medical Research Centre, Polish Academy of Sciences, Warsaw, Poland; in collaboration with dr. Michał Fiedorowicz). The system was equipped with a transmit cylindrical radiofrequency coil (8.6 cm inner diameter) and a mouse brain dedicated receive-only surface array coil (2x2 elements). Animals were anaesthetized with isoflurane (4% for induction, 1.5-2% in oxygen for maintenance) prior the imaging procedure and placed on a dedicated bed in the prone position. Respiration rate and rectal temperature was monitored with MR-compatible sensors (SA Instruments, Stony Brook, NY, USA) throughout the MR imaging sessions. The imaging protocol included four phases. First, a positioning scan was performed to adjust and choose correct location of an animal for whole experiment. Next, a structural axial (transverse) images covering the whole brain were taken. These scans were acquired with the T2-weighted TurboRARE sequence (effective echo time, TEeff=30 ms; repetition time, TR=7000 ms; rare dactor=4; number of acquisitions, NA=4; time of acquisition, TA=223 min; field of view, FOV=22 mm x 22 mm; in-plane spatial resolution=86 µm x 86 µm; 42 slices, 0.35 mm thick, no gaps). After scanning session, a global shimming procedure was followed by linear and second order local shimming with FASTMAP protocol. Finally, a localized proton MR spectroscopy (PRESS; TE=20 ms; TR=2000 ms; NA=1024; TA=34 min) was accomplished for which a water signal was suppressed using VAPOR procedure and region of interest (ROI, voxel) was centered on both hippocampi (5 mm x 2 mm x 1.2 mm).

3.10.1 Processing of structural MR data

For automated segmentation of the brain structures the National University of Singapore mouse brain atlas (NUS) (Bai et al., 2012 [15]) was employed. It provides whole mouse brain template images and labeled images with 39 brain regions. Since the NUS atlas provide no probabilistic white matter, gray matter and cerebrospinal fluid (CSF) segmentation, a NUS template image and labelled image were transformed and labelled into tissue probability maps space provided by spmmouse toolbox (Welniak-Kaminska et al., 2019 [222]). In brief, the structural images were exported in DICOM format (.dcm), then converted to NifTI format (.nii) and intensity correction of the acquired images was performed using a 3DSlicer tool (N4ITKBiasFieldCorrection). Next step included image registration using SPM8 tool, intensity correction and correction of the origin of the coordinate system. The images were segmented into gray matter, white matter, and CSF and transformed into atlas template space. In the latter step labelled atlas image was inversely transformed into the space of each input individual image using IBASPM toolbox for SPM5 (Aleman-Gomez et al., 2006 [5]). Manual segmentation of the CSF was performed blinded to the animals genotype with 3DSlicer software (version 4.10.2; http://www.slicer.org) (Fedorov et al., 2012 [60]). Finally, the "absolute" volumes of the segmented brain structures were calculated by multiplying number of voxels per structure by voxel volume. "Scaled" (normalized to the individual brain volume) volumes of the brain structures were calculated by dividing the structure volume by whole brain volume and expressed in percent.

3.10.2 Processing of proton spectroscopy data

Proton spectra obtained from voxels cantered on the hippocampi were processed with LCModel software (Provencher, 1993 [162]). Spectra with signal power to noise power ratio (SNR) less than 15 were excluded from the analysis. Relative standard error estimates of the resonance signals (Cramer-Rao lower bounds, CRLB) were used to select the metabolites that were analyzed in next steps: metabolites with mean CRLB ≤ 15 % (excluding macromolecules) were identified and their respective concentrations were calculated from the spectra. Molar concentration of the selected metabolites were normalized to total creatine concentrations (sum of creatine and phosphocreatine concentrations, tCr) and expressed as metabolite to tCr ratios.

3.11 Confocal microscopy and image processing

Fluorescence microscopy of immunolabeled brain sections and microscopy analysis were carried out at the Confocal Microscopy Facility, Nencki Institute. Images were taken using the spinning disc confocal microscope (Zeiss, Jena, Germany) equipped with PLN APO 10x/0.45, C APO 40x/1.20 and PLN APO 63x/1.40 objectives or Zeiss LSM800 Airyscan (Zeiss, Jena, Germany) provided with a PLN APO 63x/1.40 objective and Airyscan Detector (32x GaAsP detectors). ZEN software (Zeiss, Jena, Germany) was used to collect and analyze taken images. Additional analysis were done by using ImageJ/Fiji software.

The *in vivo* Purkinje cell pictures were taken with a spinning disc confocal microscope and analysis were performed using ImageJ software. Briefly, confocal Z-stacks were collected and orthogonal projections were generated for each image. The ImageJ software was used to trace morphological features of Purkinje cells: dendritic tree area, dendritic tree height and width as well as length of primary and secondary dendrites. The dendritic protrusions were classified as primary dendrites when emerged from the Purkinje cell soma, whereas secondary dendrites were defined as processes that grew out from the primary dendrites. All of the measurements were confirmed by three independent researchers and were performed in blinded manner.

3.12 Statistical analysis

The statistical analysis were performed using GraphPad Prism 7 and Microsoft Excel Software. Quantitative data were expressed as the mean ± standard error of the mean (SEM) or standard deviation (SD). The statistical methods (two-tailed and unpaired *t* tests, one-way analysis of variance followed by Tukey's post hoc test, and two-way analysis of variance followed by Bonferroni's post hoc test), *p*-values and usage of SEM or SD are defined in the figure legends. All of the observations and analyses were performed based on at least three independent experiments. The quantitative analyses of Purkinje cell morphology, measurements of cerebellar layers thickness, behavioral tests data analysis, and brain and cerebellar measurements were performed in a blinded manner. The morphogenic Purkinje neurons and cerebellar layers analysis were performed and confirmed by at least two independent researchers. Indications of significance correspond to $P > 0.05$ (ns-not significant), $P < 0.05$ (*),

$P < 0.01$ (**), $P < 0.001$ (***), and $P < 0.0001$ (****). Values of $P < 0.05$ were considered statistically significant.

4 Results

4.1 The role of Amot and Yap1 in dendritogenesis, brain morphology and mice behavior

4.1.1 Amot and Yap1 expression and localization in the adult mouse brain

Recent studies showed that Amot is expressed in the midbrain, striatum, hippocampal, cerebellar and cortical structures of an adult rat brain and that Amot is localized to synaptic compartments in mature hippocampal neurons *in vitro* (Wigerius et al., 2018 [224]). However, the expression and localization of Amot in the mouse brain has not been investigated. To verify whether Amot is also ubiquitously expressed in different regions of the adult mouse brain (P30) I performed western blot analysis of the brain homogenates. These experiment revealed that Amot is widely distributed throughout different mouse brain structures with slightly higher expression levels of both Amot isoforms observed for the cerebellar lysate (Fig. 13A) (Rojek et al., 2019 [172]). Additionally, I performed immunohistochemical analysis of the Amot localization on the hippocampal and cerebellar mouse brain slices and showed that Amot is localized to the synapses of the pyramidal neurons in the CA1 subfield of the hippocampus (Fig. 13B) and cerebellar Purkinje cells, where it overlapped with staining for synaptic marker Synaptophysin (Fig. 13C) (Rojek et al., 2019 [172]).

Recent studies by our group reveled that Amot plays a critical role for the proper development of dendritic arbors *in vitro* and that its function in neurons depends on interaction with Yap1, the Hippo pathway transcription coactivator (Rojek et al., 2019 [172]). Although Yap1 has been previously found to be expressed exclusively in neural progenitor cells and astrocytes, but not neurons (Huang et al., 2016 [91]), there were studies showing contradictory data to the one mentioned above and providing evidence of a Yap1 presence in mature neurons. For example, Mao et al. showed Yap1 immunocytochemical positive signal in the striatal neurons of C57BL/6 wild-type mice brain. Moreover, Yap1 localization has been shown for striatal and cortical neurons of a Huntington disease and control human brain samples (Mao et al., 2016 [128]; Mueller et al., 2018 [139]). Last but not least, *in vitro* data obtained from our laboratory presented that Yap1 localize to dendrites and axons in developing cultured hippocampal neurons and changes its distribution to synaptic compartments in mature cells what clearly

confirm its neuronal expression and indicate significant function in neurons (Rojek et al., 2019 [172]).

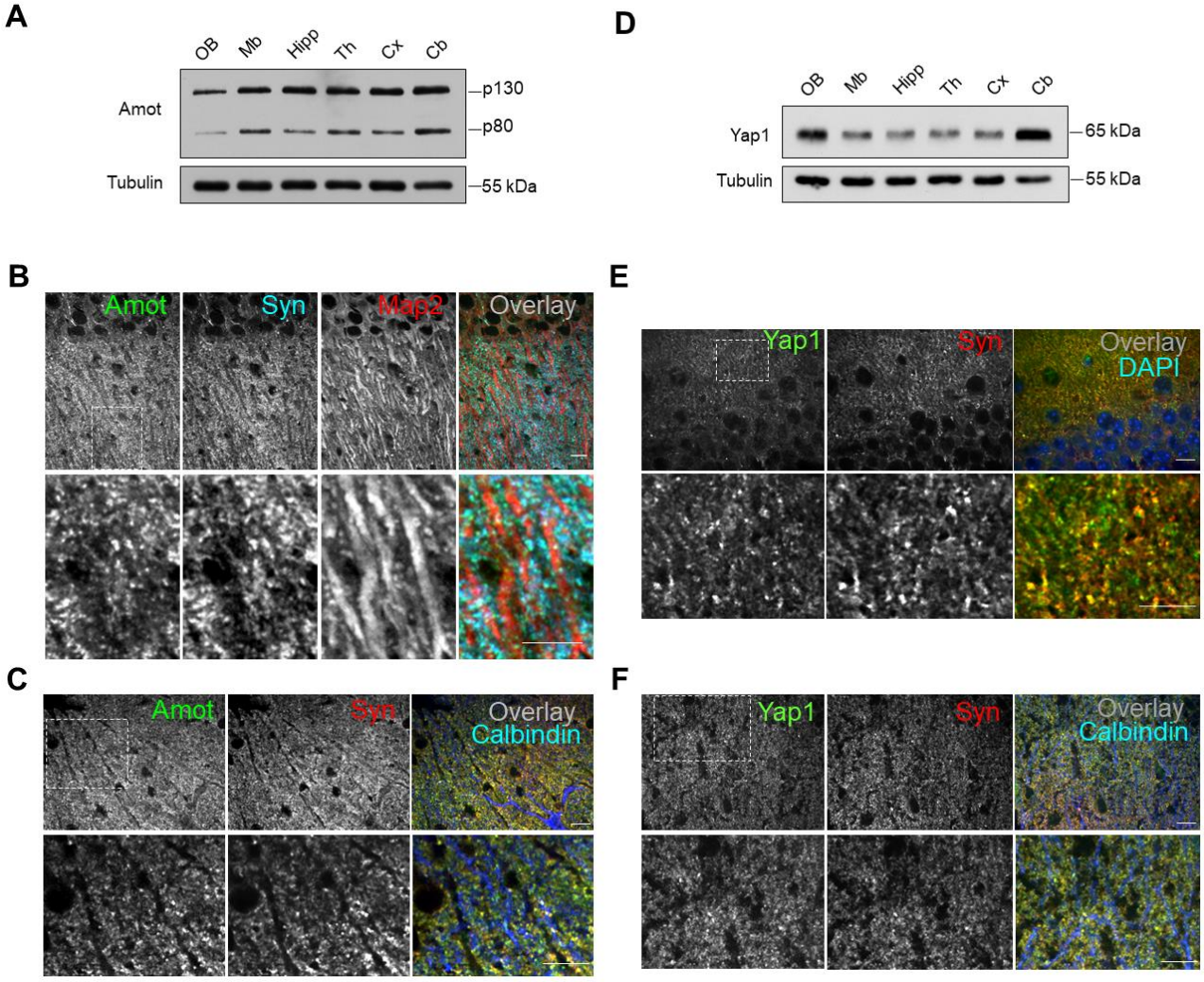

Fig. 13. Expression and localization of Amot and Yap1 proteins in the mouse brain. (A) Amot is widely expressed throughout different structures of the mouse brain. Western blot analysis of the p30 mouse brain lysates obtained from different brain regions ("OB" = olfactory bulbs; "Mb" = midbrain; "Hipp" = hippocampus; "Th" = thalamus; "Cx" = cortex; "Cb" = cerebellum). (B, C) Amot (green) localizes to synapses in pyramidal neurons of the CA1 hippocampal subfield (B) and cerebellar Purkinje cells (C) where it overlaps with Syn (red) positive puncta. The brain sections were obtained from P30 mice. Dendritic processes were stained with Map2 (red) in hippocampal slices and Calbindin (blue) in cerebellar sections. (D) Yap1 is expressed in various regions of the mouse brain. Western blot analysis of the p30 mouse brain lysates obtained from different brain structures ("OB" = olfactory bulbs; "Mb" = midbrain; "Hipp" = hippocampus; "Th" = thalamus; "Cx" = cortex; "Cb" = cerebellum). (E, F) Yap1 localization in the cryostat sections of the P30 mouse hippocampus (G) and cerebellum (H) that were stained for Yap1 (green) and Syn (red). Overlay images additionally showed nuclei, visualized with DAPI (blue in E), and Purkinje cell dendrites, visualized with anti-calbindin antibody (blue in F). The lower panels in B, C, E and

F show higher magnifications of the boxed areas in the upper panels. Scale bar = 10 µm. Amot, angiomotin; Map2, microtubule-associated protein 2; Syn, synaptophysin; Yap1, Yes-associated protein 1. Tubulin was used as a loading control in Western blot experiments (A, D).

Based on these results, I decided to analyze Yap1 expression *in vivo* throughout the mouse brain. Similarly to Amot experiment, I performed Western blot analysis and observed that Yap1 is widely expressed in various brain subregions, with the highest levels found in the cerebellum (Fig. 13D). Moreover, to verify Yap1 localization *in vivo*, I immunohistochemically analyzed cryostat sections of an adult mouse hippocampus (Fig. 13E) and cerebellum (Fig. 13F) and observed Yap1 immunoreactivity at synapses, where it colocalized with synaptophysin puncta (Rojek et al., 2019 [172]).

4.1.2 Generation of Amot or Yap1 neuron-specific knockout mice

Results obtained recently in our group showed that Amot as well as Yap1 depleted cultured hippocampal neurons have severely reduced dendritic tree complexity (Rojek et al., 2019 [172]). Collectively, these observations prompted me to investigate Amot and Yap1 functions in the brain. Therefore, I generated neuron-specific knockout mice of Amot and Yap1 using the Cre/loxP system.

In order to achieve neuron specific deletion we crossed conditional knockout mice with Syn-Cre transgenic line expressing Cre recombinase under the control of a neuronal specific Synapsin 1 promoter (*Syn-Cre*) (Zhu et al., 2001 [243]). To validate Cre activity in Syn-Cre mice we crossed these animals with a STOP-tdTomato reporter strain (*STOP-Tom*), containing STOP-of-transcription sequence flanked by LoxP sites and inserted between the constitutive CAG promoter and the tdTomato coding sequence (Fig. 14A) (Madisen et al., 2010 [125]). In *STOP-Tom;Syn-Cre* mice Cre recombinase recognizes 34 bp-long LoxP sequences, and catalyzes site-specific recombination allowing for tdTomato expression. I analyzed brain and cerebellar cross-section of the *STOP-Tom;Syn-Cre* transgenic mice and I have found heterogeneous tdTomato expression. The highest fluorescence I have observed in hippocampal CA3 and dentate gyrus area, midbrain and cerebellar Purkinje cells and low fluorescence in CA1 subfield of the hippocampus and cerebral cortex (Fig. 14B). I have concluded that despite Syn

is a pan-neuronal promoter, the chromatin position of the Syn-Cre transgene must exert certain effect on the pattern of expression.

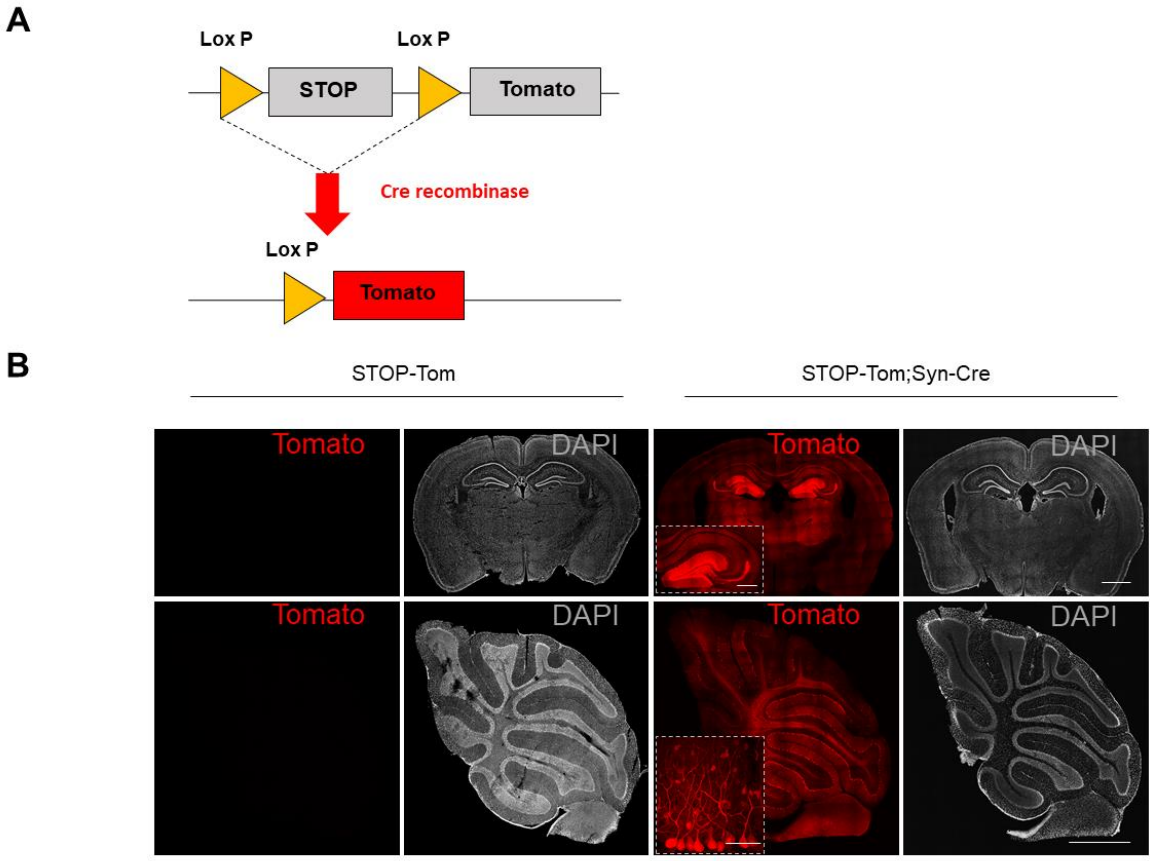

Fig. 14. Validation of the Syn-Cre activity in the STOP-Tom reporter mouse brain. (A) Schematic representation of the STOP-Tom construct. Lowers panel presents activated Tomato gene expression upon Cre mediated STOP-of-transcription cassette excision. (B) Cross-sections of the p30 mouse brains from STOP-Tom;Syn-Cre. showed high Cre activity in the hippocampus (upper panel) and the cerebellum (lower panel). TdTomato expression is shown in red. DAPI (gray) was used to visualize brain structures. Scale bars = 1 mm. The insets show higher-magnification images of the hippocampus (upper panel, scale bar = 500 µm) and Purkinje cells (lower panel, scale bar = 50 µm).

Next, to investigate the role of Amot in neuronal morphology and brain organization, I crossed *Amot* homozygous flox mice (*Amot fl/fl*), in which exon 2 of *Amot* gene was flanked by LoxP sites, to *Syn-Cre* mice (Fig. 15A). To confirm that *Amot* LoxP sites were recombined by Cre in *Amot fl/fl;Syn-Cre* mice, I performed genotyping experiments with genomic DNA isolated from the tail and brain tissue. By the electrophoresis of genotyping reaction products, I observed a 450 bp PCR fragment obtained from the brain of *Amot fl/fl; Syn-Cre* animals that corresponded

to the deleted *Amot* sequence (Rojek et al., 2019 [172]). In order to experimentally validate Amot protein downregulation in neuronal-specific knockout mice, I performed western blot analysis of hippocampal and cerebellar homogenates obtained from control *Amot fl/fl and Amot fl/fl;Syn-Cre* mice and showed significant reduction of Amot protein level in hippocampus and cerebellum of knockouts mice (Rojek et al., 2019 [172]).

To study Yap1 function in proper neuronal organization *in vivo,* I have crossed *Yap1 fl/fl mice*, that had exons 1 and 2 of a Yap1 gene surrounded by LoxP sites, with *Syn-Cre* strain (Fig. 15E). Similarly to generation of Amot conditional knockout mice, I verified the *Yap1* exons excision by genotyping experiments of a genomic DNA obtained from the mice tail and brain. The electrophoresis of a PCR reactions product revealed a 697 bp DNA fragment that represented a deleted *Yap1* gene sequence for a DNA extracted from the brain of *Yap1 fl/fl; Syn-Cre* mice (Rojek et al., 2019 [172]). To further confirm the reduction of Yap1 protein expression in the brain of Yap1 neuronal knockout mice, I prepared protein lysates from cerebellum of knockouts and *Yap1 fl/fl* control mice that were used in Western blot analysis to show lower levels of Yap1 protein in *Yap1 fl/fl; Syn-Cre* mice (Rojek et al., 2019 [172]).

Taken together, my results conducted on a DNA and protein levels confirmed that I have successfully generated neuron-specific knockout mice for Amot and Yap1 genes.

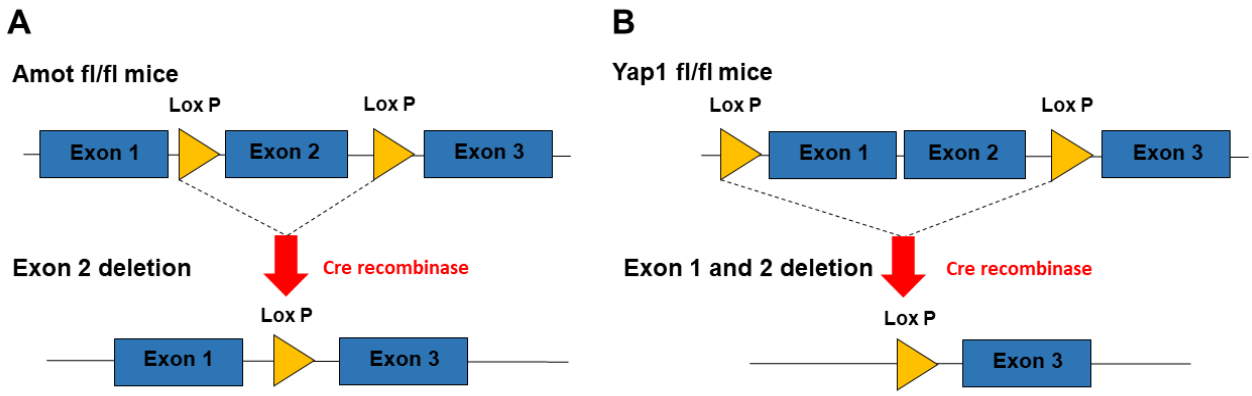

Fig. 15. Strategy for generation and validation of Amot and Yap1 conditional knockout mice. (A) The scheme of Amot flox allele (upper diagram) showing exon 2 excision after Cre-mediated recombination (lower diagram). (B) Strategy for generating Yap1 conditional knockout mice, showing the Yap1 flox allele (upper diagram) with exons 1 and 2 flanked by LoxP sites and recombined allele after Cre-mediated excision (lower diagram).

4.1.3 Analysis of body weight and gross brain anatomy of Amot or Yap1 deficient mice

Studies on the Amot function *in vivo* based on the systemic knockout mice revealed embryonic lethality soon after gastrulation that was due to defects in the cellular migration (Shimono, 2003 [183]). Nonetheless, Amot neuronal-deficient mice were born at expected Mendelian ratios and no signs of lethality could be observed. Surprisingly, mutant mice presented visible lower birth size when compared with the gender matched control littermates (Fig. 16A), that was still apparent for 30-days-old animal (p30) (Fig. 16B). Thereafter, I have measured the body weight of Amot fl/fl;Syn-Cre and control Amot fl/fl mice during their lifetime development (p0, p15, p30, p60, p70 and p110). I observed lower body weight of Amot neuronal-deficient mice than controls starting at birth, evident during adolescence and still apparent until early adulthood (p70) (Fig. 16C). Afterwards, Amot knockout mice grew to the same size and weight as their control littermates.

Yap1 fl/fl;Syn-Cre mice were born at Mendelian ratio and, likewise the Amot conditional knockouts, were significantly smaller and lighter than homozygous *Yap1 fl/fl* littermate controls of the same sex at p30 (Fig. 16D-E).

These results suggest that loss of Amot or Yap1 in neurons leads to overall developmental delay in mice, which could be a consequence of variety of pathological defects, e.g. cellular proliferation or abnormalities in the hormonal metabolism. This topic requires further investigation on developmental biology of these mice and was beyond the scope of my study.

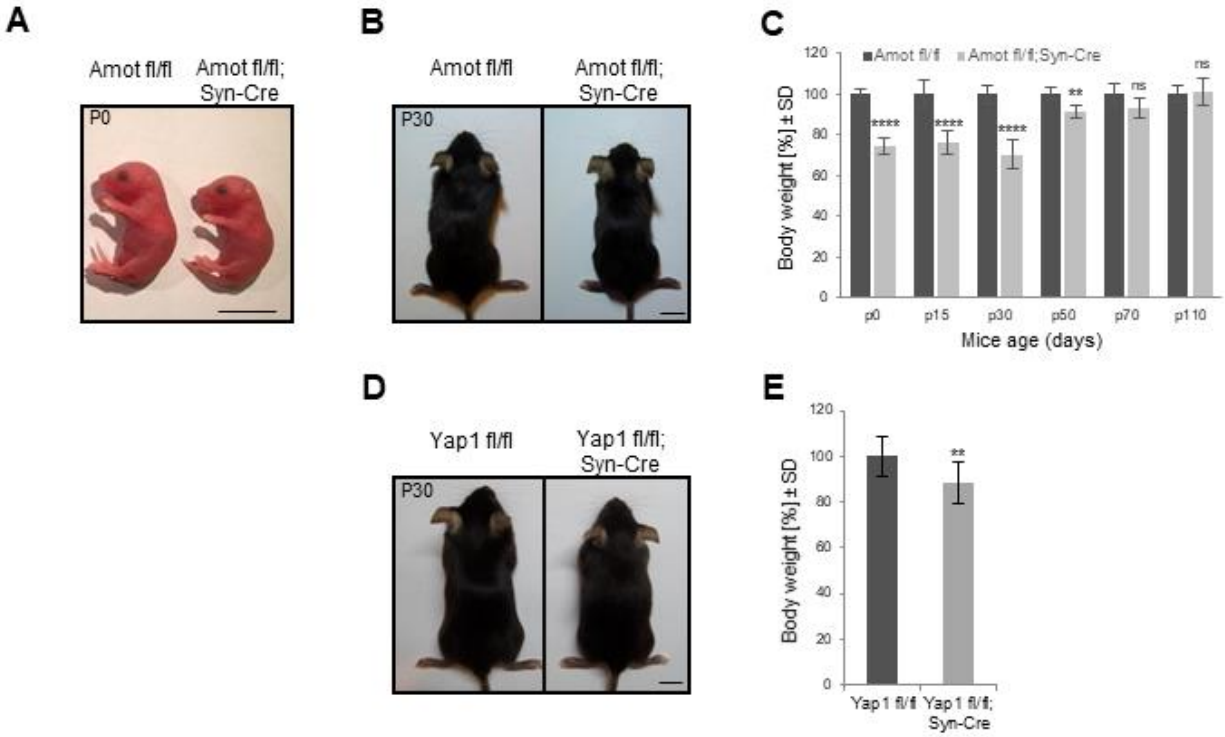

Fig. 16. Characterization of Amot and Yap1 neuronal knockout mice. (A,B) Representative images of Amot fl/fl;Syn-Cre and Amot fl/fl control littermates. Amot fl/fl;Syn-Cre mice showed reduced body size at neonatal stage (A) and on P30 (B). (C) Weight analysis of Amot fl/fl and Amot fl/fl;Syn-Cre mice (n = 8, 9, 7, 3, 4, and 4, and n = 6, 4, 9, 6, 6, and 7, respectively) on the indicated days of development. The values are shown as a percentage of control (Amot fl/fl) mouse weights at the corresponding age. (D) Images of Yap1 fl/fl;Syn-Cre and Yap1 fl/fl control littermates showing smaller body of Yap1 fl/fl; Syn-Cre mice at p30. (E) Weight analysis of Yap1 fl/fl (n = 20) and Yap1 fl/fl;Syn-Cre (n = 9) P30 mice. Values are shown as percentage of control (Yap1 fl/fl) mice weight. Scale bars = 1 cm. Statistical significance was analyzed using two-tailed unpaired t-test. **p < 0.01, ****p < 0.0001. Bars represent the mean ± SD. Ns, not significant; P, postnatal day; SD, standard deviation.

Taking into consideration that mouse brain volume is almost stable at 3 weeks of age (Hammelrath et al., 2016 [77]), I have chosen 30 days old mice for further brain analysis. Gross anatomical observation revealed that the cerebellum of Amot neuronal deficient mice appeared smaller then control animals of the same age and sex (Fig. 17A). To evaluate whether the reduction in size was specific to cerebellar area rather than the whole brain, I have quantified the cerebellar weight and normalized it to the total brain mass (Fig. 17B). These analysis confirmed significantly smaller weight of the cerebellum in *Amot fl/fl;Syn-Cre* mice then in *Amot fl/fl* controls.

Similarly to Amot mutants, Yap1 neuronal deficient mice had also smaller cerebellum comparing to control (*Yap1 fl/fl*) animals (Fig. 17C-D).

Because Syn-Cre activity was the highest in the cerebellum (Fig. 14B) and because of observed morphological defects of that brain structure upon Amot or Yap1 depletion, I have focused following experiments on the cerebellum.

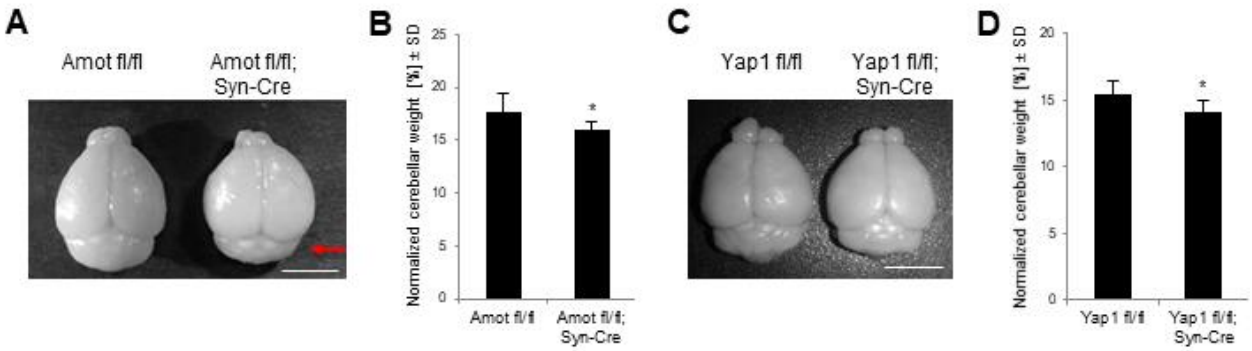

Fig. 17. Amot and Yap1 neuronal knockout mice showed reduced size and weight of the cerebellum. (A,B) Representative images of Amot fl/fl, Amot fl/fl;Syn-Cre (A) and Yap1 fl/fl, Yap1 fl/fl;Syn-Cre mice brains that show smaller cerebellum in Amot (A) and Yap1 (B) mutant mice (Amot fl/fl;Syn-Cre and Yap1 fl/fl;Syn-Cre) compared with littermate controls. Red arrow in A indicates smaller cerebellar structure in the mouse brain. (B, D) Quantitative analysis of cerebellar weight in Amot fl/fl (n = 9) and Amot fl/fl;Syn-Cre (n = 6) (B) or Yap1 fl/fl (n = 10) and Yap1 fl/fl;Syn-Cre (n = 4) mice at P30. The measurements were normalized to the whole-brain weight. Scale bars = 5 mm. Statistical significance was analyzed using two-tailed unpaired t test. *$p < 0.05$. Bars represent the mean ± SD.

4.1.4 The effects of Amot or Yap1 neuronal depletion on the cerebellar organization

The observation of reduced cerebellar weight in Amot and Yap1 mutants was made on P30 mice and for that reason all further analysis were performed on the P30 animals. To investigate in detail cerebellar structural abnormalities, I performed immunohistochemical analysis of cerebellar cross-sections from Amot and Yap1 neuronal-knockout mice.

4.1.4.1 Amot or Yap1 neuronal-deletion does not affect cerebellar foliation pattern, number of cerebellar lobes nor the number of Purkinje cells

To determine whether Amot or Yap1 depletion influenced the general organization of cerebellar cortical lobes and its foliation pattern, I immunolabeled cryosections of the cerebella with anti-calbindin and anti-NeuN antibodies. Calbindin, a member of calcium-binding protein superfamily, is a commonly used marker to visualize Purkinje cells (PC) (Bastianelli et al., 2003 [17]), whereas neuronal nuclear antigen NeuN allows for labelling posmitotic granule neurons (Weyer et al., 2003 [223]). Immunohistochemical analysis of a sagittal sections of the cerebellar vermis confirmed smaller size of cerebellum in *Amot fl/fl;Syn-Cre* and *Yap1 fl/fl;Syn-Cre* when compared to *Amot fl/fl* and *Yap1 fl/fl* controls (Fig. 18A-B). However, analysis of the stereotypical cerebellar foliation pattern, which consists of 10 lobules, revealed no general abnormalities in the cerebellar architecture in Amot nor Yap1 mutants (Fig. 18A-B).

Given that several studies have shown rodent cerebellar shrinkage associated with a clear loss of the Purkinje cells (Wang et al., 2015 [215]; Sakai et al., 2019 [176]; Long et al., 2014 [119]) due to abnormalities in the development, maturation or survival of these cells, I aimed to quantify the number of Purkinje neurons in cerebella obtained from Amot and Yap1 knockout mice. Nonetheless, detailed quantification of PCs for each cerebellar lobe showed that their number was unaffected in the absence of Amot or Yap1 (Fig. 18C-D).

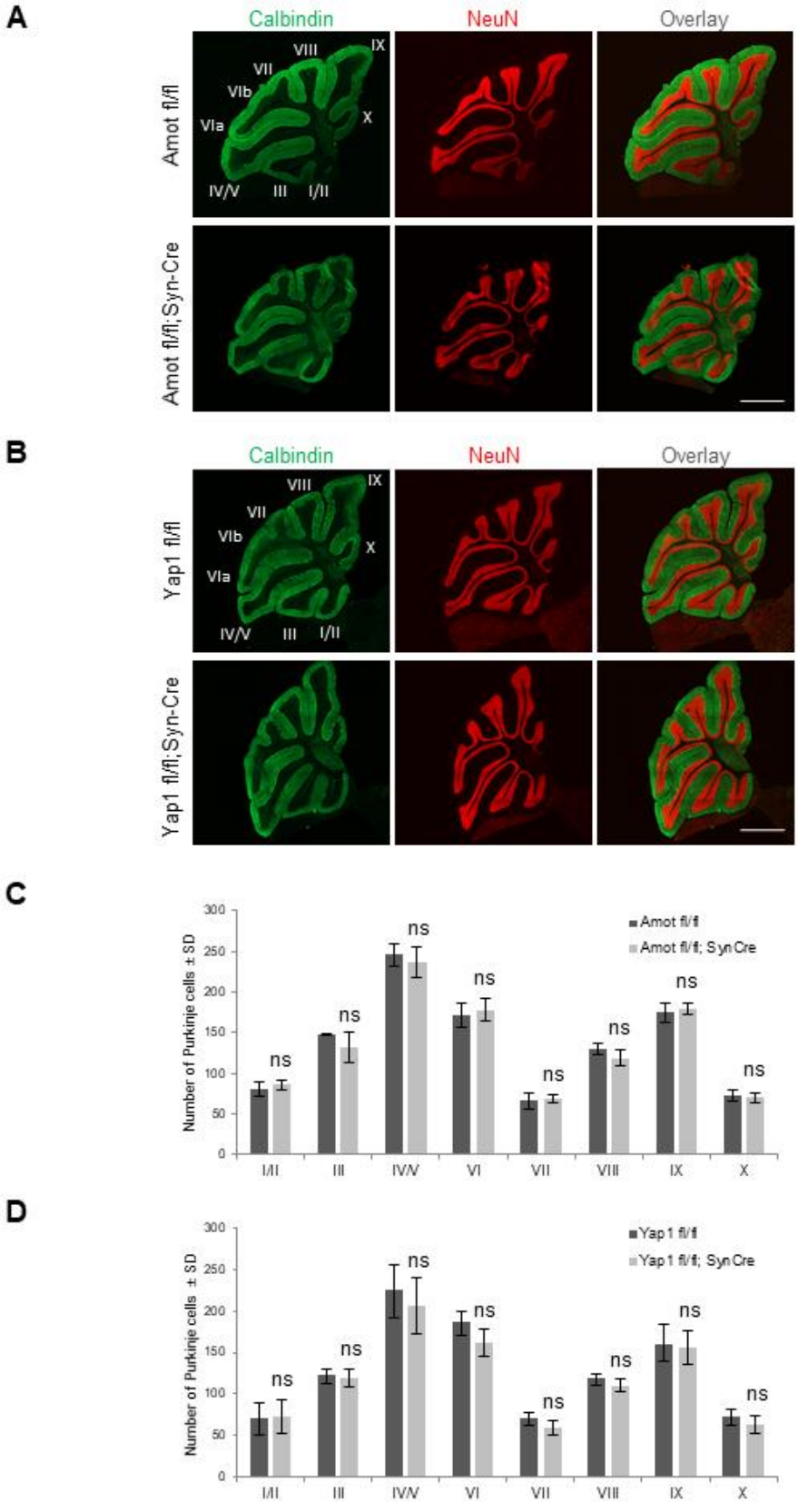

Fig. 18. The neuronal deletion of Amot or Yap1 protein does not affect the number of cortical lobules, nor the Purkinje cells number. (A, B) Sagittal cerebellar cross-sections of Amot fl/fl and Amot fl/fl;Syn-Cre (A), Yap1 fl/fl and Yap1 fl/fl;Syn-Cre mice (B) at P30. Cerebellar sections were stained with antibodies against calbindin (green)

to visualize Purkinje cells and the molecular layer and NeuN (red) to visualize the granule cell layer. Numbers indicate individual lobes. (C, D) Quantification of Purkinje cell number in sagittal sections of Amot fl/fl mice (n = 3 mice) Amot fl/fl;Syn-Cre mice (n = 4 mice) shown in C, and Yap1 fl/fl mice (n = 4 animals) and Yap1 fl/fl;Syn-Cre mice (n = 4 animals) shown in D. The analysis of Purkinje cells numbers were performed from at least three sections per mouse. Values from I/II to X indicate the concrete cerebellar lobe. Scale bars = 1000 μm. Statistical significance was analyzed using two-tailed unpaired t test. Bars represent the mean ± SD.

Collectively, my results from the general cerebellar architecture studies showed no difference between Amot or Yap1 neuronal-deficient mice and their controls, and therefore, prompted me to further analyze the structure of individual cerebellar cortex layers.

4.1.4.2 Amot or Yap1 neuronal-deficient mice show impaired structure of the molecular layer of cerebellar cortex

The cerebellar cortex is divided into three distinct layers: the innermost densely packed with granule neurons granule cell layer, a middle Purkinje cell layer made up of PCs bodies, and outer molecular layer where axons of granule cells and dendrites of PCs are located. To investigate the possibility that a particular layer of cerebellar cortex may be affected by loss of Amot or Yap1 protein, I performed measurements of individual layer thickness. In order to search for potential impairments that could be located at different cerebellar subregions, I aimed to take measurements from cerebellar sections at the sites of three different cerebellar fissures, located along the external molecular layer that separates individual cerebellar lobes: preculminate, primary and secondary fissures (Fig. 19A). Detailed analyzes of cerebellar layers showed that thickness of the molecular layer down the preculminate fissure is significantly decreased in Amot mutant mice compared with control animals (Fig. 19B), however there were no significant differences along the primary and secondary fissures (Fig. 19C). Additionally, I observed that thickness of the granular and Purkinje cell layers, along three different cerebellar subregions, was not affected by Amot depletion (Fig. 19D-E).

To reveal whether Yap1 has similar to Amot role in the cerebellar organization I performed analogous analysis of cerebellar cortical layers thickness of Yap1 depleted brains. Interestingly, I observed reduced molecular layer specifically in the site of lobe III down the preculminate fissure, whereas in other cerebellar subregions the molecular layer was not

impaired (Fig. 19F-G). Lastly, the granular and Purkinje cell layers were unaffected in the absence of a neuronal Yap1 expression (Fig. 19H-I).

Based on the above results, I concluded that both proteins, Amot and Yap1, have their roles in the organization of the cerebellar molecular layer down the preculminate fissure. Hence, I have focused further studies on the analysis of a cellular components of the molecular layer in both knockouts.

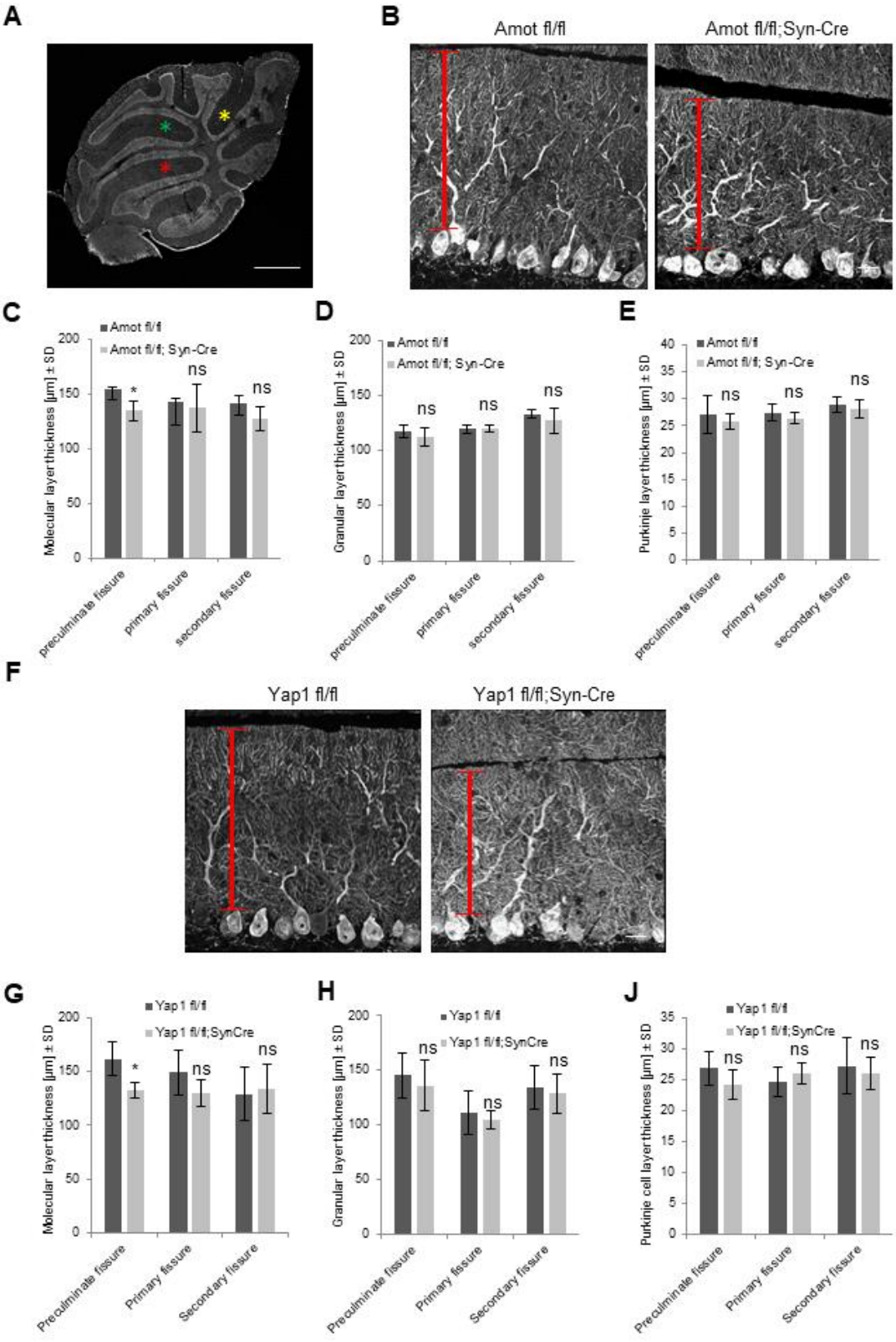

Fig. 19. Amot or Yap1 neuronal protein depletion affects the thickness of cerebellar molecular layer. (A) Representative image of a sagittal cross-section of the brain from Amot wild-type mice. Asterisks indicate localization of particular cerebellar fissures: red = preculminate, green = primary, yellow = secondary. (B, F) Images of the cerebellar molecular layer, lobe III down the preculminate fissure, in Amot fl/fl, Amot fl/fl;Syn-Cre

mice (B), and Yap1 fl/fl, Yap1 fl/fl;Syn-Cre mice at P30 (F). Red lines indicate a decreased thickness of the molecular layer in Amot and Yap1 depleted mice (Amot fl/fl;Syn-Cre, Yap1 fl/fl;Syn-Cre) when compared to control mice (Amot fl/fl and Yap1 fl/fl). Cross-sections were stained with anti-calbindin antibody. (C-E, G-J) Measurements of the molecular (C, G), granular (D, H) and Purkinje cell (E, J) layers thickness analyzed down the preculminate, primary and secondary fissures in the cerebella of Amot fl/fl, Amot fl/fl;Syn-Cre mice (C-E) and Yap1 fl/fl, Yap1 fl/fl;Syn-Cre mice (G-J) at P30 showed decreased thickness of molecular layer in Amot and Yap1 mutant mice. Quantifications were performed on at least three sections per mouse and the following numbers of animals: Amot fl/fl = 4; Amot fl/fl;Syn-Cre = 3; Yap1 fl/fl = 4; Yap1 fl/fl;Syn-Cre = 4. Scale bars: A = 50 µm; B, F = 20 µm. Statistical significance was analyzed using two-tailed unpaired t test. *$p < 0.05$. Bars represent the mean ± SD.

4.1.4.3 Analysis of the distribution of granular cells in the cerebellar molecular layer of Amot or Yap1 knockout mice

Since one the neuronal components within the cerebellar cortical molecular layer are migrating granule cells, I aimed to study numbers of granule cells for Amot or Yap1 depleted cerebella.

Cerebellar granule cells migrate radially from a thin external granular layer across the molecular layer to rich their final destination of internal granular layer. It has been reported that impairments of their migration or proliferation and thus abnormal distribution within the molecular layer can result in changes of layer thickness and therefore influence the cerebellar size (Yang et al., 2018 [228]; Men et al., 2015 [132]; Jaarsma et al., 2014 [106]).

To visualize the granular cells in molecular layer of cerebellum obtained from *Amot fl/fl;Syn-Cre*, *Yap1 fl/fl;Syn-Cre*, *Amot fl/fl* and *Yap fl/fl mice*, I performed immunohistochemical analysis of the cerebellar cross-sections stained with anti-NeuN antibody. As mentioned previously, NeuN in the cerebellum is expressed exclusively by postmitotic granule cells. My immunohistochemical experiments showed that the number of NeuN positive cells within the molecular layer over total number of nuclei (stained with DAPI), was similar in Amot knockout and control mice (Fig. 20A-B). However, in contrast to Amot, Yap1 depletion increased the number of a granule cells in the cerebellar molecular layer (Fig. 20C-D).

Together, these results indicate specific function of Yap1 in cerebellar granule cells proliferation/migration. Importantly, previous reports have shown that an increased accumulation of cells in molecular layer can contribute to either enlarged or decreased

cerebellar volume (Men et al., 2015 [132]; Jaarsma et al., 2014 [106]). These could be the secondary effect coming from another cells impairments. Lastly, smaller size of the cerebellum could indicate more possibly a decrease in granule cells proliferation then their pro-proliferative activity (Hou et al., 2014 [88]).

Based on the above mentioned observations, and the fact that Amot mutant mice have smaller cerebella but no apparent defects in granule cells distribution, I decided to study structure of PCs dendritic trees, which are another main component of the cerebellar molecular layer.

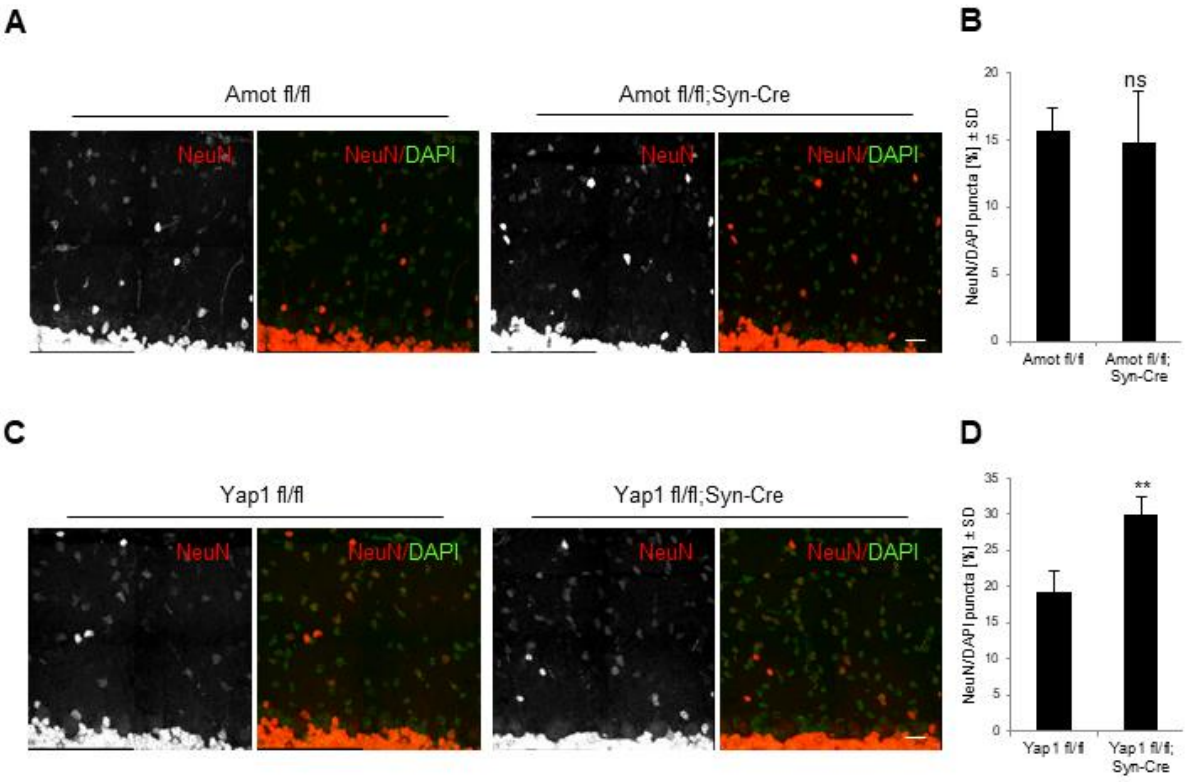

Fig. 20. The granule cell distribution in the molecular layer in Amot and Yap1 mutant and control mice. (A, B) Cross-sections of the cerebella showing the molecular layer in Amot fl, Amotl fl/fl;Syn-Cre mice (A) and Yap1 fl/fl, Yap1 fl/fl;Syn-Cre animals at P30 stained with anti-NeuN antibody (red) that visualize granule cells, and DAPI (green). (B, D) Quantification of the NeuN-positive cells over all DAPI stained nuclei per 20,000 µm2 of the cerebellar molecular layer in Amot fl/fl, Amotl fl/fl;Syn-Cre mice (B) and Yap1 fl/fl, Yap1 fl/fl;Syn-Cre animals (D) showed impaired granule cell distribution in Yap1 mutant mice (D) and no significance difference was observed in Amot depleted animals (B). Scale bar = 20 µm. Statistical significance was analyzed using two-tailed unpaired t test. **p < 0.01. Bars represent the mean ± SD. NeuN, Neuronal nuclear protein.

4.1.4.4 Amot or Yap1 depleted cerebellar Purkinje cells exhibit abnormal dendritic tree organization

Our previous *in vitro* studies identified Amot and Yap1 as a critical regulator of dendritic tree morphogenesis in cultured hippocampal neurons (Rojek et al., 2019 [172]). My results showed that Amot and Yap1 neuronal-knockout cerebella have decreased thickness of a molecular layer, where dendrites are located, I decided to focus my further study on morphological analysis of Purkinje cells that project their dendrites into the molecular layer.

In order to achieve Amot or Yap1 depletion in single Purkinje cell and to simultaneously visualize their structure, I intracerebrally injected newborn double transgenic *Amot fl/fl;STOP-Tom* and *Yap fl/fl;STOP-Tom* pups with low titter adeno-associated virus (AAV), that express recombinase Cre under the Synapsin-1 neuronal specific promoter. The *STOP-Tom* transgene allowed for Cre-mediated expression of the red fluoresce tdTomato reporter protein in all cells infected with virus (Fig. 21A). When TdTomato is expressed it nicely fills entire neuronal cells including dendritic processes what allows to study their structure. To achieve Purkinje cell specific Cre expression through the viral infection, I have used AAV serotype 8 (AAV8), that have been previously shown to have high tropism to Purkinje neurons (Gibson et al., 2011 [68]). The development of Purkinje cells dendritic trees occurs during the first three postnatal weeks in mice (Sotelo et al., 2009 [192]). Therefore, I harvested the injected animals brains at P21 and performed confocal microscopy analysis of 100-µm thick cerebellar cross-sections. I visualized the morphology of dendritic trees in Amot depleted Purkinje cells and in control cells from *STOP-Tom* mice infected with the same virus (Fig. 21B). In order to characterize Amot depleted Purkinje cells dendritic tree structure I performed the quantitative analysis of dendritic tree area, its height and width, length of primary and secondary dendrites and the number of dendritic branching points (Fig. 21C-G). I found that all of these parameters were reduced in Amot knockout Purkinje cells compared with control neurons.

To verify whether Yap1 also plays a role in the organization of Purkinje cells dendritic trees *in vivo* I have knocked out Yap1 in individual PCs in *Yap fl/fl;STOP-Tom* or *STOP-Tom* using AAV8, and analyzed their structure in the same manner as for Amot depleted Purkinje cells. As expected, Yap1 deficient cells showed significant reduction of dendritic field area, dendritic tree width, the length of primary and secondary branches, and the number of dendrite branching points compared with control cells (Fig. 21I, 21K, 21M 21N). At the same time, I

could not detect significant differences in dendritic tree height (Fig. 21J) between Yap1 knockout and control cells.

Summing up, I concluded that both proteins, Amot and Yap1, play an important role in the regulation of dendritic tree architecture in mouse Purkinje cells *in vivo*.

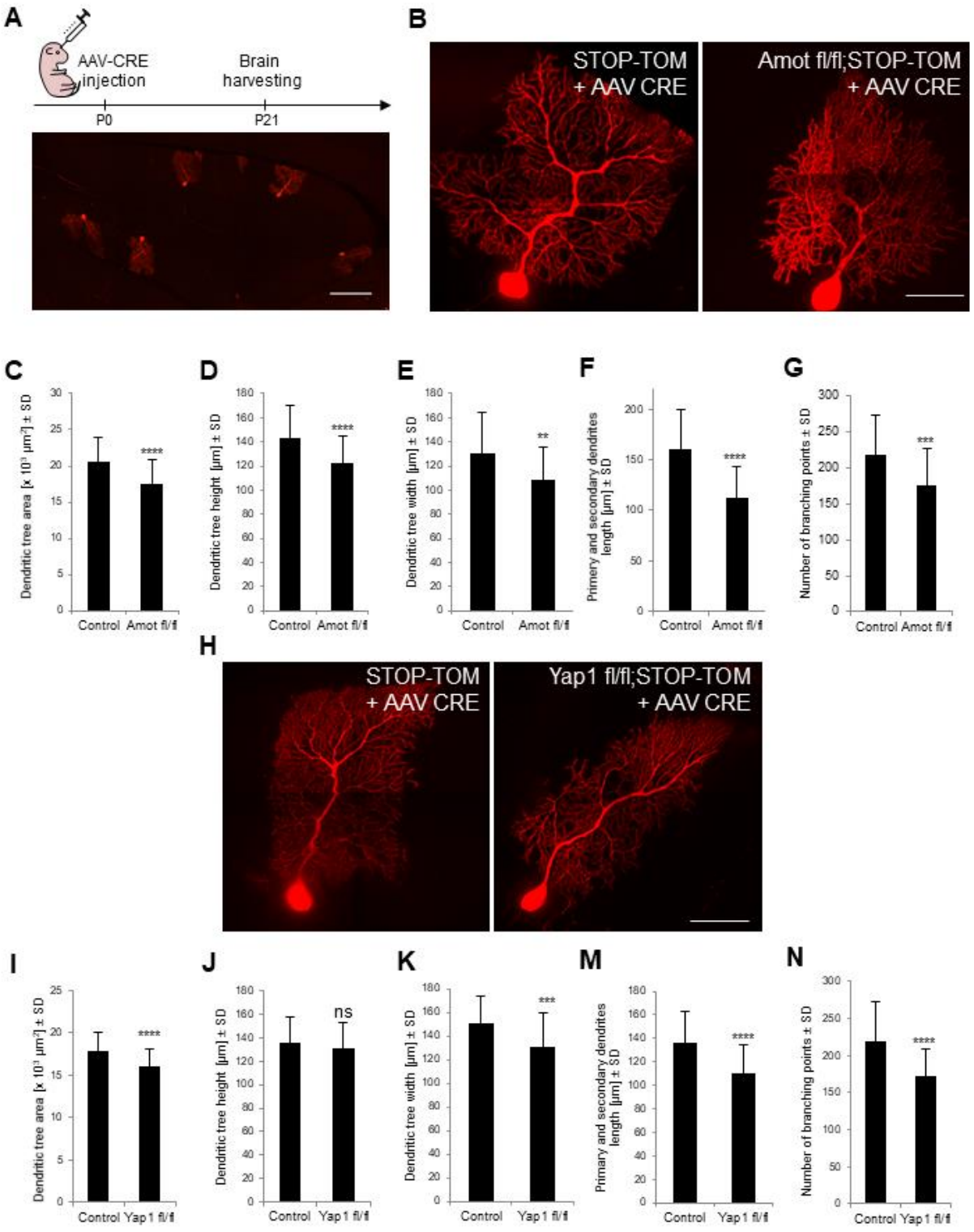

Fig. 21. Amot or Yap1 depleted Purkinje cells exhibit impaired structure of the dendritic tree. (A) TdTomato expression (red) in single Purkinje cells in STOP-Tom reporter mice indicates Cre activity in virus infected cells. The schematic illustration of the experimental procedure is shown in the upper panel shows. P0 STOP-Tom pups were injected with 1.7×10^9 AAV8-Syn-Cre viral genomes and euthanized on P21. (B, H) Purkinje cells morphology images from the cerebellar cross-sections of Amot fl/fl;STOP-Tom and control STOP-Tom mice (B) as well as Yap1 fl/fl;STOP-Tom and STOP-Tom animals (H) that were infected with AAV8-Syn-Cre. Tomato expression is shown in

red. (C-G, I-N) Quantitative analysis of the dendritic tree area (C, I), height (D, J), width (E, K), primary and secondary dendrite length (F, M) and the number of dendrite branching points (G, N) of Purkinje cells from Amot fl/fl;STOP-Tom, control STOP-Tom (C-G) and Yap1 fl/fl;STOP-Tom, STOP-Tom (I-N) brains injected with AAV8-Syn-Cre. Measurements were performed on the following number of cells and mice: (C-F) STOP-Tom (control), n ≥ 45 cells and 4 mice; Amot fl/fl;STOP-Tom (Amot fl/fl), n ≥ 43 cells and 4 mice; (G) STOP-Tom (control), n = 35 cells and 4 mice; Amot fl/fl;STOP-Tom (Amot fl/fl) n = 39 cells and 4 mice; (J-M) STOP-Tom (control), n ≥ 28 cells and 5 mice; Yap1 fl/fl;STOP-Tom (Yap fl/fl), n ≥ 68 cells and 8 mice, (N) STOP-Tom (control), n = 33 cells and 5 mice; Yap1 fl/fl;STOP-Tom (Yap fl/fl), n = 48 cells and 6 mice. Scale bars: A = 200 µm, B, H = 50 µm. Statistical significance was analyzed using two-tailed unpaired t tests. **p < 0.01, ***p < 0.001, ****p < 0.0001. Bars represent the mean ± SD.

4.1.4.5 Amot or Yap1 knockout mice show normal distribution of synaptic markers in the molecular layer of cerebellar cortex

Knowing that Amot and Yap1 localize to Purkinje cell synaptic compartments *in vivo* (Fig. 13C, 13F) and that they regulate arborization of Purkinje neuron dendrites (Fig. 21B-L), it was intuitive to investigate possible impact of Amot and Yap1 depletion on synaptic deficiency. To address this subject, I used immunohistochemistry and confocal microscopy to analyze the distribution of synaptic markers, within the molecular layer in cerebella obtained from *Amot fl/fl;Syn-Cre* and *Yap1 fl/fl;Syn-Cre* knockout mice, as well as *Amot fl/fl* and *Yap fl/fl* control animals. I used the antibody against the vesicular γ-aminobutyric acid transporter (VGAT) antibody to label inhibitory synaptic puncta, and vesicular glutamate transporter 1 (VGLUT1) and VGLUT2 for efficient visualization of excitatory synapses. These experiments revealed that Amot depletion has no effect on number of VGAT (Fig. 22A, 22D), VGLUT1 (Fig. 22B, 22E), nor VGLUT2 (Fig. 22C, 22F) positive synapses along the cerebellar molecular layer. My results are consistent with the previously published report showing that number of synapses in hippocampal neurons *in vitro* was unaffected upon knockdown of Amot p130 isoform (Wigerius et al., 2018 [224]). Moreover, I could not detect any defects in inhibitory (VGAT) or excitatory (VGLUT1, VGLUT2) synapses number within the cerebellar molecular layer in Yap1 neuronal-knockout mice (Fig. 22G-M).

Collectively, my results showed that Amot and Yap1 play important roles in the regulation of Purkinje cells dendritic tree morphology, the structure of cerebellar molecular layer and in the organization of the mouse cerebellum.

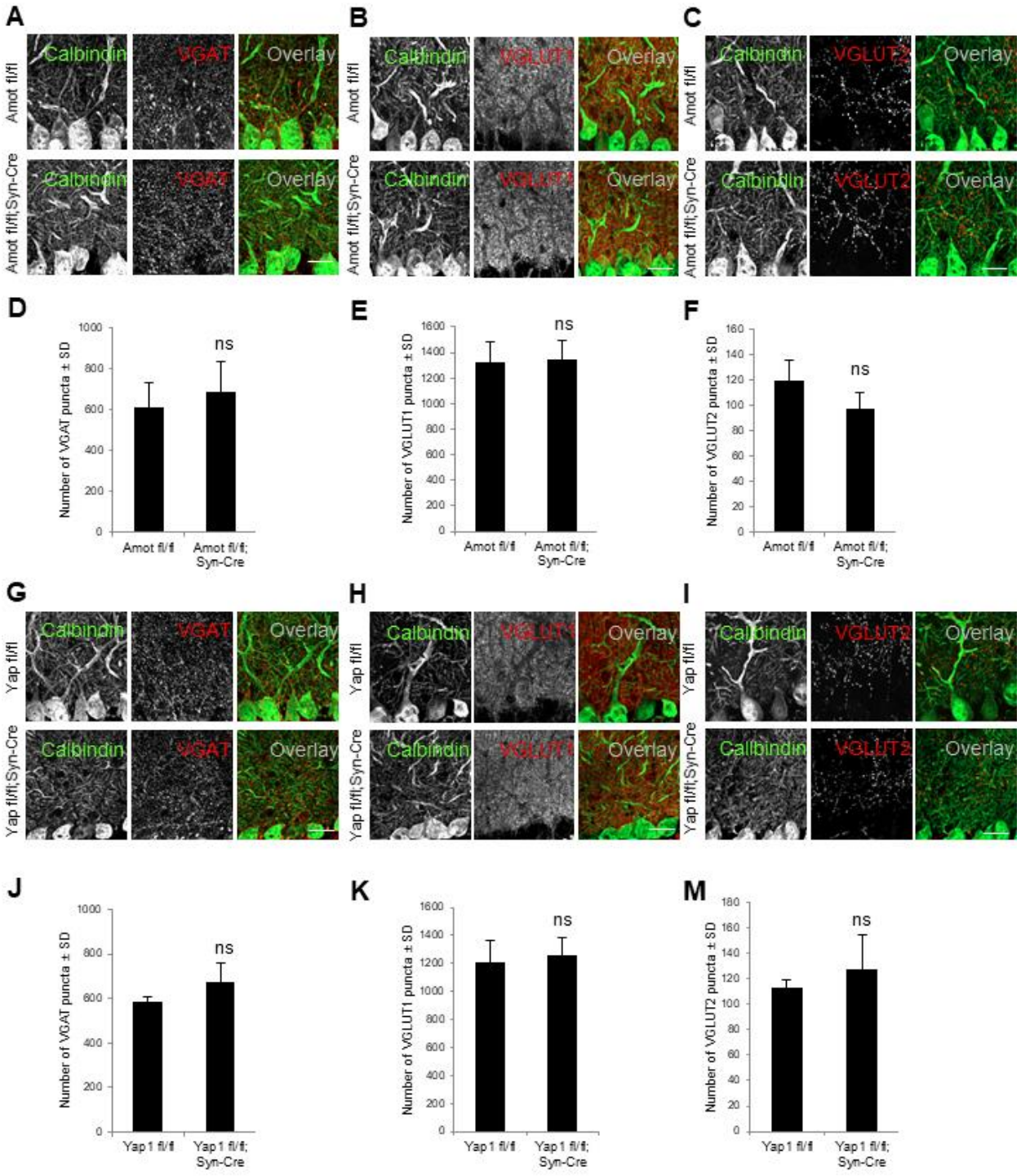

Fig. 22. Amot or Yap1 depletion did not affect the distribution of inhibitory and excitatory synapses in the cerebellum. (A-C, G-I) Cerebellar sagittal sections obtained from Amot fl/fl, Amot fl/fl;Syn-Cre mice (A-C), and Yap1 fl/fl, Yap1 fl/fl;Syn-Cre animals (G-I) were immunostained for VGAT (A, G), VGLUT1 (B, H), and VGLUT2 (C, I). Anti-calbindin antibody was used to visualize Purkinje cells. (D-F, J-M) Quantification of VGAT (D,J), VGLUT1 (E, K), and VGLUT2 (F, M) puncta per 1,000 µm2 in Amot mutant and control brains (D-F) as well as Yap1 mutant and control brains (J-M). At least four mice and three sections per mouse were analyzed. Scale bar = 50 µm.

Statistical significance was analyzed using two-tailed unpaired t tests. Bars represent the mean ± SD. VGAT, vesicular γ-aminobutyric acid transporter; VGLUT, vesicular glutamate transporter.

4.1.5 The role of Amot and Yap1 in general locomotion and locomotor coordination in mice

The cerebellum is a motor coordination center and variety of previous studies have shown association between reduced complexity of the cerebellar Purkinje cells dendritic trees and impaired locomotor coordination in mice (Wischhof et al., 2017 [225]; Quevedo et al., 2010 [165]; Donald et al., 2008 [51]). My results showed important role of Amot and Yap1 in organizing dendritic trees of Purkinje cells *in vivo*, hence I hypothesized that these proteins may also have function in maintaining proper locomotor coordination in mice. To test this hypothesis I performed a battery of behavioral experiments to evaluate mice locomotor coordination and balance for Amot and Yap1 knockouts. My previous experiments showed that Amot and Yap1 knockout mice have lighter body weight then control animals that was visible until approximately P70 (Fig. 16C, 16E). In order to eliminate possible impact of knockout and control animals weight differences on their locomotor ability I conducted all behavioral test on P150 mice, knowing that Amot deficient mice reached the stable weight of their control littermates at that age (Fig. 16C). Additionally, I aimed to analyze the cerebellar weight of these knockouts at the age of behavioral testing. Importantly, the cerebella of both *Amot fl/fl;Syn-Cre* and *Yap1 fl/fl;Syn-Cre* had continually lower weight when compared with the littermate controls (*Amot fl/fl* and *Yap fl/fl*) (Fig. 23A-B), even though their body weight got already normalized.

These results suggest that the phenotype of a smaller cerebellar size in Amot or Yap1 deficient mice develop independently on their lower body weight. However, a conclusion on that subject would require more data and analysis on the developing young animals.

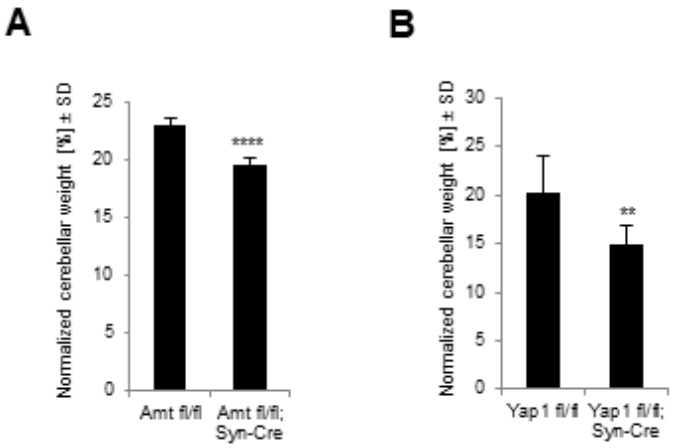

Fig. 23. Amot and Yap1 neuronal knockout mice showed decreased cerebellar weight at P150. Quantitative analysis of the cerebellar weight in Amot fl/fl and Amot fl/fl;Syn-Cre mice (A) and similarly in Yap1 fl/fl and Yap1 fl/fl;Syn-Cre animals (B). Values are shown as a percentage of cerebellar weight to the whole-brain weight. The following number of animals were analyzed: Amot fl/fl = 7; Amot fl/fl;Syn-Cre = 3; Yap1 fl/fl = 7; Yap1 fl/fl;Syn-Cre = 9. Statistical significance was analyzed using two-tailed unpaired t test. **p < 0.01, ****p < 0.0001. Bars represent the mean ± SD.

4.1.5.1 Amot or Yap1 neuronal depletion do not affect animal mobility during Open Field experiment

To evaluate whether the defects in cerebellar structure affects an animal general mobility, I performed an Open Field experiments. Open Field test is widely used to assess rodents basic behaviors, such as general locomotor ability or anxiety-related behaviors (Seibenhener et al., 2015 [181]). Each animal was placed on the center of round Open Field plexiglas arena (Fig. 24A) and allowed to freely explore the apparatus. General locomotion of Amot or Yap1 knockout mice was similar to control animals. The quantified amount of time spend immobile or distance traveled during the test did not reveal any abnormalities for Amot or Yap1 knockouts (Fig. 24B-E). This indicates that Syn-Cre mediated deletion of Amot or Yap1 does not affect the animal general locomotor activity.

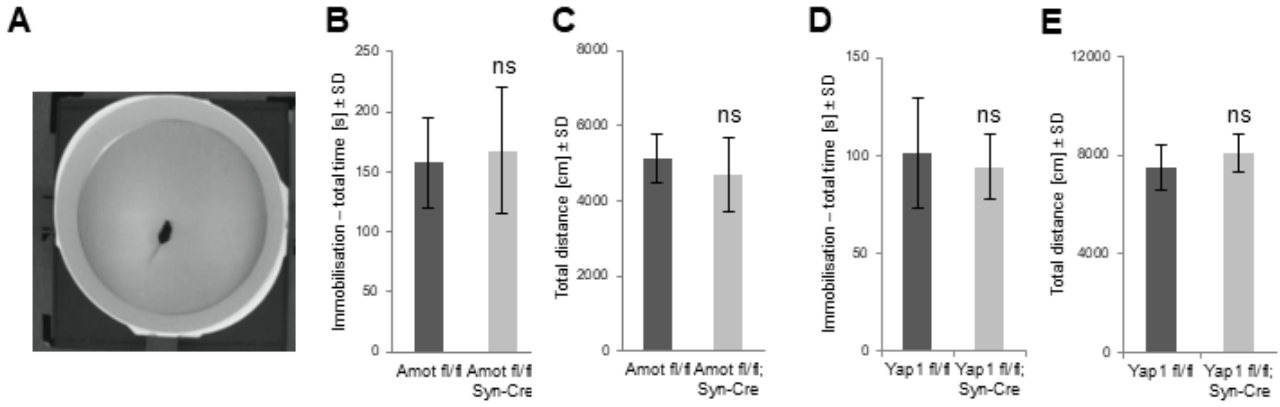

Fig. 24. The Open Field analysis of a locomotor activity in Amot and Yap1 mutant mice. (A) Image of Open Field arena. (B, D) Quantification of total time spend immobile for Amot (B) and Yap1 (D) mutants and control animals. (C, E) Total distance traveled by Amot (C) and Yap1 (E) mutant and control mice. The experiments were performed on P150 mice. Following number of animals were subjected to test: Amot fl/fl;Syn-Cre n = 9; Amot fl/fl n= 9; Yap1 fl/fl;Syn-Cre n = 6; Yap1 fl/fl n = 8. Statistical significance was analyzed using two-tailed upaired t test. Bars represents the mean ± SD.

4.1.5.2 Deficits in locomotor coordination of Amot or Yap1 knockout mice observed in RotaRod test, CatWalk experiment, and Foot-Fault analysis

Knowing that Amot and Yap1 neuronal-knockout mice present normal locomotor activity, I performed studies of motor coordination and balance that depends on the proper function of the cerebellum. For that, I performed a set of behavioral experiments that consisted of RotaRod test, CatWalk gait analysis and the foot-fault assay.

Firstly, I placed animals on an horizontally oriented rod that was suspended above the floor of the RotaRod apparatus (Fig. 25A). Naturally, animals would avoid falling, and would try to remain on the rotating rod as long as they are able to keep the balance and effectively coordinate their movements. In the experiment the rod has started to rotate 20-30sec after the animal was placed into the apparatus and increased the speed of rotation from 4 to 40 per minute over 240 seconds. I have measured the latency to fall from the platform in *Amot fl/fl;Syn-Cre* and *Yap1 fl/fl;Syn-Cre* and control mice. Over 4 constitutive days of the experiment Amot and Yap1 mutants fell down from the platform earlier then littermate controls indicating their coordination and balance impairments (Fig. 25B-C).

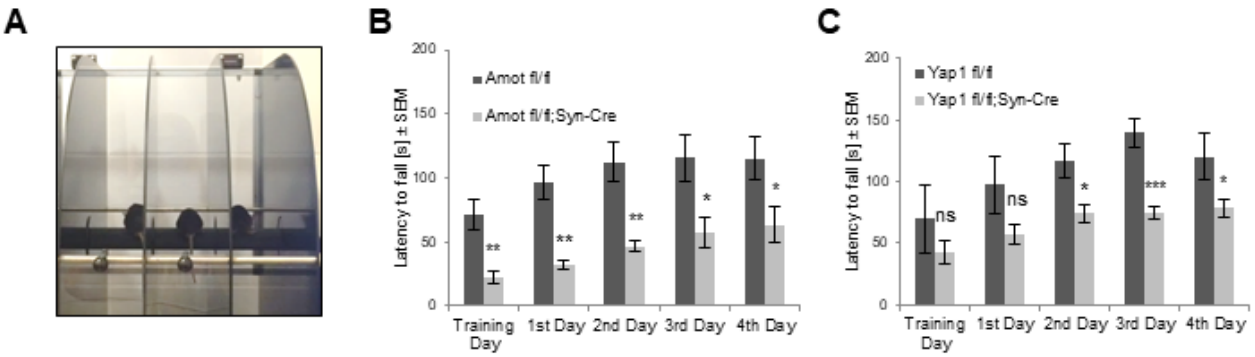

Fig. 25. Amot and Yap1 neuronal depletion leads to impairments in mice locomotor coordination on the RotaRod test. (A) Image of the RotaRod apparatus. (B-C) Locomotor coordination in Amot fl/fl and Amot fl/fl; Syn-Cre mice (B), as well as Yap1 fl/fl and Yap1 fl/fl; Syn-Cre animals (C) measured over the training and four constitutive days of experiment. Values are shown as a total time that mice remained on the RotaRod (Latency to fall). Following number of animals were used in the test: Amot fl/fl n = 10; Amot fl/fl;Syn-Cre n = 6; Yap1 fl/fl n = 4; Yap1 fl/fl;Syn-Cre n = 6. Statistical significance was analyzed using two-tailed unpaired t test. Statistical significance was analyzed using two-tailed unpaired t test. *p < 0.05, **p < 0.01, ***p < 0.001. Bars represent the mean ± SEM (standard error of the mean).

Secondly, for gait analysis of Amot and Yap1 knockout mice I performed the CatWalk experiments. In this test a mouse walks across a 130-cm long illuminated glass runway and the camera records the paw prints from below. Next, the CatWalk software enables for detailed analysis of the basic gait parameters, such as stride length or the distance between two forepaws or hind paws (Base of support, BOS) (Fig. 26A), and the analysis of more precise animal coordination units of its step-cycle dynamic. My analysis of the base of support for both hind and forepaws in Amot/Yap1 mutant mice did not reveal apparent changes between knockouts and their controls (Fig. 26B, 26C). Yap1 neuronal-deficient mice, however, had significantly increased paw stride measurements of a fore- and hindlimbs (Fig. 26E), whereas that gait parameter was not affected by Amot depletion in neurons (Fig. 26D). Importantly, the study of step-cycle dynamics, revealed that the percentage of stand phase duration to the whole step duration (duty cycle) for hindpaws in both Amot and Yap1 mutants was significantly decreased (Fig. 26F-G). These automated analysis of mutant mice gait parameter clearly indicated that Amot and Yap1 neuronal depleted mice exhibit gait disturbances and coordination impairments, however, the abnormalities were more apparent for the *Yap1 fl/fl;Syn-Cre* mice.

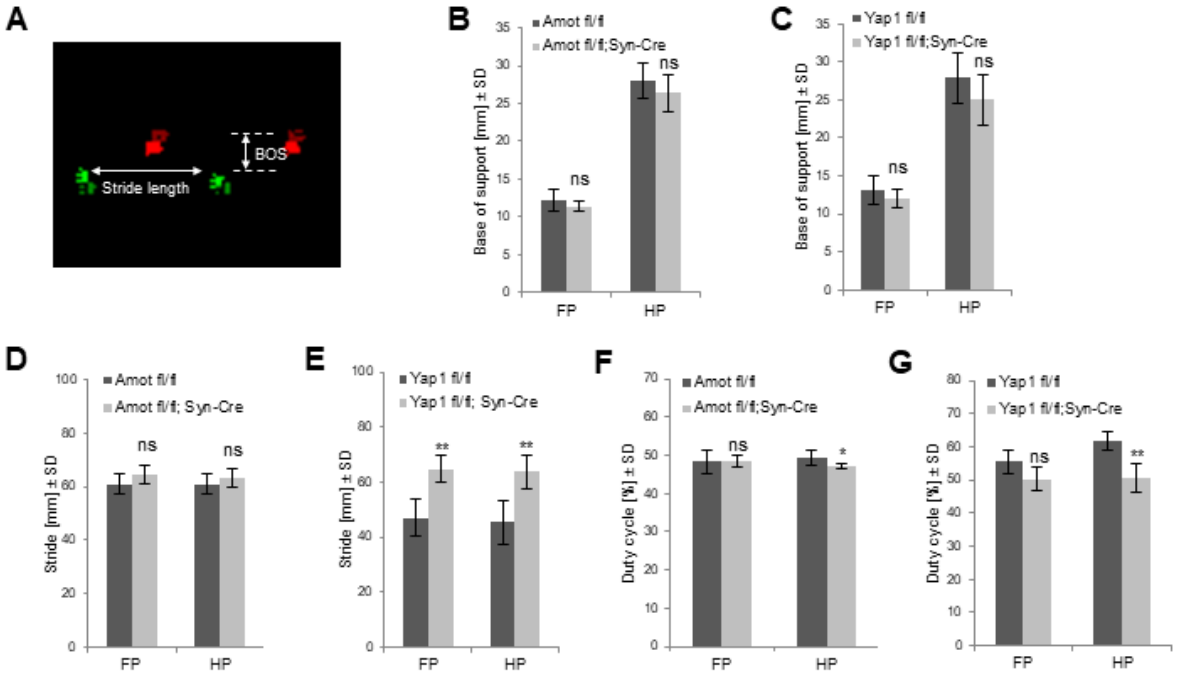

Fig. 26. Amot and Yap1 mutant mice exhibit abnormal coordination in the CatWalk automated gait analysis. (A) Image from the CatWalk gait analysis showing the mouse footprints (red = left paws; green = right paws). (B, C) The measurements of a distance between forepaws or hind paws (base of support) made by Amot fl/fl, Amotl fl/fl;Syn-Cre mice (B) and Yap1 fl/fl; Yap1 fl/fl;Syn-Cre animals (C). (D, E) The analysis of forepaws and hind paws stride length in by Amot fl/fl, Amotl fl/fl;Syn-Cre mice (D) and Yap1 fl/fl; Yap1 fl/fl;Syn-Cre animals (E). (F-G) The duty cycle analysis in Amot fl/fl;Syn-Cre (F), Yap1 fl/fl;Syn-Cre mice (G) and their control littermates. Following number of animals were used in the test: Amot fl/fl n = 11; Amot fl/fl;Syn-Cre n = 5; Yap1 fl/fl n = 4; Yap1 fl/fl;Syn-Cre n = 6. Statistical significance was analyzed using two-tailed unpaired t test. Statistical significance was analyzed using two-tailed unpaired t test. *$p < 0.05$, **$p < 0.01$. Bars represent the mean ± SD. FP, forepaws; HP, hind paws; BOS, base of support.

Knowing that the animal performance during the RotaRod task could be interpreted as indication of a motor learning skills that hides the precise information about a subject motor coordination (Buitrago et al., 2004 [30]), I decided to conduct additional motor coordination behavioral experiment that would not engage the learning process. For that, I aimed to design a foot-fault test, in which the animal could freely run over a metal rod runway towards a darkened shelter located at the end of the platform (Fig. 27A). During the experiments animals performances were recorded and movies were analyzed in slow motions mode. From each run I have analyzed the total number of foot slips from the rods and the time needed to traverse the runway. I found that the performances of Amot and Yap1 knockouts were

significantly worse than control mice; they required more time to complete the run and made more foot slips during each run (Fig. 27B-E).

Collectively, my results obtained from motor coordination experiments showed that Amot and Yap1 knockouts had shorter latency to fall from RotaRod, abnormal duty cycle coordination parameter analyzed with Catwalk experiments and more foot slips as well as needed longer time for completing the foot-fault test than control animals. These results strongly indicate that neuronal deletion of Amot or Yap1 leads to impaired motor coordination in mice.

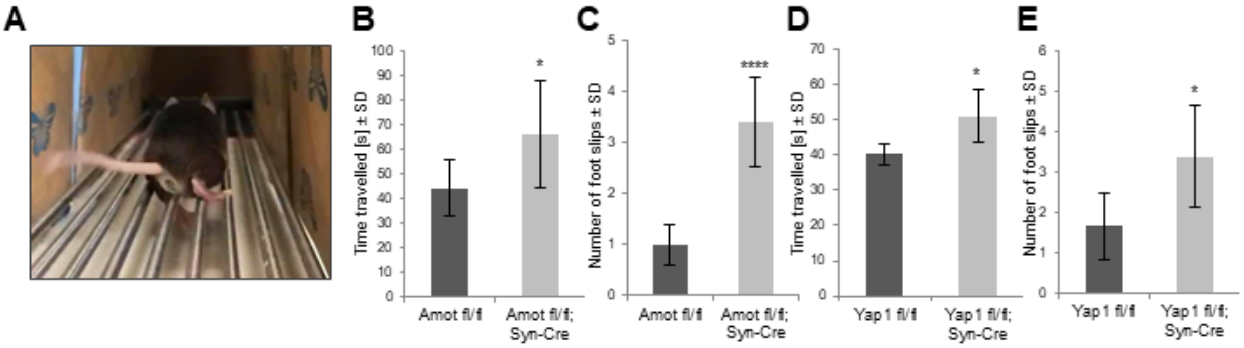

Fig. 27. Amot and Yap1 mutant mice showed impairments in coordination during foot-fault experiments. (A) Image of a mouse performing the foot-fault test. (A) Analysis of the time that Amot fl/fl and Amot fl/fl;Syn-Cre mice needed to traverse the metal-rod platform and (B) the number of their foot slips showed impairments in mutant mice coordination. (D) Time for complete traverse and (E) the number of foot slips for Yap1 fl/fl and Yap1 fl/fl;Syn-Cre. The following number of animals were used in the experiment: Amot fl/fl n = 7; Amot fl/fl;Syn-Cre n = 5; Yap1 fl/fl n = 4; Yap1 fl/fl;Syn-Cre n = 6. Statistical significance was analyzed using two-tailed unpaired t test. Statistical significance was analyzed using two-tailed unpaired t test. *p < 0.05, ****p < 0.0001. Bars represent the mean ± SD.

4.1.5.3 Analysis of the potential vestibular system dysfunction on the motor coordination impairments of Amot and Yap1 knockout mice

The vestibular system dysfunction may result in impairments of locomotor coordination. Inner-ear abnormalities often lead to increased circling behavior in rodents (Isgrig et al., 2019 [103]). Therefore, to exclude the impact of Amot and Yap1 depletion on the potential vestibular system dysfunction and to highlight the cerebellar-driven coordination impairments in Amot and Yap1 mutants, I performed more detailed analysis of mice trucks during the Open Field tests (Fig. 28A, 28B, 28D, 28E). Importantly, I could not detect a significant differences in the number of rotations performed by Amot or Yap1 knockout mice compared to control

littermates. These results suggest that the vestibular system is unlikely to cause the defects observed in RotaRod and gait analysis tests.

Altogether, using variety of experimental approaches, I showed that Amot and Yap1 are indispensable for complex dendritic arborization of Purkinje cells *in vivo*, proper cerebellar organization, and are essential for normal motor coordination in mice.

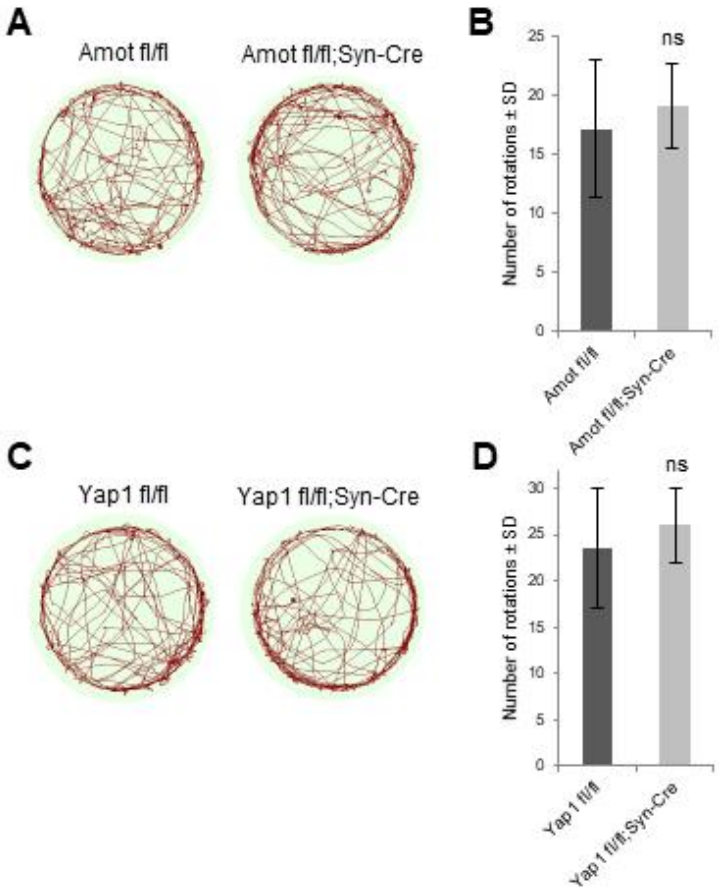

Fig. 28. Amot and Yap1 depletion in neurons does not lead to increased number of rotations in Open Field experiment. (A, C) Representative track plot tracings demonstrate ambulatory activity of Amot fl/fl, Amot fl/fl;Syn-Cre mice (A) and Yap1 fl/fl Yap1 fl/fl;Syn-Cre mice (C). (B, D) Quantification of the number of rotations performed by Amot mutant and control mice (B) and by Yap1 mutant and control littermates (D). The following number of animals were used in the experiment: Amot fl/fl n = 9; Amot fl/fl;Syn-Cre n = 9; Yap1 fl/fl n = 8; Yap1 fl/fl;Syn-Cre n = 6. Statistical significance was analyzed using two-tailed unpaired t test. Statistical significance was analyzed using two-tailed unpaired t test. Bars represent the mean ± SD.

4.2 The role of Amotl1 protein in the mouse brain organization and behavior

Knowing that Amot plays important functions in the brain organization and animals behavior I decided to study the second protein from Angiomotin family, Angiomotin-like 1 (Amotl1). The expression, localization and function of endogenous Amotl1 protein in the CNS have not been investigated so far. I hypothesized that Amotl1 may also play an important role in neurons and brain organization that influences behavioral responses.

4.2.1 Expression and localization of Amotl1 in cultured neurons and adult mouse brain

To address this hypothesis I firstly aimed to investigate Amotl1 expression and localization in mature cultured hippocampal neurons. Microscopic analysis on immunostained cells revealed that Amotl1 is expressed in neurons (Fig. 29A). Higher magnification of dendritic processes showed Amotl1 localization to synaptic compartments, where its immunoreactivity overlapped with anti-postsynaptic density protein 95 (PSD95) and anti-synaptophysin positive puncta, commonly used as synaptic markers (Fig. 29A). To determine whether Amotl1 is widely expressed throughout the mice brain I performed the protein detection experiments in lysates obtained from various mouse brain structures at P30. My western blot analysis revealed that, similarly to Amot, Amotl1 is expressed in different mouse brain areas, however its levels noticeably differ between individual structures (Fig. 29B). The highest Amotl1 expression level was observed in the thalamus, whereas lower protein levels could be detected in the hippocampus, cortex, amygdala, and cerebellum.

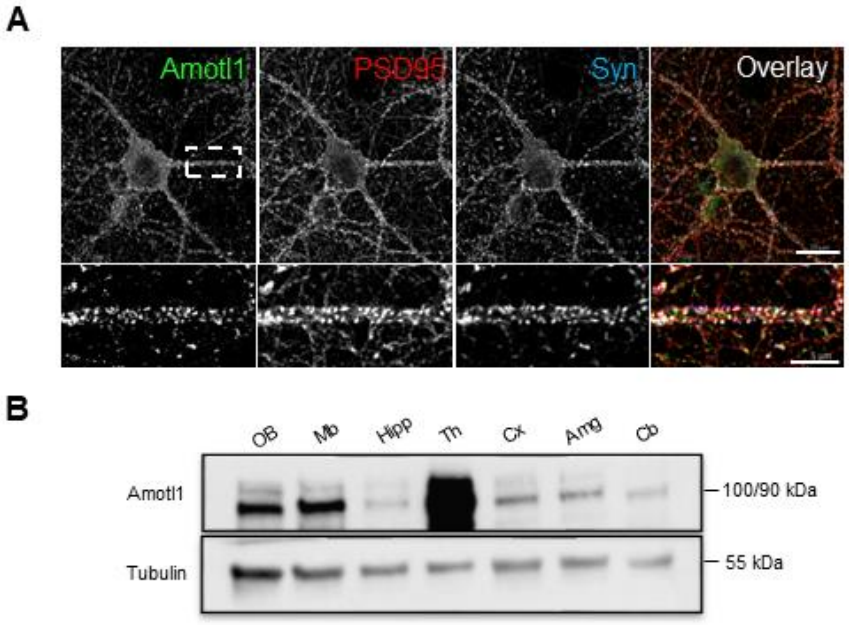

Fig. 29. Amotl1 localizes to synapses in neurons and is widely expressed in the mouse brain. (A) Amotl1 localization in cultured rat hippocampal neurons (DIV 21). Neurons were immunolabeled for Angiomotin like 1 protein (Amotl1, green), postsynaptic density protein 95 (PSD95, red) and synaptophysin (Syn, blue). Anti-PSD95 and anti-synaptophysin antibody was used to visualize synapses. The lower panel shows the higher magnification of the boxed area showed in upper panel. (B) Amotl1 expression in different structures of the mouse brain. Western blot analysis of lysates obtained from different brain regions from P30 mouse ("OB" = olfactory bulbs; "Mb" = midbrain; "Hipp" = hippocampus; "Th" = thalamus; "Cx" = cortex; "Amg" = amygdala; "Cb" = cerebellum). Tubulin was used as the loading control. Scale bars: A upper panel = 10 µm, A lower panel = 5 µm.

4.2.2 Strategy for generation of Amotl1 knockout mice

To determine Amotl1 function in the brain, I designed the breeding strategy to achieve systemic knockout of *Amot1* gene from Amotl1 conditional-knockout mice, which was a kind gift from Lars Holmgren Laboratory (Fig. 30). In the first cross, homozygotes transgenic mice containing two LoxP sites that flank critical exons 5 and 6 of the *Amotl1* gene (Amotl1 fl/fl) were crossed to heterozygotes animals that express Cre recombinase under the control of a human cytomegalovirus promoter (*CMV-Cre*) which is active in most of cells and tissues (Fig. 30A). In the F1 population, all mice that carry *Amotl1* flox allele and *CMV-Cre* transgene have floxed alleles converted into null allele (KO) due to Cre activity. In the second cross, *Amotl1 KO/WT;CMV-Cre* heterozygotes animals were bred to the heterozygous mice *Amotl1 fl/WT*.

This results in generation of *Amotl1 KO/KO;CMV-Cre* animals. In the next step I outbred the CMV-Cre transgene to generate *Amotl1 KO/KO* mice.

In parallel to assess Cre recombinase activity in *CMV-Cre* mice, I breed these animals *to STOP-Tom* reporter strain (see section 4.1.2). I observed wide expression of the Tomato gene by its visible fluorescence throughout the whole mouse body (Fig. 30B), which means that Cre was successfully produced in various tissues. To evaluate whether Cre effectively recombined LoxP sites of the *Amotl1* gene I performed the PCR analysis of the genomic DNA obtained from the various tissues of Amotl1 homozygous knockout-mice (*Amotl1 KO/KO*) and control wild-type littermates (*Amotl1 WT/WT*) (Fig. 30C). The agarose gel electrophoresis of the PCR reaction products confirmed the tissue-wide generation of 382 base-pare DNA fragment in *Amotl1 KO/KO mice* corresponding to the *Amotl1* gene where exon 2 was successfully excised. Lastly, I performed a western blot analysis of the Amotl1 knockout and control brain homogenates and I observed a lack of the Amotl1 protein in mutant mice (Fig. 30D).

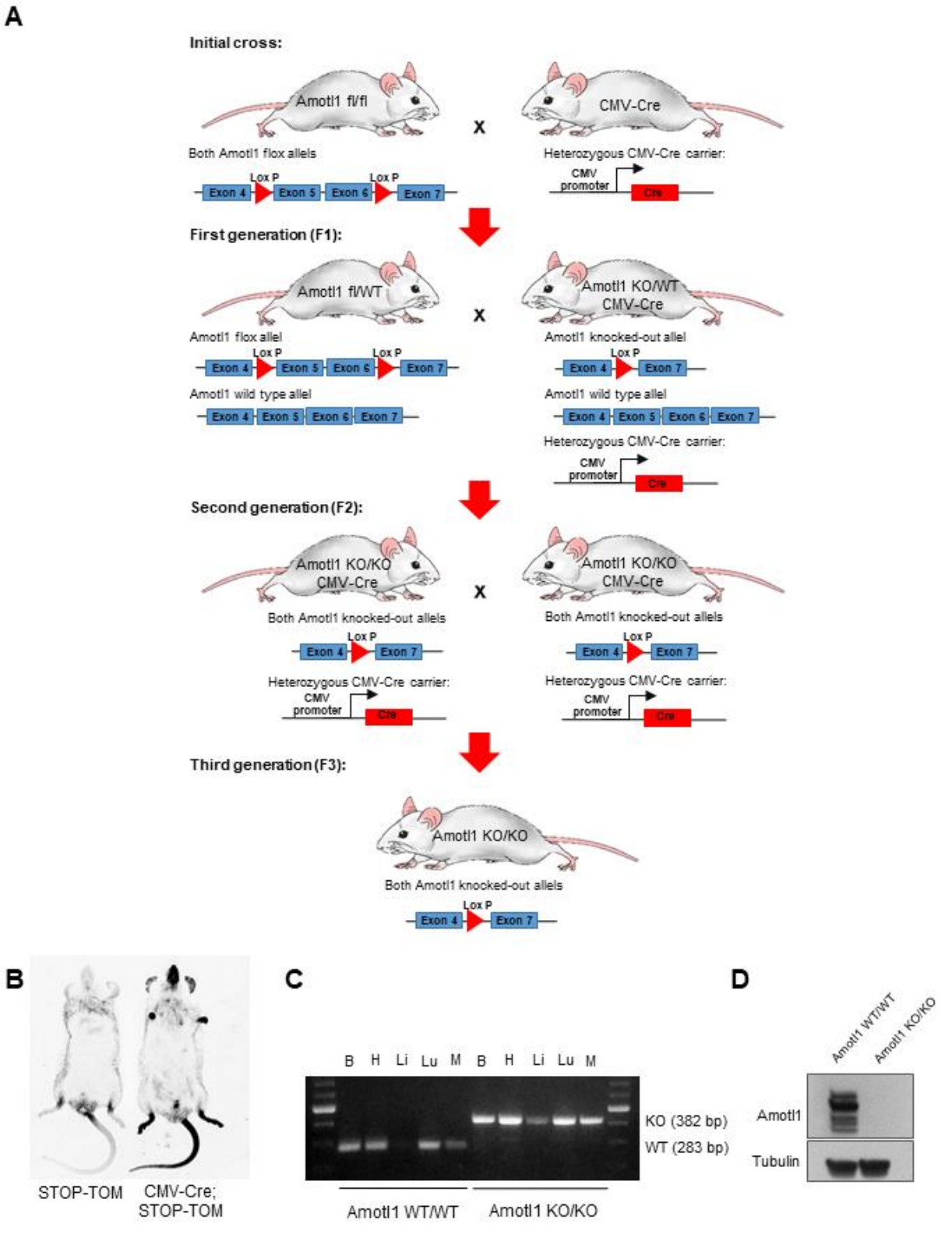

Fig. 30. Strategy for generation and validation of the Amotl1 knockout mice. (A) The schematic diagram of generating the Amotl1 knockout mouse (Amot1 KO/KO). Homozygous Amotl1 flox mice that have exon 5 and 6 of the Amotl1 gene flanked by LoxP sites (Amotl1 fl/fl; top left panel) were bred with the heterozygous mice caring Cre under the cytomegalovirus promoter (CMV-Cre; top right panel) to produce the heterozygous Amotl1

flox/WT mice (Amotl1 fl/WT; middle left panel) and heterozygous knockout animals in which the LoxP surrounded fragment of the gene was deleted due to Cre recombination (Amotl1 KO/WT,CMV-Cre; middle right panel). These mice were bred to Amotl1 fl/WT animals to produce the second generation F2 offspring, double Amotl1 knockout mice (Amotl1 KO/KO, CMV-Cre; third panel). The last breeding point allowed for outbreeding of the CMV-Cre transgene (bottom panel). (B) The photograph of the STOP-Tom mouse (control) and STOP-Tom;CMV-Cre animal that shows active Tomato expression throughout the whole mouse body visualized by exposure to ultraviolet light. (C) Amotl1 genotyping reaction. The PCR fragments amplified from the brain ("B"), heart ("H"), liver ("Li"), lung ("Lu") and skeletal muscle ("Mu") genomic DNA of the WT (Amotl1 WT/WT) and knockout mice (Amotl1 KO/KO). Amotl1 wild-type allel (WT) = 283 bp, Amotl1 knockout allel = 382 bp. (D) Lak of Amotl1 expression in the Amotl1 KO brain shown by the Western blot experiments. Tubulin was used as loading control in Western blot analysis.

These results demonstrated that I have generated mice with systemic deletion of *Amotl1*. *Amotl1 KO/KO* mice were born at expected Mendelian rations and showed no obvious signs of any gross abnormalities. This is different to Amot, which systemic deletion leads to embryonic lethality.

4.2.3 Body weight and brain gross anatomy analysis of Amotl1 KO/KO animals

I firstly aimed to analyze *Amotl1 KO/KO* mice general body and brain weight, similarly to experiments I have previously conducted on Amot mutants. Amotl1 mutant animals did not differ from WT controls in overall body weight (Fig. 31A) and their brains did not show any obvious changes in the general organization (Fig. 31B). However, I found a significant increase in their brain weight (Fig. 31C). In order to investigate the potential enlarged structure in these brains I prepared the coronal sections of *Amotl1 KO/KO* and WT mice brains that were stained with DAPI (Fig. 31D). I found significantly increased surface area of the lateral ventricles in Amotl1 depleted brains compared to WT controls (Fig. 31E).

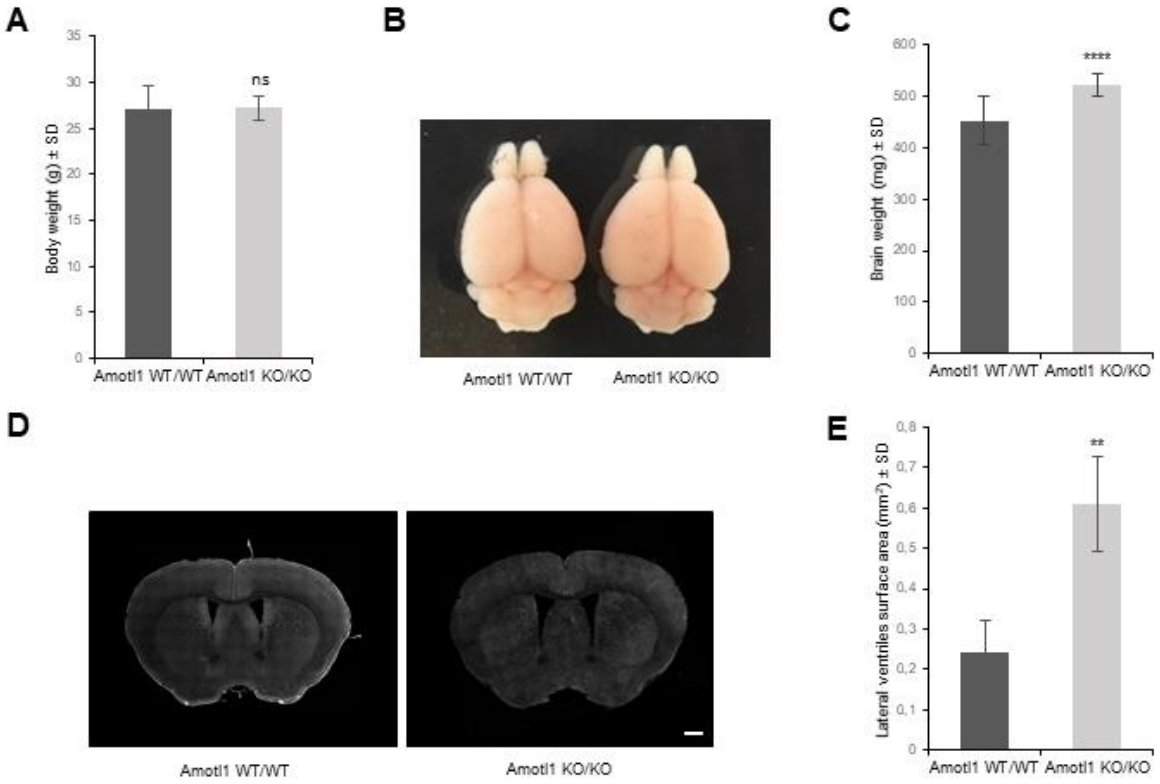

Fig. 31. Amotl1 knockout mice exhibit increased weight of brains and enlarged lateral ventricles compared to control Amotl1 WT/WT animals. (A) The body weight measurements of the Amotl1 WT/WT and Amotl1 KO/KO mice. (B) The representative image of the Amotl1 WT/WT and Amotl1 KO/KO mice brains. (C) Increased Amotl1 knockout brain weight when compared to wild-type control. (D) The cross-section through Amot1 WT/WT and Amotl1 KO/KO brains and quantification of lateral ventricles surface area (E) showed enlarged lateral ventricles in Amotl1 knockout mice. Scale bar = 1000µm. Quantifications were performed on the following number of animals: (A) Amot WT/WT = 14; Amotl1 KO/KO = 17, (C) Amot WT/WT = 15; Amotl1 KO/KO = 17, (E) Amot WT/WT = 4; Amotl1 KO/KO = 4 and at least four sections per mouse were analyzed. Statistical significance was analyzed using two-tailed unpaired t test. **p < 0.01, ****p < 0.0001. Bars represent the mean ± SD.

4.2.4 Amotl1 KO/KO mice have no abnormalities in locomotor coordination and gait pattern

The results of my previous studies on Amot neuronal-depleted mice revealed impaired coordination in these mice (see section 4.1.5). I suspected that the brain morphological abnormalities found in *Amotl1 KO/KO* mice will lead to different behavioral impairments in these animals compared to Amot neuronal depleted mice. To test this hypothesis, I decided to evaluate motor coordination, balance and gait of Amotl1 mutants. During two constitutive days of RotaRod locomotor coordination experiment I could not detect significant differences

in the latency to fall between Amotl1 knockout and WT control mice (Fig. 32A). Additionally, I examined *Amotl1 KO/KO* mice in a standard foot-print assay to analyze their gait pattern. Mouse paws were painted with non-toxic dyes of different colors for fore and hind limbs and animals were allowed to walk over a shit of white paper (Fig. 32B). The footprint analysis of stride length and width showed no significant gait disturbance for the Amotl1 knockout mice (Fig. 32C, 32D). These results suggest that Amotl1 ablation have no effect on mice locomotor coordination.

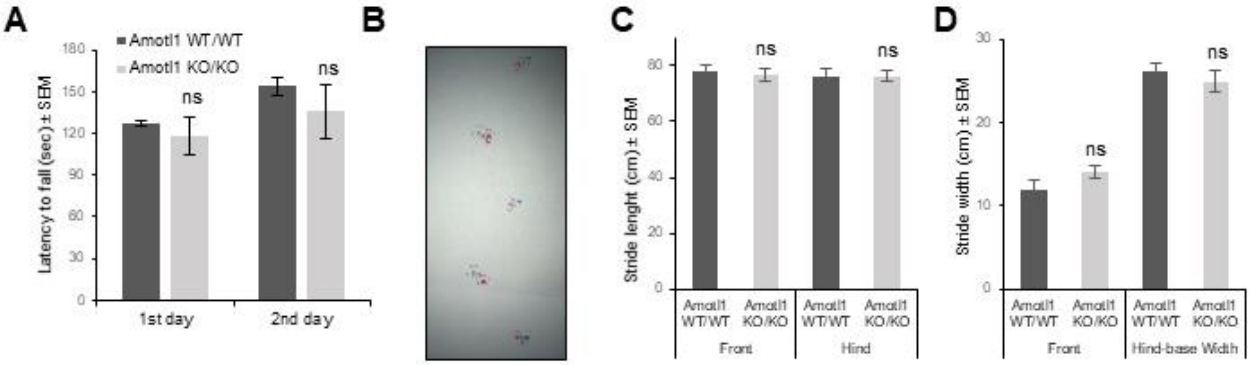

Fig. 32. Amotl1 depletion do not affect mice locomotor coordination. (A) Amot1 WT/WT and Amotl1 KO/KO mice were tested at RotaRod for 2 days and their latency to fall from the platform was measured. (B) Representative image of the wild-type mouse footprints made on the white sheet paper during the foot-print experiments (red = front paws, blue = hindpaws). (C, D) The foot-print test analysis of Amotl1 WT/WT and Amotl1 KO/KO stride length (C) and stride width (D) for their front and hindpaws. Quantifications were performed on the following number of animals: (A) Amot WT/WT = 9; Amotl1 KO/KO = 9, (C, D) Amot WT/WT = 7; Amotl1 KO/KO = 6. Statistical significance was analyzed using two-tailed unpaired t test. Bars represent the mean ± SEM.

4.2.5 Amotl1 mutant mice display hyperactivity and decreased anxiety in the Open Field experiment

In order to investigate the general locomotor activity and basic emotional responses of Amotl1 deficient mice, I performed an Open Field test. Mice were placed individually at the center of an open round arena and allowed for undisturbed exploration for 10 min. To assess their motor behavioral performance I quantified the distance traveled by each animal. The detailed analysis of an animal locomotion showed that Amotl1 knockouts traveled longer distances in each minute over first 6 min of the experiment (Fig. 33A). Therefore, I quantified total distance traveled over that time and I found that Amotl1 mutant mice displayed significant increase in

locomotor activity (Fig. 33B). Additionally, a decreased time that these mice have spent immobile (Fig. 33C) supported the observation of *Amotl1 KO/KO* hyperactivity.

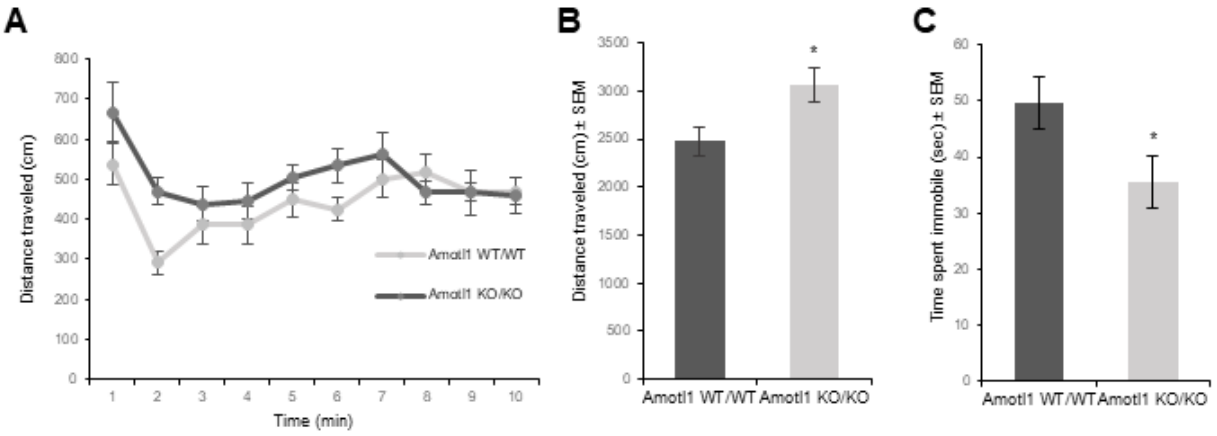

Fig. 33. Amotl1 knockout mice show hyperactivity in the Open Field. (A, B) Amotl1 KO/KO mice traveled greater distances than Amotl1 WT/WT during first six minutes of the Open Field test as shown in a time course for distance traveled in one minute time bins (A) and cumulative distance traveled during first six minutes (B). (C) Amotl1 knockouts have spent less time immobile than controls for six minutes of the Open Field experiments. N = 9 mice of each genotype were tested. Statistical significance was analyzed using two-tailed unpaired t test. *p < 0.05. Bars represent the mean ± SEM.

Increased thigmotaxis in the Open Field could be connected with anxiety-like behavior in rodents due to their fear of open and illuminated spaces (Simon et al., 1994 [185]). To assess whether the increased locomotion of Amotl1 knockout mice is a symptom of their elevated anxiety-related behavior I analyzed the spatial preference in the Open Field. Surprisingly, Amotl1 mutants spend more time in the central zone of the apparatus, as shown by the group heat maps of the animal position (Fig. 34A) and analysis of the time that animal spend in the zone-center (Fig. 34B). Therefore, I concluded that Amotl1 deficient mice show reduced anxiety. Increased locomotion over first 6 min of the test could indicate their enhanced interest and curiosity of the novel environment.

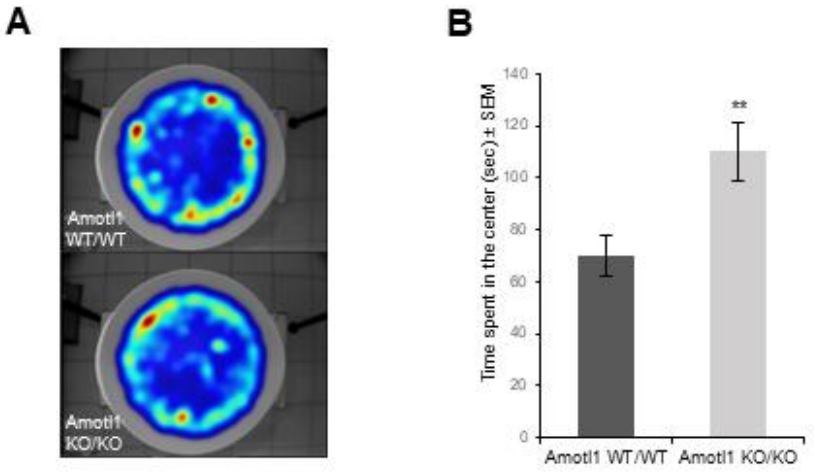

Fig. 34. Amotl1 knockouts exhibit reduced anxiety-related behavior in the Open Field. (A) Heat maps representing the Amotl1 wild-type (upper panel) and Amotl1 knockout (lower panel) time spend in different Open Field area (wormer color = more time). (B) Quantitative analysis of the time that mice have spent in the center zone of the Open Field apparatus was significantly higher for the Amotl1 knockouts. N = 9 mice of each genotype were tested. Statistical significance was analyzed using two-tailed unpaired t test. **p < 0.01. Bars represent the mean ± SEM.

4.2.6 Impaired anxiety-like responses of Amotl1 knockouts during mice handling and in marble burying test

In rodent behavioral phenotyping, it is of a great importance to minimalize the stress of animals before and during the experiments. The gentle handling procedure may allow habitation to the experimenter and thus significantly reduce animal anxiety. I habituated individual mouse prior to each behavioral testing. Naive WT mice show natural avoidance of human when handled for the first time (Fig. 35A). This diminishes over time with repetitive contact. Strikingly, Amotl1 mutants did not show any symptoms of distress or anxiety when handled for the first time (Fig. 35B). This observation, together with the Open Field locomotion analysis prompted me to investigate more carefully anxiety behaviors of the Amotl1 mutants.

In order to confirm the observed anxiolytic phenotype of *AmotI1 KO/KO* mice I conducted the marble burring test (MBT). This approach is based on mice digging and burrowing performance, a natural defense behavior that occurs under stressful conditions (novel environment). In MBT glass marbles are equally spaced on the mouse bedding. Animal with a high degree of anxiety tent to burry most of the marbles over the time, and this reaction can be suppressed by administration of anxiolytics drugs (Njung et al., 1991 [149]; Ichimaru et al.,

1995 [102]; Li et al., 2006 [114]). I found that after 30 min Amotl1 knockout mice buried less marbles when compared to WT control mice (Fig. 36A, 36B). Additionally, based on the quantification of buried marbles, I divided the experimental groups of WT and mutant mice into three levels of anxiety: subject that were not anxious (anxiolytic), middle class and the most anxious group. More than 60% of WT mice tested buried at least 10 over 15 marbles that were introduced, whereas the similar anxiety individuals were not detected over the Amotl1 mutants group (Fig. 36C).

Fig. 35. Amotl1 KO/KO mice show decrease anxiety during handling. During handling Amotl1 WT/WT mice presented strong avoidance behavior (left) whereas Amotl1 KO/KO mice showed reduced stress level and did not avoid the contact with experimenter (right). Different behavior during handling procedure is presented on the movies uploaded on youtube. For the Amotl1 WT/WT visit website: https://youtu.be/zYMAFB2DbXM, for the Amotl1 KO/KO visit website: https://youtu.be/WTXcrq4yzQo.

Taken together, the results obtained from the Open Field experiments, marble burring approach, and the observation during mice handling supported the conclusion of a decreased anxiety-like behavior in mice.

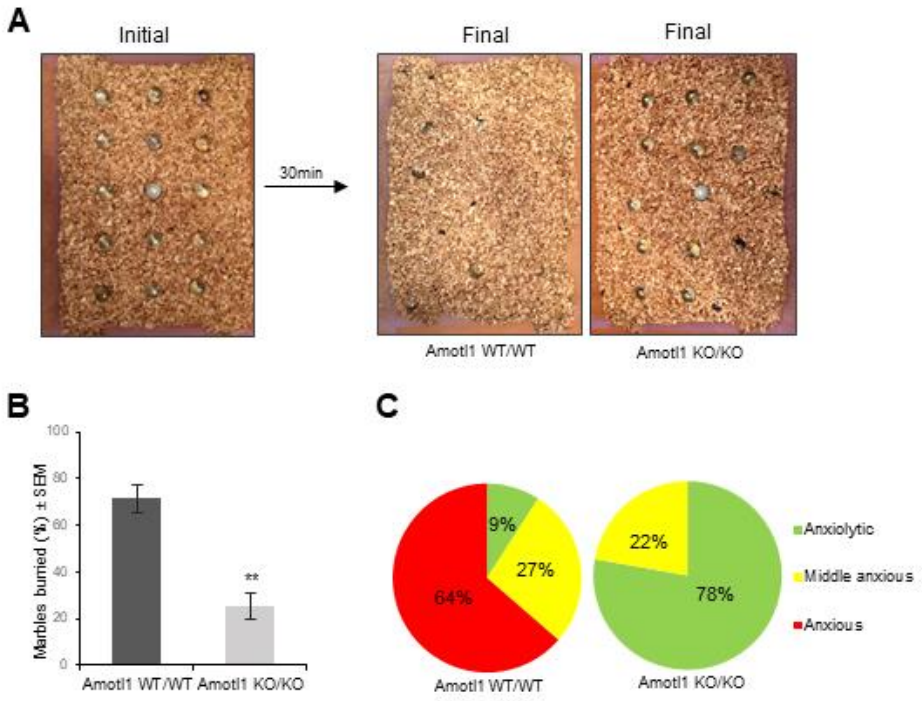

Fig. 36. Amotl1 KO/KO mice showed suppressed marble burying behavior. (A) Example images of the equal spaced marbles placed on the bedding at the initial experimental set up (left) and marbles buried by wild-type and knockout mice after 30 min (right). (B) Qunatification of the marbles buried by mice from each genotype shown as a percentage of the fifteen in total marbles presented. (C) The circular diagrams that shows the percentage of anxiolytic, middle anxious and the most anxious mice within the tested groups of Amotl1 WT/WT (left) and Amolt 1 KO/KO (right) animals. The subgroups were defined based on the number of marbles buried: anxiolytic n ≤ 6, middle anxious < 10, anxious ≥10. Quantifications were performed on the following number of animals: (A) Amot WT/WT = 11; Amotl1 KO/KO = 9. Statistical significance was analyzed using two-tailed unpaired t test. **p < 0.01. Bars represent the mean ± SEM.

4.2.7 Analysis of repetitive behavior

The animal anxiety could be reflected in increased digging behavior that not always translates to increased number of marbles buried. Therefore, I analyzed the total time spend on digging behavior over the marble burying test. As expected, *Amotl1 KO/KO* mice spend less time on digging behavior than WT control animals (Fig. 37A).

It is worth mentioning that there is controversy over the marble burring test when used as anxiety assessing task rather than representation of compulsive-like behaviors in mice (Taylor et al., 2017 [200]; Mehta et al., 2011 [131]; Angoa-Pérez et al., 2013 [7]). The self-grooming is the other representative of rodent repetitive behavior that could complete with digging during

marble burying. Hence, to evaluate whether Amotl1 mutants show symptoms of repetitive-like behavior I quantified total time spend on self-grooming. However, I could not detect any differences in the time spend on self-grooming between *Amotl1 KO/KO* and WT mice (Fig. 37B).

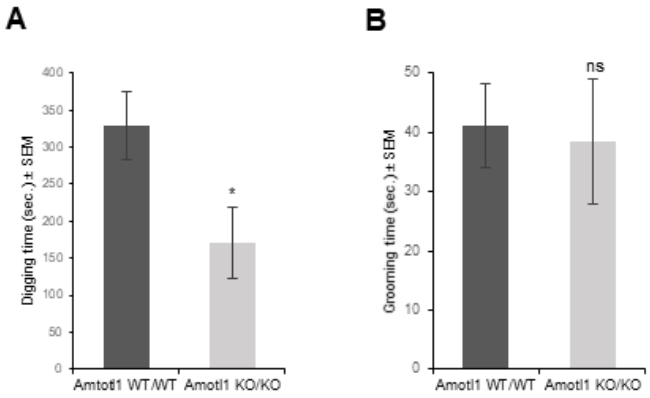

Fig. 37. Amotl1 knockout in mice does not lead to increased repetitive behavior during marble burying test. (A, B) Quantification of a cumulative time spend on digging (A) and self-grooming for Amotl1 WT/WT and Amotl1 KO/KO mice during the 30 min marble burying experiment. Quantifications were performed on the following number of animals: (A) Amot WT/WT = 11; Amotl1 KO/KO = 9. Statistical significance was analyzed using two-tailed unpaired t test. *$p < 0.05$. Bars represent the mean ± SEM.

My result from marble burying test suggest that there are no signs of increased repetitive behavior in Amotl1 mutant mice. To confirm these results independently in an experimental setup where digging does not interfere with grooming, I performed a simple self-grooming test in the cages that contained minimal 1cm-thin layer of bedding (Fig. 38A). As expected, I found that self-grooming time did not differ significantly between the experimental groups (Fig. 38B), confirming that Amotl1 ablation do not cause increase in repetitive behavior.

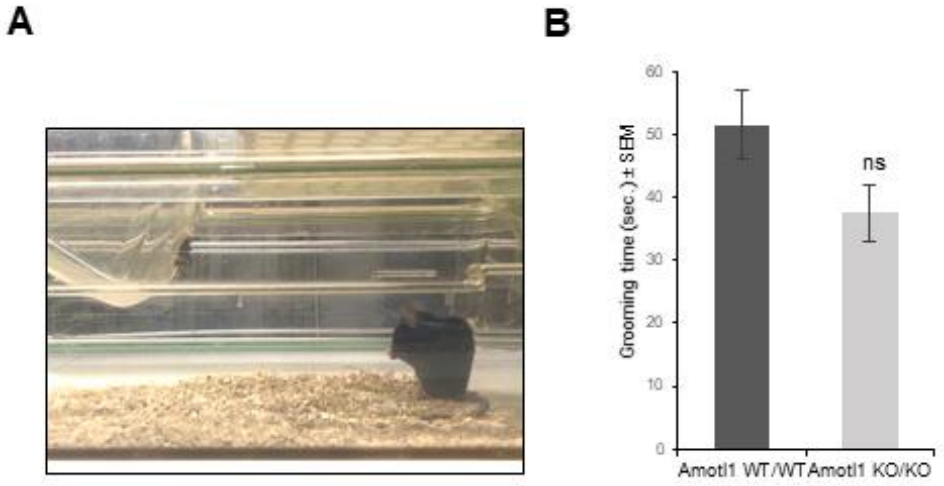

Fig. 38. Amotl1 knockout mice do not show enhanced repetitive self-grooming behavior during self-grooming test. (A) Representative image of a mouse grooming all body parts during self-grooming testing. (B) Total duration of self-grooming in Amotl1 KO/KO and Amotl1 WT/WT mice during 20 minutes experiment showed normal self-grooming behavior in Amotl1 depleted mice. Quantifications were performed on the following number of animals: Amot WT/WT = 9; Amotl1 KO/KO = 8. Statistical significance was analyzed using two-tailed unpaired t test. Bars represent the mean ± SEM.

4.2.8 The role of Amotl1 protein in mice social behavior

4.2.8.1 Impairments of the nest building behavior

The observation of mice home-cage activities of daily living often gives insights into animals welfare, simultaneously pointing out potential behavioral impairments and therefore providing a direction for further studies. Nest building is one of the most important rodents spontaneous activities because it provides save shelters allowing to hide from predators, enable for warming and keeping optimal body temperature. To shed more light on *Amotl1 KO/KO* mice possible behavioral impairments I performed simple nest building experiment. In order to assess nesting ability I introduced a piece of paper towel into the mouse cage overnight. Surprisingly, I observed abnormal and less complex construction of the nests prepared by Amotl1 mutants (Fig. 39A). Most of the studies evaluate nesting impairments by assigning scores from 1 to 5 arbitrary points reflecting the nests quality (Carreno-Munoz et al., 2018 [36]; Hagiwara et al., 2020 [76]). In order to evaluate nesting in more objective and quantitative manner I have analyzed the surface area of the tissue perforation (Fig. 39A, lower panel). I found that the total area of perforations within the nesting tissue was smaller for

Amotl1 knockouts when compared to tissue introduced to WT mice (Fig. 39B). Therefore, according to the amount of material used for nesting and observation of the shape of nests, I concluded that Amotl1 KO mice display strongly impaired nesting behavior.

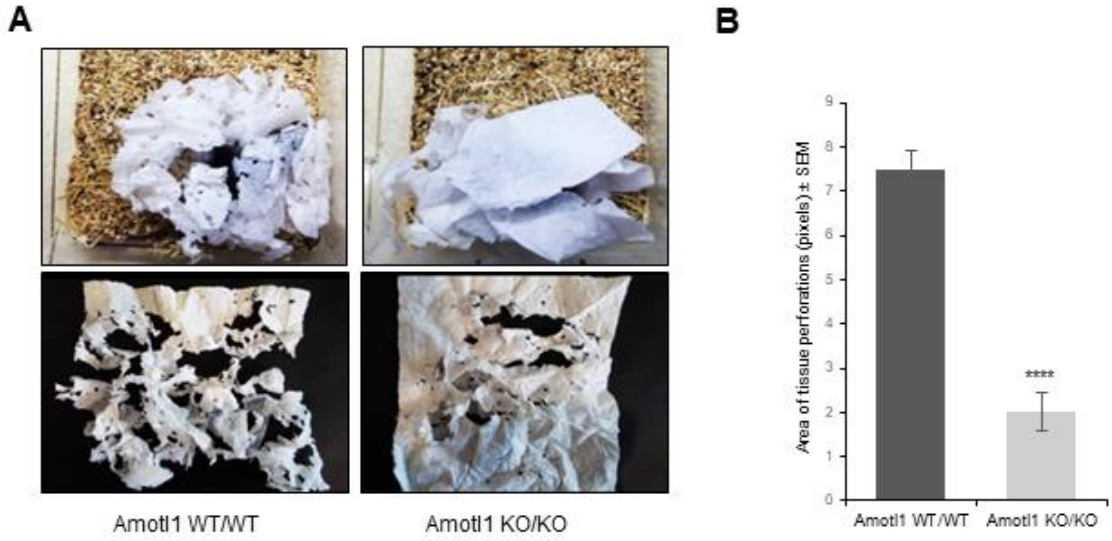

Fig. 39. Amotl1 ablation causes impaired nesting behavior. (A) Representative photographs of nests made by Amotl1 WT/WT (left) and Amotl1 knockout (right) mice. Bottom panel shows perforation made by mice in paper towel used as nesting material. (B) Quantification of the cumulative area of a tissue perforations during revealed significant decrease in material used for nesting by Amotl1 KO/KO mice. Quantifications were performed on the following number of animals: Amot WT/WT = 5; Amotl1 KO/KO = 6. Statistical significance was analyzed using two-tailed unpaired t test. ****$p < 0.0001$. Bars represent the mean ± SEM.

4.2.8.2 Amotl1 mutants sociability in the three-chamber experiment

Abnormal nest building behavior often indicates impairments in mice sociability. Thus, I was curious whether the deletion of Amotl1 will have an impact on mice sociability. To address this hypothesis, I performed a standard three-chamber social approach experiment. In this test animal voluntary move around the apparatus consisting of 3 connected arenas: a chamber with unfamiliar conspecific placed under an inverted wire cup, the center neutral chamber and a third chamber where an empty wire cup is located (Fig. 40A). Mice have a natural interest to investigate a stranger mouse. Therefore, mice sociability can be determined as comparison of time spend in the arena that contains another animal vs. the one with an empty object (wire cup). Firstly, I habituated the animals individually to the empty apparatus allowing them for 5 minutes undisturbed locomotion across all three chambers. During that phase of

experiment neither WT mice, nor Amotl1 mutants showed preference for spending time in a particular chamber (Fig. 40B). Next, the unfamiliar mouse and wire cups were placed to the chambers and the social task began. I found that both experimental groups (WTs and Amotl1 knockouts) displayed similar preference for spending time in the chamber that contained the stranger than the chamber with a novel object (Fig. 40C). Finally, I decided to analyze the time that mouse has spent in direct exploration of the conspecific or empty cup. I have calculated the percentage of time that mouse spend exploring a stranger mouse/empty cup over the total time that mouse has spent in the chamber (direct interest index). WT mice had significantly greater preference for direct exploration of conspecific than empty object. They explored the stranger mouse for about 50% of total time spend in that arena, whereas for 30% of their time spend in the other chamber they showed interest in empty object (Fig. 40D). Surprisingly, the same analysis of Amotl1 mutants behavior showed no difference for the percentage of time they willed to explore the animal or the empty cup. Thus, I concluded that Amotl1 depletion leads to deficits in mice sociability.

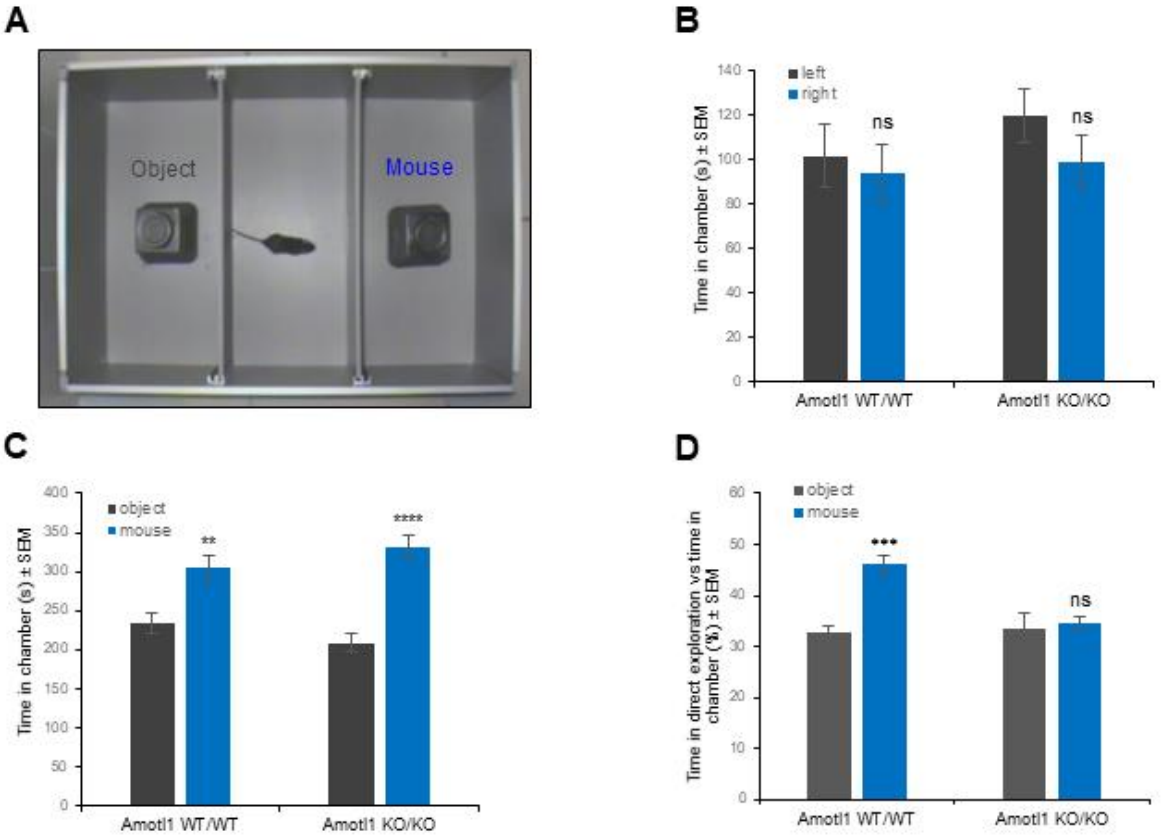

Fig. 40. Altered social behavior of the Amotl1 knockout mice in three-chambered test. (A) A photograph of the three-chambered apparatus. A mouse is freely exploring the chambers where it makes a choice between the

area containing the novel object (left, grey), stranger mouse (right, blue) or neutral middle chamber. (B) The cumulative duration in chambers during the first habituation phase of the sociability testing. Mice of each genotype do not show preference for any chamber. (C) The sociability tests showed preference for the time that mice spent in chamber with stranger over the novel object. (D) Quantification of the time spent exploring the object and stranger mouse, shown as a percentage of total time spent in the chamber. Amotl1 WT/WT mice spent more time when entered to the chamber investigating the mouse than the object, whereas Amotl1 KO/KO animals showed no preference between these two. N = 13 mice of each genotype were tested. Statistical significance was analyzed using two-tailed unpaired t test. **p < 0.01, ***p < 0.001, ****p < 0.0001. Bars represent the mean ± SEM.

4.2.8.3 Assessment of interest in the novel social stimuli and in-cohort sociability behavior of Amotl1 depleted animals using the Eco-Hab

My results of previously conducted experiments showed altered nesting behavior and deficits in social preference for *Amotl1 KO/KO* mice suggesting a social withdrawal phenotype. To analyze further and confirm independently social impairments in Amotl1 mutants I conducted the Eco-Hab experiments in collaboration with Ewelina Knapska group from the Laboratory of Emotions Neurobiology located at the Nencki Instiute of Experimental Biology (Puścian et al., 2016 [164]). The Eco-Hab approach represents variety of advantages over a standard three-chamber testing. It allows for automated tracking of each animal, provides reduced level of stress by limitation of the contact with humans, and allows for prolonged time analysis of individuals behavior that are maintained in a large groups. The apparatus consists of 4 compartments resembling animal home-cages connected with a narrow tunnels that enables for voluntary locomotion and location to preferred areas within the available territory (Fig. 41A). Moreover, it enables for measuring different aspects of animals sociability such as approach to unfamiliar social odor or the time that animals spent in cohorts. The olfaction plays an important role in rodents social preferences and approach to social odor is considered as one of the most crucial aspect of animals social behavior. Therefore, I have analyzed the social behavior of 10 Amotl1 knockout mice housed together in the Eco-Hab apparatus based on their scent-based approach to bedding taken from unfamiliar mice of the same gender, age and genotype. These experiments reveled that Amotl1 mutants display no preference for the scent based social odor vs a clean bedding (Fig. 41B), that could represent another evidence of their impaired sociability. In order to evaluate whether lack of interest in social odor in the *Amotl1 KO/KO* specifically represents their social withdrawal phenotype mice and is not the

effect of olfaction deficits, I performed the simple buried food experiment (Fig. 42A), a test widely used to assess olfactory deficits in rodents (Alberts and Galef, 1971 [4]; Li et al., 2013 [113]). For this purpose mice were habituated to a food pellet covered with peanut butter that is one of the highest sense attractant for rodents. Mice were food deprived over-night and on the next day were allowed to search for food hidden beneath the bedding in the animal's cage. The latency to uncover the food pellet did not increase for Amotl1 mutant mice, what indicates that the sense of smell is not affected in Amotl1 knockouts (Fig. 42B).

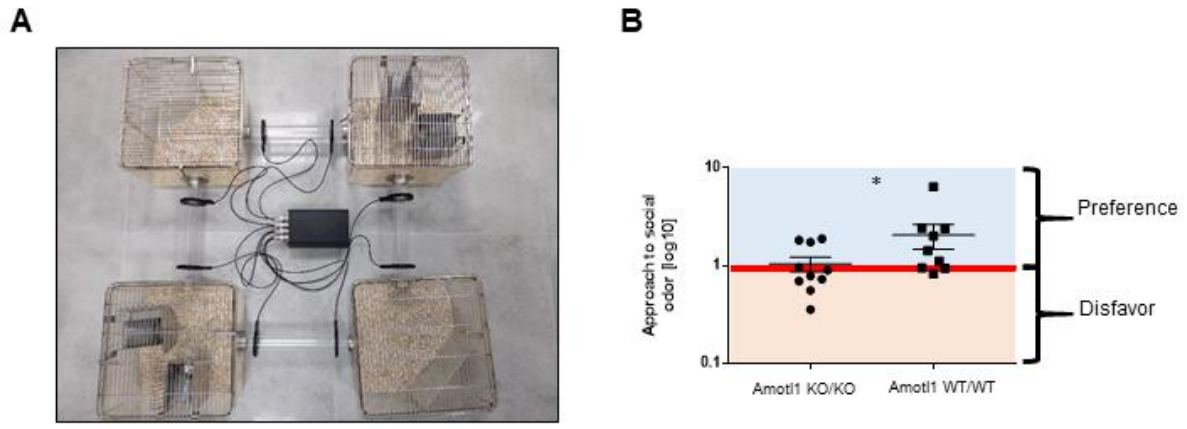

Fig. 41. Amotl1 KO/KO mice showed impaired approach to social odor during the Eco-Hab automated experiment. (A) Representative image of the Eco-Hab apparatus that consists of 4 cages connected by narrow tunnels. (B) Amotl1 KO/KO mice showed no preference for the time that mice spent in cage with social stimuli vs the control non-odor bedding, meaning that the approach to social odor was affected. N = 10 mice of each genotype were tested. Statistical significance was analyzed using two-tailed unpaired t test. *p < 0.05. Bars represent the mean ± SEM.

Altogether, I showed that Amotl1 deficient mice display a social withdrawal phenotype that was apparent by abnormal nest-building behavior, decreased interest in unfamiliar conspecific, and lack of approach to social odor stimuli.

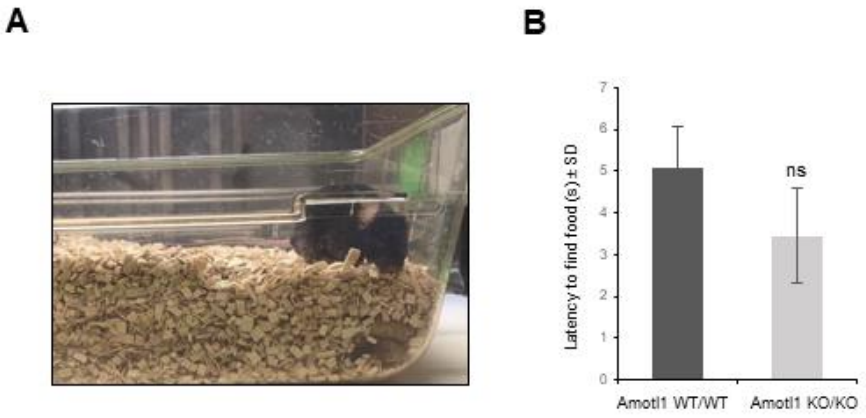

Fig. 42. Amotl1 knockout does not affect mice olfaction. (A) Image of a mouse performing buried-food experiment where the food pellet is hidden underneath the 5 cm bedding layer. (B) The amount of time required for mice to find the food showed no significant difference in the olfactory abilities of Amotl1 WT/WT and Amotl1 KO/KO mice. Experiments were performed on the following number of animals: Amot WT/WT = 7; Amotl1 KO/KO = 9. Statistical significance was analyzed using two-tailed unpaired t test. Bars represent the mean ± SEM.

4.2.9 Amotl1 knockout mice exhibit episodes of backward walking and increased circling behavior

Through the detailed analysis of the Open Field experiment recording I observed that Amotl1 depleted mice exhibit abnormal locomotor activity shown as backward walking episodes (Fig. 43A). I defined the backward walking phenotype as more than two steps that mice made in the backward direction. I observed that about 80% of mice from the experimental group showed backward walking phenotype, whereas I could detect the backward steps in 20% control group animals (Fig. 43B). Additionally, to verify if the Open Field test conditions induce the observed abnormal locomotor activity in *Amotl1 KO/KO* mice or it would be the animal reaction to novelty I analyzed recordings from three chambered experiment. Similarly to Open Field performance, 60% of the tested Amotl1 mutants exhibited backward walking phenotype (Fig. 43C) that was scored an average of 4 times for each animal when analyzed recordings from the Open Field and tree-chamber experiments together (Fig. 43D). Although, there is not much of data describing the mice backward locomotion, previously published study showed that hallucinogenic drugs could provoke the abnormal locomotor such as backward walking and increased circling behavior (Curzon et al., 1979 [44]), suggesting that this could be the animal reaction to hallucinations. Therefore I analyzed the Open Field recording to assess whether Amotl1 mutants show increased circling behavior. Both, track plots and quantitative analysis

showed increased circling locomotion in *Amotl1 KO/KO* when compared to WT control mice (Fig. 43E, 43F).

Summing up, my experiments revealed that Amotl1 is involved in different aspects of mice behavior. Hyperactivity, abnormal anxiety-like behavior and impaired sociability has been previously observed in animal models of various neuropsychiatric disorders such as Autism spectrum disorder, fragile X syndrome and schizophrenia (Kazdoba et al., 2016 [98]; Kazdoba et al., 2014 [99]; Park et al., 2015 [155]). Importantly, I found that Amotl1 deficient mice showed these phenotype of a potential mood disorder mouse model, together with abnormal locomotion represented in backward walking episodes and increased circling behavior.

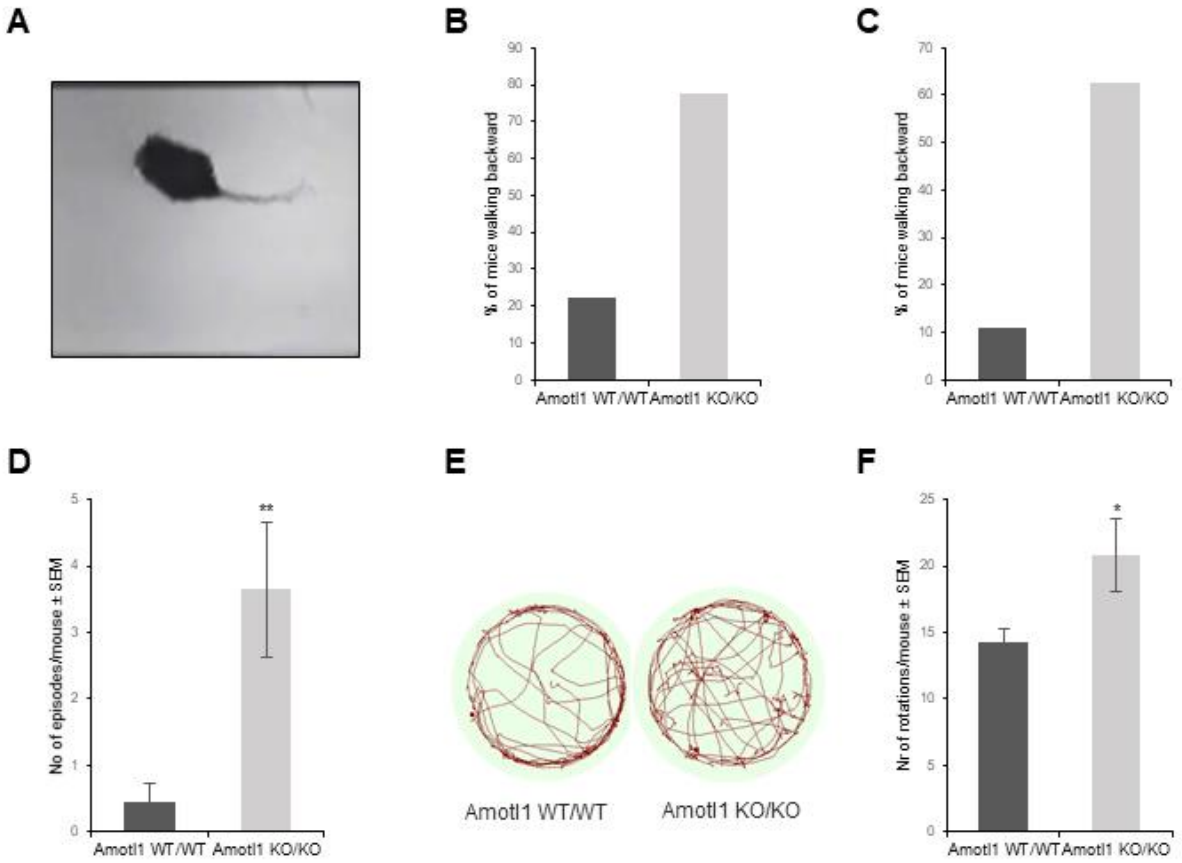

Fig. 43. Amotl1 knockout mice have backward walking episodes and increased circling behavior. (A) An image of mouse in position during the backward walking activity. Visit the following website to watch recording of Amotl1 backward walking phenotype: https://youtu.be/WHChu9PmIsM. (B, C) The percentage of mice from each group that showed the backward walking during Open Field (B) and three-chambered (C) tests. (D) The number of backward walking episodes in Open Field and three-chambered experiments. (E) Representative track plots demonstrate ambulatory activity of Amotl1 WT/WT and Amotl1 KO/KO mice. (F) Quantification of rotations performed by Amotl1 knockout and control. Analysis were performed on the all animals that were used in the

Open Field and three-chambered experiments. Statistical significance was analyzed using two-tailed unpaired t test. *p < 0.05, **p < 0.01 Bars represent the mean ± SEM.

4.2.9 In vivo magnetic resonance imaging (MRI) studies of the Amotl1 knockout brains

Knowing that Amotl1 depletion leads to a severe abnormalities in mouse behavior I aimed to investigate in detail the structure of Amotl1 deficient brains. Therefore, in collaboration with Small Animal Magnetic Resonance Imaging Laboratory located at Mossakowski Medical Research Centre I performed *in vivo* magnetic resonance imaging of the whole brains, which allows for detailed volumetric analysis of different brain structures (MRI). This method allows to avoid artifacts that could be potentially generated due to histological processing and thus, has the advantages over a standard histological procedures. The scans of Amotl1 depleted brains showed a strong increase in the area of the lateral ventricles (Fig. 44A), which was in agreement with my previous histological experiments (see section 4.2.3). Thus, I decided to quantify the volume of cerebrospinal fluid that fills brain ventricles. This fluid helps to circulate nutrients and remove waste from the brain structures. The volumetric MRI analysis showed higher volume of the cerebrospinal fluid in Amotl1 knockout mice than in WT animals (Fig. 44B).

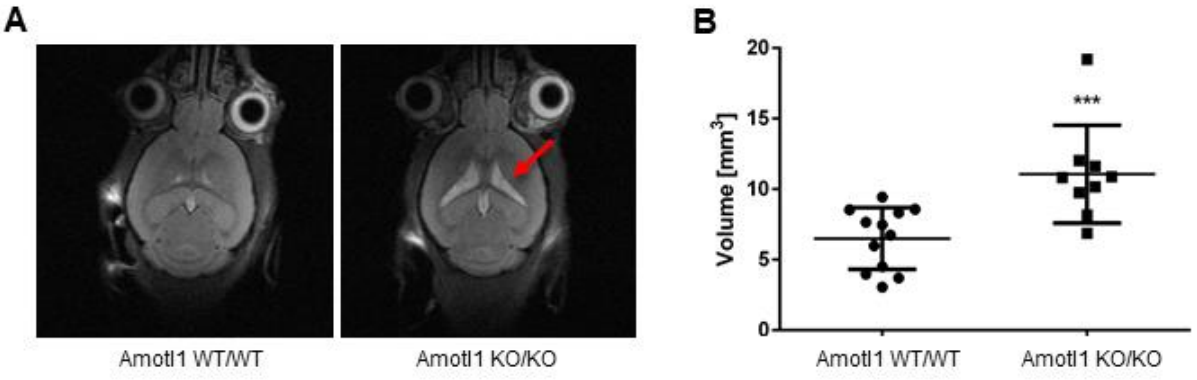

Fig. 44. Increased area of lateral ventricles and volume cerebrospinal fluid in Amotl1 depleted brains showed by magnetic resonance imaging (MRI) experiments. (A) The images of wild-type (left) and knockout (right) brains acquired *in vivo* in the MRI studies. Red arrow points enlarged lateral ventricles structures in Amotl1 KO/KO mouse. (B) The quantitative analysis of the volumes of the cerebrospinal fluid showed an increase for the Amotl1 depleted brains. Experiments were performed on the following number of animals: Amot WT/WT = 12; Amotl1 KO/KO = 9. Statistical significance was analyzed using two-tailed unpaired t test. ***p < 0.001. Lines represent medians, dots represent individual values. Bars represent the mean ± SD.

In order to investigate whether Amotl1 depletion affects different brain areas besides the increase in lateral ventricles and in cerebrospinal fluid volume, I performed the volumetric analysis on numerous major brain structures. The MRI scans showed increased volume of the whole brain in Amotl1 mutant mice (Fig. 45A), which was not detect previously by the gross brain anatomy analysis, however it was in agreement with increased weight that I have previously observed (see section 4.2.3). Further volumetric measurements revealed that brain ventricles (lateral, third) together with connecting ventricles cerebral aqueduct structure were bigger in *Amotl1 KO/KO* mice than WTs (Fig. 45B-D). Lastly, I found that the relative total cortex volume was also increased in mutants, the phenotype that was mostly visible for the motor and somatosensory cortical subfields (Fig. 45E-J). I have also confirmed that in contrary to Amot neuronal deficient mice, the cerebellum of Amotl1 mutants was not affected (Fig. 46A). Additionally, the amygdala that is strongly related to animals sociability and thalamic structures that had strong Amotl1 protein expression (see section 4.2.1), did not significantly differ in volume (Fig. 46B-D) between experimental and control mice groups.

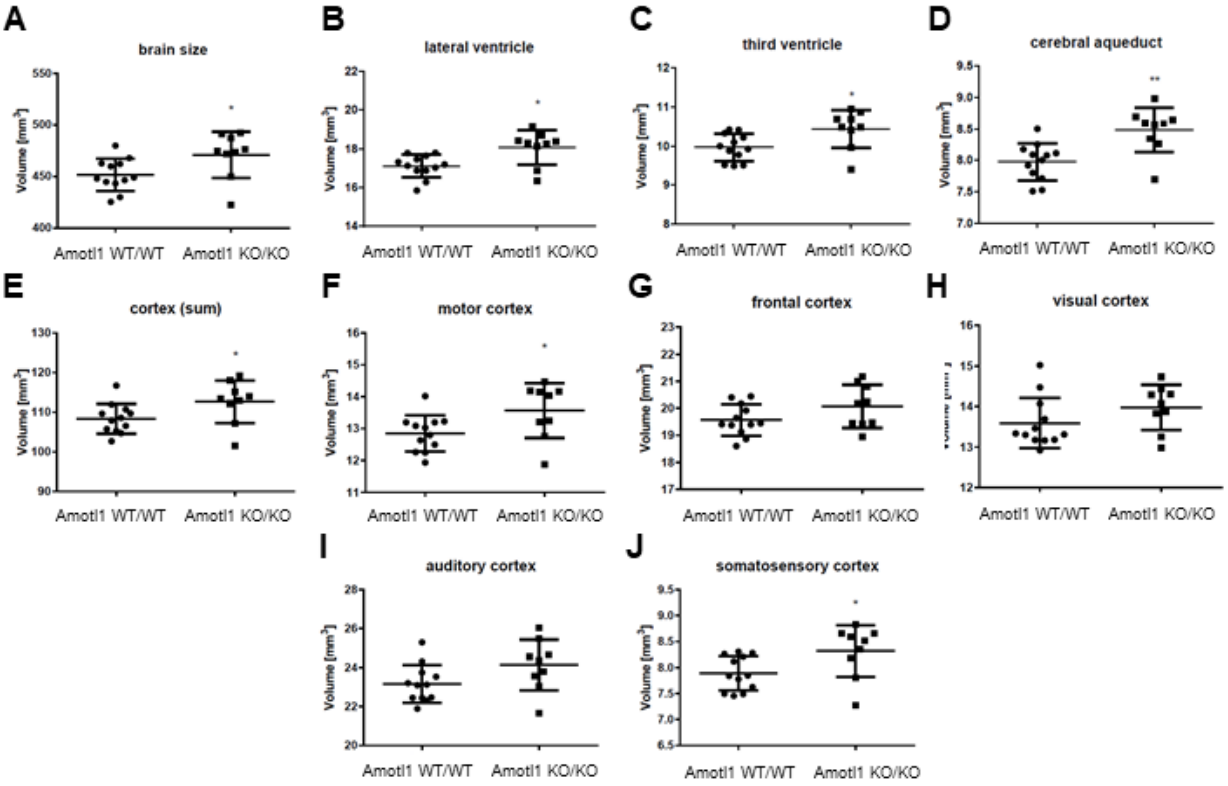

Fig. 45. Amotl1 knockout brains show increased size and larger volume of the brain ventricles and cortical structures. (A-J) MRI volumetric analysis of wild-type and knockout brains *iv vivo* showed an increase in brain size of Amotl1 knockouts (A), increased volume of the lateral (B) and third (C) ventricles and larger cerebral aqueduct structure (D). Additional analysis of the mouse brain cortex demonstrated that Amotl1 depletion leads

to larger cortical structures (E) with significant differences found in motor cortex (F) and somatosensory cortex (J), and no volumetric defects in the frontal G), visual (H) and auditory (I) cortical subfields. Experiments were performed on the following number of animals: Amot WT/WT = 12; Amotl1 KO/KO = 9. Statistical significance was analyzed using two-tailed unpaired t test. *p < 0.05. Lines represent medians, dots represent individual values. Bars represent the mean ± SD.

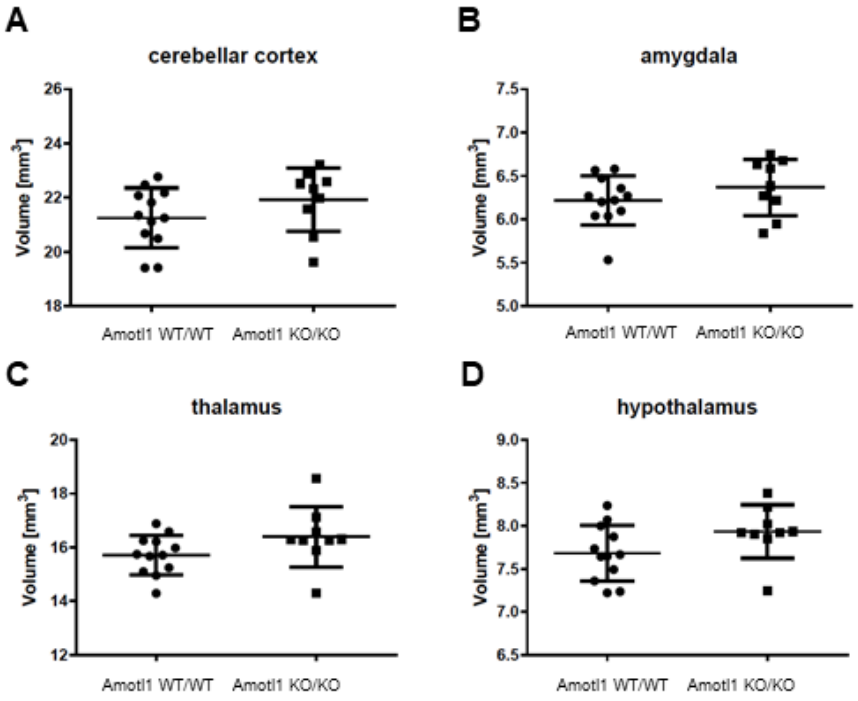

Fig. 46. Relative volumes of different brain structures in Amotl1 KO/KO mice brain. Volumetric MRI analysis showed no difference in the volume of cerebellar structure (A), amygdala (B), thalamus (C) and hypothalamus (D) between knockout and control groups. Analysis were performed on the following number of animals: Amot WT/WT = 12; Amotl1 KO/KO = 9. Statistical significance was analyzed using two-tailed unpaired t test. Lines represent medians, dots represent individual values. Bars represent the mean ± SD.

Altogether, MRI volumetric analysis showed that Amotl1 ablation causes strong increase in the whole brain volume, affecting mostly ventricles, cerebrospinal fluid volume and cortical structures.

In order to investigate and characterize the pathological processes that appear in Amotl1 depleted brains, I analyzed the brain metabolite levels through the magnetic resonance spectroscopy (MRS). N-Acetyl Aspartate (NAA) is one of the most abundant metabolite in the brain (Birken et al., 1989 [24]). I observed that Amotl1 depleted hippocampal structures have a decrease in NAA levels over the WT hippocampi (Fig. 47A). Moreover, I found an increase of

ratio between N-Acetylaspartylglutamic acid (NAAG) and NAA, whereas the levels of NAA and NAAG together was not affected (Fig. 47B-C). Interestingly, previously conducted studies have found that decreased hippocampal NAA levels are one of the features of schizophrenic brains in patients (Steen et al., 2005 [193]). Therefore, I proceeded to analysis of the metabolites related to neurotransmission, known to be affected in schizophrenia disorder, namely glutamate (Glu) and glutamine (Gln). Strikingly, the concertation of Gln was significantly increased in Amotl1 depleted brains, however the total Glu level was similar between WT and knockout mice (Fig. 48), indicating possible glutamatergic dysfunction. Importantly, increased glutamine, glutamate or its ratio have been found in the early stages of schizophrenia and in unmedicated patients (Tibbo et al., 2004 [204]; Hashimoto et al., 2005 [82]; Brandt et al., 2016 [25]; Merritt et al., 2016 [134]).

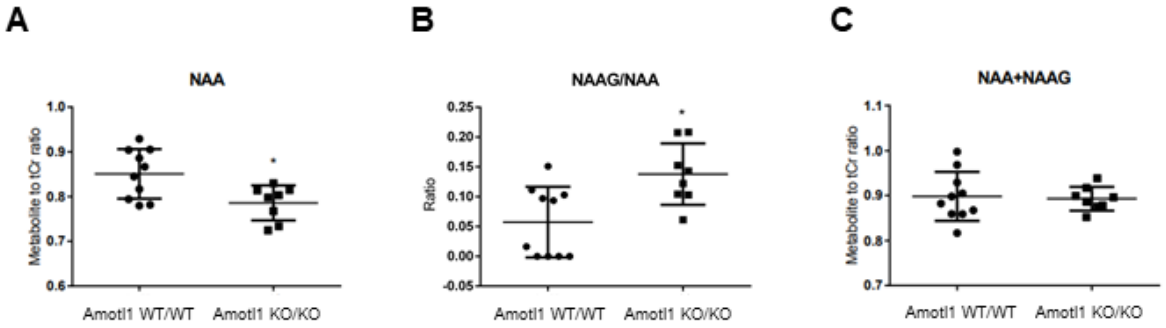

Fig. 47. Analysis of the brain metabolites distribution in Amotl1 knockouts by magnetic resonance spectroscopy. Valueas are shown as ratio of the particular metabolite to the creatine concentration. (A) Amotl1 KO/KO mice had lower level of the N-Acetyl Aspartate metabolite (NAA) and higher ratio of N-Acetylaspartylglutamic acid (NAAG) to NAA (B). (C)Cumulative NAA and NAAG concentrations were not affected by the Amotl1 deletion in the mouse brain. Analysis were performed on the brain hippocampal structure using the following number of animals: Amot WT/WT = 10; Amotl1 KO/KO = 8. Statistical significance was analyzed using two-tailed unpaired t test. Lines represent medians, dots represent individual values. Bars represent the mean ± SD.

Altogether, by using variety of experimental approaches ranging from the behavioral experiments, to morphological and molecular brain analysis, I have shown that Amotl1 knockout mice represent the features of a schizophrenia-like disorder and could be the potential model for studying this disease.

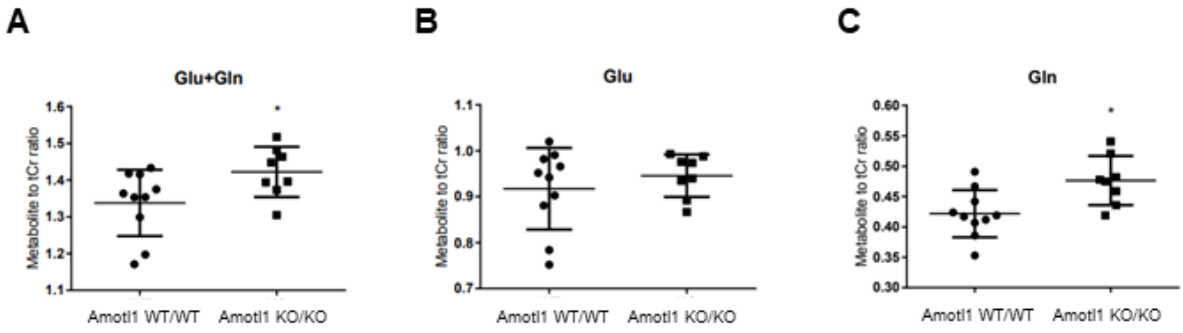

Fig. 48. Analysis of the Amotl1 knockout and control brain metabolites by magnetic resonance spectroscopy. Values are shown as ratio of the particular metabolite to the creatine concentration. (A) Amotl1 KO/KO mice showed increased level of the glutamate (Glu) and glutamine (Gln) in the hippocampal structures when compared to control brain. The level of Glu was similar in both groups, however increased Gln was detected in Amotl1 depleted hippocampi than in control wild-type brain structure. Analysis were performed on the following number of animals: Amot WT/WT = 10; Amotl1 KO/KO = 8. Statistical significance was analyzed using two-tailed unpaired t test. Lines represent medians, dots represent individual values. Bars represent the mean ± SD.

5 Discussion

The principal objective of this PhD thesis was to investigate a putative role of Amot and Amotl1 in the organization of mouse brain and behavior. Angiomotins have been studied for over a decades and their role in cellular motility, polarity, embryogenesis and cancer development has been documented. Their function in the brain is still unknown. Recently published results by Wigerius and colleagues have demonstrated that Amot p130 isoform localizes to the synaptic compartments of mature cultured hippocampal neurons where it interacts with scaffolding proteins MUPP1 and PSD95, and regulates postsynaptic specialization (Wigerius et al., 2018 [224]). Meanwhile, our group demonstrated Amot role in developing hippocampal neurons, and we showed that Amot regulates dendritic tree morphogenesis *in vitro*, where it function depends on the interaction with a Hippo pathway transcriptional co-activator, Yap1 (Rojek et al., 2019 [172]). Our experiments demonstrated that Yap1 is also indispensable for dendritic architecture in cultured hippocampal neurons. My project focused on understanding function of Amot, Amotl1 and Yap1 in the brain *in vivo*.

The molecular mechanisms of dendritogenesis have been mostly studied in cultured neuronal cells due to relative simplicity of this minimalistic system. However, the main disadvantage of the *in vitro* model is the elimination of all the possible external cues produced by surrounding environment that could have a great impact on the cellular response to the applied modifications. Studies based on cell culture do not provide insights into the consequences of genetic manipulations on the whole organism. Taking into account that behavior is a complex and the most important outcome of the brain activity, it is of a great importance to study behavioral responses *in vivo*. That became possible thanks to pioneering work of Capecchi, Evans and Smithies, who working independently developed methodology to produce knockout mouse, and that discovery has been awarded the Nobel prize in Physiology and Medicine in 2007 (Evans and Kaufman, 1981 [58]; Smithies et al., 1985 [188]; Thomas and Capecchi, 1987 [203]; Vogel, 2007 [213]). Although human brains show more complex physiological characteristic over small rodents, mice are considered as valuable model for studying human development and disease processes due to over 99% genes similarities between these two species (Capecchi, 1994 [33]). Nowadays, the mouse models have become a valuable tool for investigating the molecular and structural pathologies underlying the human neuropsychiatric disorders (Nestler and Hyman, 2010 [142]; van der Staay et al., 2009 [211]; Belzung et al., 2011 [20]).

Based on our findings on the Amot role in dendritic organization obtained from *in vitro* studies, the first part of my work concentrated on evaluating Amot and Yap1 functions in mouse brain organization and behavior. I found that Amot neuronal depletion in mice: a) leads to impaired dendrite growth in cerebellar Purkinje cells, b) inhibited cerebellar growth due to reduced thickness of its cortical molecular layer, c) affected locomotor coordination. Amot is well known for its interaction with Yap1 in many cell types. Similarly, Rojek et al. have demonstrated that these two proteins interact also in the brain (Rojek et al., 2019 [172]). Yap1 knockdown turned out to have similar phenotype in cultured cells to Amot. My work has demonstrated that the conditional knockout of Yap1 in the Purkinje cells leads to reduced Purkinje cells dendritic trees, cerebellar abnormalities and coordination impairments. Results of this part of my study have been recently published in PLOS Biology (Rojek, Krzemien* et al., 2019; * co-first author [172]). In the second project I focused on Amotl1 role in the organization of the brain. My results revealed that, in contrast to Amot mutants, Amotl1 knockout mice do not show impairments in locomotor coordination. Instead, Amotl1 depletion leads to mice hyperactivity in the open field, decreased anxiety-like behavior, social withdrawal phenotype and abnormal walking episodes and increased circling behavior. Moreover, contrary to smaller cerebellum of Amot knockouts, Amotl1 mutants have increased brain weight and size. Through the histological and magnetic resonance imaging (MRI) studies I showed that Amotl1 depletion causes increased volume of the brain ventricles and cerebrospinal fluid. In addition to ventricles enlargement, Amotl1 knockout brains present higher cortical volume with significant volumetric changes in motor and somatosensory cortical areas. Lastly, the spectroscopic analyzes of the brain metabolites concentration in Amotl1 depleted hippocampi revealed abnormal N-Acetyl Aspartate (NAA) and glutamine (Gln) levels. Hence, I found a novel function of Amotl1 protein that has significant implication in the brain organization and its depletion affects multiple aspects of a mouse behavior (unpublished work).

5.1 The neuronal function of Amot and Yap1 proteins in the mouse brain organization and behavior

5.1.1 A possible molecular mechanisms underlying Purkinje cell dendritic abnormalities and cerebellar dysfunction upon Amot and Yap1 neuronal knockout

The role of Amot and Yap1 proteins in the organization of Purkinje neurons has not been addressed in previously conducted studies. Interestingly, Yap1 expression has been found enriched in the population of progenitor cells of external granular cell layer in human fetal cerebellar tissue and has been reported as one of causative factors for the brain tumors with cerebellar origin, meduloblastoma (Orr et al., 2011 [153]).

5.1.1.1 Interaction with F-actin

Based on results obtained in our laboratory on cultured hippocampal neurons we proposed the molecular mechanism underlying the abolishment of dendritic tree complexity upon Amot protein depletion (Rojek et al., 2019 [172]). Kasia Rojek has found that Amot regulates dendritic morphogenesis through the interaction with Yap1, as neuronal transfection with Amot construct mutated Yap1-binding site did not rescue the dendritic abnormalities observed in Amot knockdown neurons. On the other hand, it is widely known that Amot, through its N-terminal ID domain, associates to F-actin and promotes actin fibers formation in a different cellular context (Ernkvist et al., 2006 [55]; Chan et al., 2013 [38]; Mana-Capelli et al., 2014 [126]). Its overexpression in endothelial cell is associated with accumulation of the actin fibers and alteration in cell shape leading to an increase in cellular area (Ernkvist et al., 2006 [55]). Moreover, recently Wigerius and rest have shown that Amot role in neuronal postsynaptic organization involves the actin cytoskeleton regulation (Wigerius et al., 2018 [224]). Importantly, actin organization is crucial for establishing neuronal shape, polarity, and it is widely involved in dendritogenesis. Different factors that control neuronal F-actin dynamics, such as actin nucleators (Arp 2/3 complexes), actin coupling proteins (cofilin-1) and extracellular neural cell adhesion molecules 1 (NCAM1) are involved in dendritic architecture (Pinyol et al., 2007 [159]; Noguchi et al., 2016 [150]; Frese et al., 2017 [63]). However, experiments performed in our laboratory suggest that Amot function in dendritic organization does not involve Amot binding to F-actin, because the phenotype observed in Amot knockdown neurons could be reversed with overexpression of Amot construct that lacked actin binding site (Rojek et al., 2019 [172]). Thus, Amot plays its role in cultured hippocampal neurons dendritogenesis in cooperation with Yap1 and independently of its interaction with F-actin. Moreover, Kasia found that Amot-Yap1 role in this process does not involve the canonic Hippo-signaling pathway. The phenotype of abnormal dendritic tree formation upon Yap1 knockdown neurons could be

rescued with ectopic expression of Yap1 mutants unable to bind to TEAD transcription factors and Amot depletion in neurons did not affect the expression of the Hippo pathway-controlled genes (Rojek et al., 2019 [172]). Instead, she demonstrated that Amot and Yap1 control dendritic tree formation through the S6 kinase (S6K) phosphorylation and its downstream target S6 ribosomal protein, which could be regulated by the mTOR complex 1. Importantly, these findings from our *in vitro* studies seem to be relevant for Amot and Yap1 neuronal function *in vivo*. First, Kasia showed that Amot coprecipitates with Yap1 from a wild-type mouse brain confirming their interaction in the brain *in vivo*. Secondly, Amot neuronal depletion in mice does not alter Hippo pathway-dependent gene expression (Rojek et al., 2019 [172]). Lastly, the levels of phosphorylated S6K and S6 ribosomal protein were significantly reduced in the cerebella of both Amot and Yap1 neuronal knockout mice.

5.1.1.2 A link to mTOR signaling

An increasing number of studies report association between Yap1, S6 kinase and mTOR regulation of organ size (Tumaneng et al., 2012 [208]; Domínguez-Calderón et al., 2016 [50]; Liu et al., 2017 [118]). Domínguez-Calderón and colleagues have shown that ablation of the tight junction-enriched protein Zona Occludens 2 (ZO-2) is linked to increased activity of Yap1, activation of mTOR pathway and S6 kinase which in summary causes increased protein synthesis and cell enlargement in the renal compensatory hypertrophy (Domínguez-Calderón et al., 2016 [50]). Importantly, the crosstalk between Angiomotins, Yap1 and mTOR has been observed recently in a mouse model and human samples of glioblastoma (GMB), the most common brain tumor composed mainly of astrocytes (Artinian et al., 2015 [12]). Here authors found that Amotl2 is phosphorylated at Ser760 via mTORC2, which blocks its binding site for Yap1, therefore, leading to increased Yap1 activity, and enhanced expression of its target genes. This in consequence causes GBM cell growth, migration and invasiveness. Although this study did not find conserved Ser760 site for mTOR2 phosphorylation in other Angiomotins, it cannot be excluded that different secondary modifications are required to promote other Motins phosphorylation by mTORC2. Thus, taking into account an increasing evidence of Angiomotins, Yap1, and mTOR cooperation in regulation of cellular shape and size, it is possible that miss-regulation of these pathways underlies the reduction of size and complexity in Amot and Yap1 Purkinje knockout cells. It has been shown that hyperactivation of mTOR1

and S6 protein in mouse Purkinje cells caused an increase in their dendritic arborization together with altered mice gait pattern and poorer RotaRod performance (Sakai et al., 2019 [176]). Furthermore, ablation of the mTORC2 component Rictor in mouse Purkinje cells leads to reduction in dendrites length and volume (Thomanetz et al., 2013 [202]). Our results on decreased S6 ribosomal protein found in cerebellar homogenates of Amot and Yap1 neuronal knockout mice additionally strengthen the hypothesis on the mTOR involvement in Amot and Yap1 dependent Purkinje cell morphogenesis. In consequence, S6 protein ablation could potentially lead to reduced translation of other proteins involved in Purkinje cells development resulting in abolished dendritic tree complexity. Another line of evidence suggests involvement of phosphatase and tensin homologue (PTEN), an upstream regulator of mTOR, in Amot and Yap1 role in Purkinje cells dendritogenesis. Yap1 has been shown to regulate PTEN expression, while Purkinje cell-specific PTEN knockout mice display abnormalities in their dendrite organization and coordination impairments among other features (Tumaneng et al., 2012 [208]; Cupolillo et al., 2016 [43]). Interestingly, mutations in PTEN have been reported as a causative factor in around 10% of Autism patients and recently Amot has been found associated with Autism spectrum disorders (McBride et al., 2010 [130]; Schanzenbächer et al., 2016 [176]). Summing up, Amot and Yap1 function in Purkinje cells dendritic organization may involve mTOR, s6 ribosomal protein and S6 kinase phosphorylation, or/and PTEN, and other mechanisms however this needs further molecular investigation that would concentrate specifically on the Purkinje neurons biology.

5.1.2 The granular cells distribution in the Amot and Yap1 knockout mice

My experiments on Amot and Yap1 neuronal knockout mice revealed decreased thickness of the cerebellar molecular layer, where dendrites of Purkinje cells are located. That morphological changes was the most pronounced in the lobes located down the preculminate fissure, which consists of neuronal leg and foot representations (Nitschke et al., 1996 [148]; Stoodley et al., 2010 [194]). Interestingly, Fujita and colleagues have recently reported that overexpression of Yap1 during development of mice modeling spinocerebellar ataxia type 1 disorder restored the reduction in molecular layer thickness and mice locomotor impairments indicating Yap1 role in the organization of this cerebellar layer and mice coordination (Fujita et al., 2017 [64]). The cerebellar molecular layer, besides enrichment of Purkinje cells dendritic

trees, contains also another type of neurons called granule cells. This small cells migrate from the external granular layer, through the molecular layer to populate their final destination in the cerebellum, the internal granule layer (Fig. 49). Recently, it has been presented that impaired radial migration of the cerebellar granule cells and their enrichment in the molecular layer is associated with a decrease in latency to fall from RotaRod and abnormal gait parameters in mice (Shintani et al., 2012 [184]). Yap1 expression has been observed in cerebellar granule neural precursor cells and its overexpression enhances proliferation of these cells (Fernandez et al., 2009 [62]; Yang et al., 2019 [229]). Thus, I aimed to analyze the distribution of granule cells over the molecular layer in Amot and Yap1 neuronal knockout mice. Surprisingly, I found a significant increase in granule cell distribution inside the cerebellar molecular layer upon neuronal Yap1 depletion, however I could not detect any similar abnormalities in Amot depleted mice (Fig. 20). This observation could explain more pronounced locomotor impairments observed in Yap1 performance assessed by the CatWalk gait analysis, where Yap1 showed significant increase in stride length that was not observed for Amot mutants. Whether this is the effect of impaired granular cell migration or abnormal proliferation would require further investigation of the cell proliferation in the external granular cell layer. Knowing that Yap1 has been previously linked to granule cells, it could have more important functions for the cerebellar organization than Amot and that subject needs deeper investigation in future.

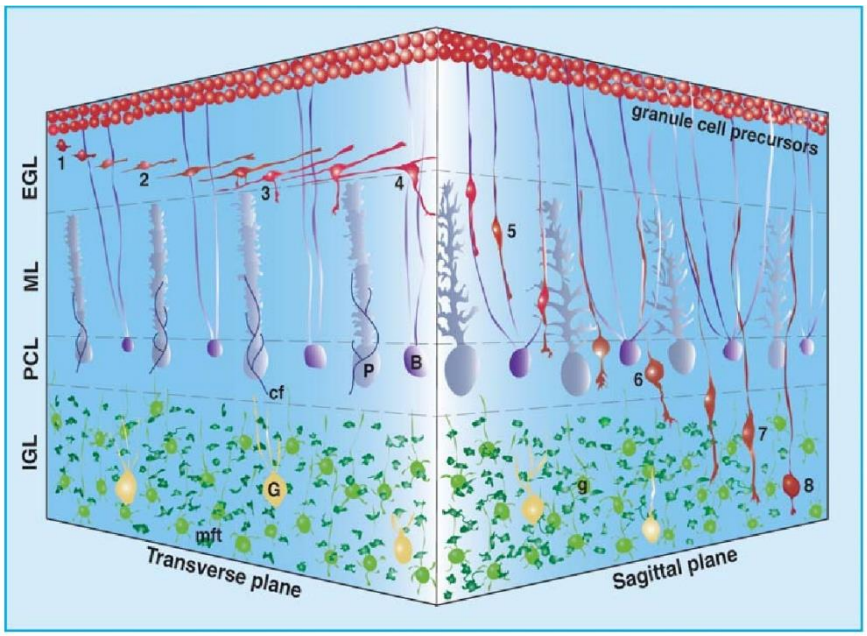

Fig. 49. Schematic representation of the granule cell migratory trail over the cerebellar cortical layers. The granule cell precursors originate from the outer external granular layer where their extensive proliferation is observed. At later stages granule cells migrate firstly in horizontal manner through external granular layer (steps 1-4 steps), following by radial migration via the molecular and the Purkinje cell layer (steps 5-6) to rich their final destination in the internal granular layer (steps 7-8). EGL- external granular layer; ML- molecular layer; PCL- Purkinje cell layer; IGL- internal granular layer; P- Purkinje cell; B- Bergmann glia; G- Golgi cell; g- postmigratory granule cell; cf- climbing fiber; mft- mossy fiber terminal. (Komuro and Yacubova, 2003).

5.1.3 The possible Amot and Yap1 functions in the brain

My analysis of the brain morphological alteration upon Amot and Yap1 neuronal depletion reveled reduced cerebellar size in both knockouts, and no gross abnormalities for the structure of both brain hemispheres. The initial experiments on *Synapsin-Cre* transgenic mice line crossed with a *STOP-Tomato* reporter strain revealed previously unknown limitation of the Cre expression under Synapsin promoter in mice. I found the abundant Cre expression in cerebellar Purkinje cells, whereas only certain in the hippocampal subfields. This could potentially explain why observed phenotypes were restricted to cerebellar regions. Importantly, Huang and co-workers have found that Yap1 depletion in glial cells leads to reduction in whole brain size, however the authors have used nestin-Cre line to drive excision of the Yap1 sequence and interpreted their result as a consequence of the loss of Yap1 function solely in glial cells. In these mice Cre is expressed in progenitors of both glial and neural lineages, and thus the observed phenotype could result from Yap1 depletion in neurons

simultaneously (Huang et al., 2016 [91]). Therefore, based on the above and on our *in vitro* experiments that were performed on hippocampal neurons I hypothesize that if broader Cre-mediated deletion could be achieved in neurons, I would find more brain regions affected by Amot and Yap1 depletion. Thus, further research should address the possible Amot and Yap1 neuronal function in the other brain regions.

Summing up, this part of my PhD dissertation uncovered unknown Amot and Yap1 functions in the mouse Purkinje cell dendritic tree architecture, cerebellar organization, and locomotor coordination. Further research should refer to questions about the link between Amot, Yap1, and mTOR. Interesting direction to study would be to investigate in more detail Yap1 role in granule cells *in vivo*. Lastly, further studies should assess the Amot and Yap1 neuronal function in the organization of other brain structures.

5.2 The function of Amotl1 in the brain

5.2.1 Amotl1- the potential molecular mechanisms

The second part of my PhD studies was concentrated on the second Angiomotin family member, Amotl1. This protein has never been studied in the context of neuronal organization, nor brain morphogenesis. I found that Amotl1 depletion causes increase in the total brain weight, which provides another important insight into Angiomotins involvement in organs size and growth control (Zhao et al., 2011 [235]; Zhao et al., 2011 [236]; Zhao et al., 2010 [234]; Zhao et al., 2007 [237]). Similarly to Amot, Amotl1 has been shown to bind directly Yap1 protein, and Yap1 glial and neuronal knockout brains were smaller in size (Zhao et al., 2011 [235]; Huang et al., 2016 [91]). The possible relationship between Amotl1, Yap1 and Hippo pathway dependent regulation of the brain cells proliferation and the brain size serves as novel interesting subject to study. Although this year report from Zhou and colleagues indicated the Amotl1 has a role in Yap1 activation of pro-proliferating genes in gastric cancer, it is widely known that Angiomotins differently regulate Yap1 function depending on the tissue context (Zhou et al., 2020 [241]). Another study has shown that in tight junctions of cardiomyocytes Amotl1 forms a complex with Yap1 and protocadherin Fat4, an upstream regulator of Hippo signaling, and Fat4 knockout leads to overexpression of the Hippo-dependent genes, increased cardiomyocyte size and proliferation, and heart growth (Ragni et al., 2017 [166]). In MDCK and

HEK293T cells knockdown of Angiomotins causes loss of Yap1 from the tight junctions, drop of Yap1 phosphorylation and its increased nuclear localization (Zhao et al., 2011 [235]). Depending on the available partners and cellular context Amotl1 might act as inhibitor or facilitator of Yap1. Thus, it cannot be excluded that Amotl1 function in brain tissue involves regulation of Yap1 protein resulting in preventing its translocation to the cell nucleus.

5.2.1.1 The cause of enlarged lateral ventricles upon Amotl1 depletion

My further histological and magnetic resonance imaging experiments revealed that Amotl1-depleted brains have enlarged volumes of the brain ventricles and cortical tissue, which most likely contributes to observed increase in the brain weight. Interestingly, it has been shown that FAT Atypical Cadherin 4 (Fat4) is implicated in the pathogenesis of cortical malformations, such as periventricular neuronal heterotopia, where mislocalization of cortical neurons are observed and could lead to increased cortical thickness (Cappello et al., 2013 [34]; Watrin et al., 2015 [218]). Cappello and colleagues found that Fat4 depletion in the mouse developing neuroepithelium, which line the ventricle walls, leads to increased neuronal progenitor proliferation and defects in neuronal migration through the cortical layers (Cappello et al., 2013 [34]). Moreover, authors demonstrated that in cerebral cortex Yap1 acts downstream of Fat4 in mediating neuronal proliferation. Because Amotl1 interacts with Fat4 protein in cellular junctions, and radial glial cells that produce all cerebral neurons are anchored in neuroepithelium by junctional complexes, it is possible that this molecular mechanism is involved in increased cerebral volume of Amotl1 depleted brains. Importantly, the Amotl1 knockout mouse line that I have generated has systemic deletion of the Amotl1 in all cells and tissues. Amotl1 is widely involved in the tight junctional complexes integrity and stability in epithelial cells. Thus, this Amotl1 function may contribute to some features of observed Amotl1 KO/KO phenotype, such as increased volume of CSF and ventricles enlargement. Recently, it has been reported that ablation of the Alix TJs protein results in disassembly of actomyosin-TJs polarity complex in choroid plexus structure, which resulted in exclusions of cells from epithelial layer, dysfunction in primary and motile cilia, loss of the control over CSF production and hydrocephalus in mice (Campos et al., 2016 [32]). The authors indicated involvement of Alix interaction with ZO-1 in these processes, the cell junctional marker protein which together with Amotl1 stabilize TJs integrity (Patrie et al., 2005 [156]; Skouloudaki et al.,

2012 [187]). Moreover, numbers of reports indicated another TJs protein that is involved in ventricles enlargement and increased CSF volume, the Mupp1/MPDZ protein (Feldner et al., 2017 [61]; Saugier-Veber et al., 2017 [177]; Yang et al., 2019 [227]). Felder and colleagues have found that although the global MPDZ knockout mice develop these hydrocephalus features, no changes in the brain vasculature could be detected and endothelial specific MDPZ ablation did not cause that phenotype. Instead, authors indicated the crucial role of radial glial cells in these process by using the Nestin promotor-driven Cre expression, that in fact leads to MDPZ depletion in all neuronal cells. Amotl1 protein has been also found to interact with MPDZ polypeptide in epithelial cells and more importantly Amot-p130 interacts and colocalizes with Mupp1/MPDZ protein at synapses in mature hippocampal neurons (Wigerius et al., 2018 [224]; Sugihara-Mizuno et al., 2007 [198]). Felder interpreted their results of MPDZ driven hydrocephalus phenotype as the effect of abnormalities in radial glia cells and there is no studies so far indicating synaptic dysfunction involvement in developing brain ventricles enlargement. Future studies should address this subject of potential neurotransmission impairments. Thus, knowing that Amotl1 localizes to synapses in mature neurons where it potentially could interact with MPDZ protein, we cannot exclude that neuronal Amotl1 function at synapses contributes to observed phenotype in Amotl1 KO/KO mice of enlarged ventricles and higher CFS volumes.

Although during my studies I found significant changes in the size of lateral and third ventricles, and increased CFS volume in the brain upon Amotl1 depletion, Amotl1 knockout animals did not develop a visible hydrocephalic features, with swollen and enlarged skull. Importantly, an increased lateral ventricles volume is recognized as the brain morphological hallmark of schizophrenia disorder both in patients and mouse models of the disease (Fig. 50; Jaaro-Peled et al., 2010 [105]). Recent study indicated the claudin-5 tight junction protein, that is strongly enriched in the blood-brain barrier of endothelial cells, as a potential risk factor for schizophrenia development (Greene et al., 2018 [73]). Its targeted ablation in mouse hippocampus or medial prefrontal cortex area led to distinct behavioral changes that authors linked to psychosis. Moreover, they found claudin-5 expression aberrant in schizophrenia patients and they showed that antipsychotic drugs increased claudin-5 expression both *in vitro* and *in vivo*. To date, no other TJs enriched protein have been implicated in schizophrenia development.

My structural and volumetric analysis of *Amotl1 KO/KO* brains revealed several significant abnormalities upon Amotl1 ablation. That results open a novel and wide subject for further research which should concentrate on the molecular and cellular mechanisms underlying brain structural impairments. One line of studies should address the question of the cell type origin of observed impairments, whether endothelial, neuronal or other cells contribute to these abnormalities. Importantly, the neurogenesis inside the cerebral cortex during development and in adult ages should be addressed. Moreover, the integrity of epithelial cells lying the ventricle walls and the blood-brain barrier should be investigated in these mice. Another important aspect to study would consider ventricular walls ciliary number and structure, choroid plexus organization and the flow of the CSF upon Amotl1 depletion. This could help explain the origin of increased CSF volume found in *Amotl1 KO/KO* brains. Lastly, the molecular mechanisms underlying *Amotl1 KO/KO* brain structural phenotype and identification of Amotl1 binding partners in neurons should be investigated.

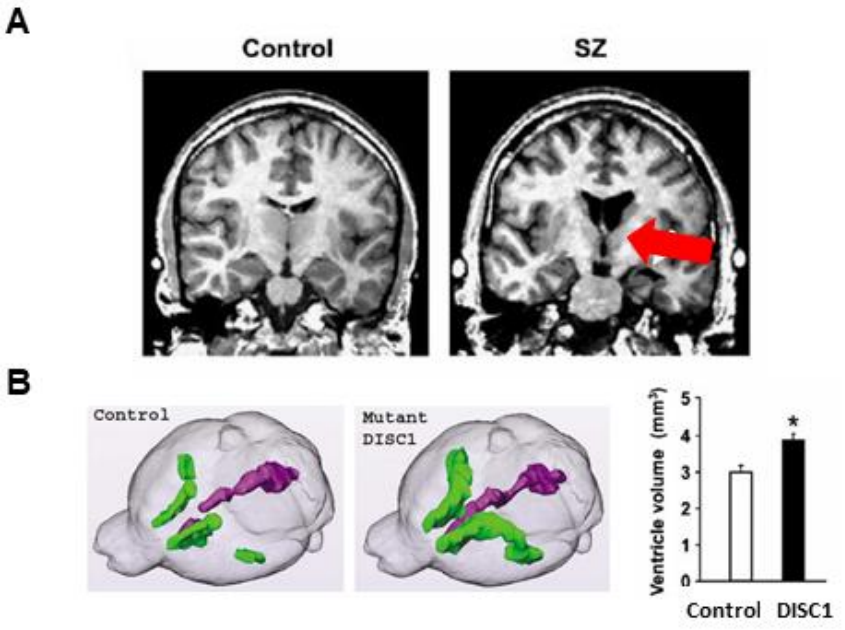

Fig. 50. Enlarged lateral ventricles observed in Schizophrenia patients and mouse model of the disease. A) In vivo resonance magnetic imaging scans of healthy individual (control) and schizophrenia patient (SZ). Red arrow indicate the lateral ventricle area B) Results of in vivo magnetic resonance scanning of the mouse schizophrenia model, DISC1 knockout. On the left side is the 3D reconstructions of control (wild-type) and DISC1 mutant mice brains. Green color represents the lateral ventricles, whereas purple shows third and fourth ventricles. Quantification of the lateral ventricles volumes from the wild-type controls and DISC1 knockouts are presented on the right side. (Pletnikov et al., 2008; Jaaro-Peled et al., 2009; modified).

5.2.2 The relevance of behavioral abnormalities found in Amotl1 knockout mice to neuropsychiatric disorders

The behavioral experiments that I have conducted on *Amotl1 KO/KO* mice revealed great number of aberrations. Interestingly, in contrast to Amot mutants, Amotl1 deficient mice do not seem to have impaired locomotor coordination as shown by RotaRod and foot-print assay. The MRI volumetric analysis also did not detect any gross abnormalities in the *Amotl1 KO/KO* mice cerebella. *Amotl1 KO/KO* mice exhibit increased locomotion and reduced anxiety measured by the time spent in center arena of the Open Field. Thus, longer distance traveled presents rather their hyperactive behavior in response to novelty then reaction to stressful conditions because at the same time they did not avoid the center, anxiogenic arena. Their anxiolytic phenotype I further confirmed with the marble burying experiments, and their tendency to burry much fewer marbles then wild-type age and sex matched control mice. Strikingly, these mice do not exhibit any signs of anxiety during handling procedures. Moreover, Amotl1 depletion causes social withdrawal phenotype in mice indicted by impaired nesting behavior, no preference for direct contact with unfamiliar conspecific over novel object and no approach to social odor assessed with the automated Eco-Hab approach. Lastly, I observed abnormal locomotor activity in Amotl1 mutants, such as backward walking and increased circling behavior.

Altogether several behavioral abnormalities found in Amotl1 mutants demonstrate their emotional and possible cognitive impairments that could model the features of neurodevelopmental disorders found in human. Hyperactivity, abnormal anxiety and social deficits have been previously observed in animal models of numerous neuropsychiatric disorders such as Autism spectrum disorder, Fragile X syndrome and Schizophrenia (Kazdoba et al., 2016 [98]; Kazdoba et al., 2014 [99]; Park et al., 2015 [155]). Among two others, one of the core symptoms of Autism is increased repetitive/stereotyped motor behaviors, which is widely reflected in mouse models of the disease in more frequent grooming of their body parts or increased digging in their home-cage bedding (Patterson et al., 2011 [157]). Interestingly, recent brain structural imaging study found association between Autism spectrum disorder and enlarged brain lateral ventricles in human (Turner et al., 2016 [209]). Considering enlargement of brain ventricles volume in Amotl1 mutants and all their behavioral abnormalities, I analyzed

their self-grooming and digging behavior. Although these mice showed no tendency to increased repetitive behaviors, I could not fully exclude their relevance to Autism at that stage of my study, due to heterogeneity of that disorder and diversity of behavioral impairment presented by mouse models of Autism spectrum disorder.

My further analysis of *Amotl1 KO/KO* mice activity brought me to the surprising observation of their recurring locomotion in backward direction. To date, backward walking in rodents is rarely observed. A study by Becker and colleagues found that mice carrying loss-of-function mutation in gene encoding a transient receptor potential channel 3 protein (TRPC3) display backward walking phenotype and on the cellular level abnormal Purkinje cell growth, differentiation and aberrant dendritic arborization has been reported (Becker et al., 2009 [18]). However, these so called "moonwalker" mice, presented severe cerebellar ataxia phenotype with impaired locomotor coordination showed in increased gait width, reduced latency to fall from rod and visible defects in basic locomotion resulting in the constant flat body position. Similarly, one more recent study linked the cerebellar ataxia phenotype in mice to their moonwalking behavior (Kumar et al., 2011 [111]). Interestingly, with the beginning in 1960s, the administration of hallucinogenic drugs to rats, such as amphetamine or fenfluramine which leads to increased dopamine and serotonin brain levels, has been linked with backward walking and increased circling behavior (Smythies et al., 1967 [189]; Schneider et al., 1968 [179]). Thus, this abnormal locomotion has been suggested as the animal behavioral response to hallucination, similar to the schizophrenia-like visual and auditory hallucinations caused by high dosage of amphetamine in human (Davis et al., 1978 [49]; Curzon et al., 1979 [44]; Snyder et al., 1973 [190]). Strikingly, the backward walking phenotype that I have observed in Amotl1 mutants was associated with increased circling behavior, while no coordination impairments was detected. Thus, I hypothesize that their abnormal locomotion could be the result of increased dopamine/serotonin levels and impaired neurotransmission which cases abnormal brain activity and hallucinations. Moreover, Genome-wide Association Study revealed that Amotl1 could be the potential factor related to a mood disorders and several studies implicated *Amotl1* locus with schizophrenia (Roussos et al., 2016 [175]; Mohamoud et al., 2018 [137]; GeneCards). Thus, my results from Amotl1 mutants behavioral studies together with published records strongly suggest that Amotl1 has a fundamental role in mice behavior and its ablation could result in schizophrenia-like phenotype in mice. Future studies should

address the brain serotonin/dopamine neurotransmission and investigate more detailed aspects of *Amotl1 KO/KO* mice behavior, such as ultrasonic vocalization and pre-pulse inhibition that are often affected in schizophrenia mice models.

5.2.3 The possible explanation of abnormal NAA/NAAG and glutamate metabolite levels in the Amotl1 knockout brain and its relevance to the schizophrenia

All of the described above brain morphological and behavioral impairments found in Amotl1 KO/KO indicate that depletion of Amotl1 causes serious abnormalities in the brain function that could be relevant to schizophrenia-like features in humans and mice models of the diseases. Because abnormal concentrations of brain metabolites play an important role in the pathology of the brain disorders and may mediate the cognitive impairments I aimed to analyze the main brain metabolites in Amotl1 mutants. The proton magnetic resonance spectroscopy analysis revealed that over several other metabolites found at normal concentrations, there are lower NAA levels, increased NAAG to NAA ratio and significantly elevated Glu and Gln (Glx) concertation in Amotl1 depleted hippocampi. Strikingly, similar affection of metabolites levels are broadly found in brains of schizophrenic patients, and are generally interpreted as markers of glutamatergic dysfunction (Steen et al., 2005 [193]; Tibbo et al., 2004 [204]; Hashimoto et al., 2005 [82]; Brandt et al., 2016 [25]; Merritt et al., 2016 [134]; Duarte et al., 2019 [52]). The possible explanation of the increased Glx levels in the brains of schizophrenia patients is the impairments in neuronal-glial interactions found by several studies (Mitteraurer et al., 2014 [136]; Bernstein et al., 2009 [22]). In proper glutamatergic neurotransmission Glu is released from the presynaptic neuron to the synaptic cleft where it binds to the NMDA receptors located on the postsynaptic cell membrane. Later it is actively transported into adjacent glial cell, converted by glutamine synthetase into Gln and transported back into the neuron, which again synthetizes Glu (Daikhin et al., 2000 [46]). And although NAA does not act directly in glutamatergic neurotransmission, it is the precursor for NAAG synthesis, which in fact modulates Glu synaptic release (Agarwal et al., 2012 [2]). This complex local cellular network is called tripartite synapse. When the receptors on astrocytes are nonfunctional or the neuronal-astrocyte connection is lost it could lead to uncontrolled synaptic information flux, resulting in abnormal information processing in brought neuronal-glial networks and generalization of the information processing underlying delusions and

hallucinations in schizophrenia patients (Mitteraurer et al., 2014 [136]). Whether Amotl1 protein is engaged in the proper organization of tripartite synapses in the brain and if so, which domain of this network is affected upon Amotl1 depletion (e.g. neural-astrocyte junctional connection, NMDA receptors function, Gln synthesis) is far from our understanding. Thus my results presenting impaired metabolite concentration in Amotl1 depleted brains provide the novel, wide and extremely interesting field to study for neuroscience research.

Hence, taking together the results of my studies on the Amotl1 function in the brain organization and mice behavior, insight from GWAS and already published data obtained from patients and mice models of schizophrenia disorder, I propose the hypothesis that Amotl1 is a novel molecular factor involved in the development of schizophrenia-like disorder in mice. Future studies should analyze in more detail the a possible behavioral cognitive impairments, molecular mechanisms underlying the brain structural abnormalities and aberrant metabolites concentrations in Amotl1 knockout mice. Additionally, the analysis of neuronal structures, dendritic organization and particular neuronal circuits connectivity would be desirable. Lastly, further studies should investigate whether the epithelial cells, neurons or astrocytes are the primary source for all these impairments. However, taking into account that schizophrenia is among the most heterogeneous neurodevelopmental disorders, I hypothesize that Amotl1 depletion causes simultaneous abnormalities possibly in all these cell types that altogether result in schizophrenia-like features visible on multiple levels of the organism.

6 Concluding remarks

Proper organization of neuronal dendritic arbors is crucial for the formation of functional neuronal circuits, and hence appropriate transmission of information within the central and peripheral nervous system. Alterations in dendritic tree morphogenesis, such as dendrites shrinkage, reduced number of branching points or abnormal density of dendritic spines have been reported in the brains of individual's diagnosed with various neurodevelopmental or neuropsychiatric disorders like Rett syndrome, Autism spectrum disorders, Down's syndrome or Schizophrenia. Results of my studies presented in this dissertation indicate a novel important role of Angiomotin proteins (Amot and Amotl1) in the brain organization and behavior. Regarding similarities in their domain organization, these two proteins often present a diverse function for multiple physiological and pathological conditions. Here I found that Amot is implicated in organization and function of mice cerebellum, whereas Amotl1 has its role in multiple levels of the brain organization and mice emotional responses. However, the conclusion about its diverse function in CNS is not accurate at that stage of our knowledge, due to different models used in my study (Amot neuronal specific knockout, Amotl1 global mutant). Further research should investigate the role of residual Angiomotin family member, Amotl2 protein, in the CNS organization and function. My results open a novel interesting field to study that in the long-term could lead to the establishment of a new treatment modalities for neurodevelopmental disorders.

7 References

1. Aase K, Ernkvist M, Ebarasi L, et al. Angiomotin regulates endothelial cell migration during embryonic angiogenesis. Genes Dev. 2007;21(16):2055-2068.
2. Agarwal N, Renshaw PF. Proton MR spectroscopy-detectable major neurotransmitters of the brain: biology and possible clinical applications. AJNR Am J Neuroradiol. 2012;33(4):595-602.
3. Agarwala S, Duquesne S, Liu K, et al. Amotl2a interacts with the Hippo effector Yap1 and the Wnt/β-catenin effector Lef1 to control tissue size in zebrafish. Elife. 2015;4:e08201.
4. Alberts JR, Galef BG Jr. Acute anosmia in the rat: a behavioral test of a peripherally-induced olfactory deficit. *Physiol Behav*. 1971;6(5):619-621.
5. Alemán-Gómez, Y., L. Melie-García, and P. Valdés-Hernandez. 2006. "IBASPM: Toolbox for automatic parcellation of brain structures." In 12th Annual Meeting of the Organization for Human Brain Mapping. Neuroimage.
6. Alves-Sampaio A, Troca-Marín JA, Montesinos ML. NMDA-mediated regulation of DSCAM dendritic local translation is lost in a mouse model of Down's syndrome. J Neurosci. 2010;30(40):13537-13548.
7. Angoa-Pérez M, Kane MJ, Briggs DI, Francescutti DM, Kuhn DM. Marble burying and nestlet shredding as tests of repetitive, compulsive-like behaviors in mice. *J Vis Exp*. 2013;(82):50978.
8. Arikkath J, Israely I, Tao Y, Mei L, Liu X, Reichardt LF. Erbin controls dendritic morphogenesis by regulating localization of delta-catenin. J Neurosci. 2008;28(28):7047-7056.
9. Arikkath J. Molecular mechanisms of dendrite morphogenesis. Front Cell Neurosci. 2012;6:61.
10. Armstrong D, Dunn JK, Antalffy B, Trivedi R. Selective dendritic alterations in the cortex of Rett syndrome. J Neuropathol Exp Neurol. 1995;54(2):195-201.
11. Armstrong DD. Rett syndrome neuropathology review 2000. Brain Dev. 2001;23 Suppl 1:S72-S76.
12. Artinian N, Cloninger C, Holmes B, Benavides-Serrato A, Bashir T, Gera J. Phosphorylation of the Hippo Pathway Component AMOTL2 by the mTORC2 Kinase Promotes YAP Signaling, Resulting in Enhanced Glioblastoma Growth and Invasiveness. J Biol Chem. 2015;290(32):19387-19401.
13. Ascoli GA. Progress and perspectives in computational neuroanatomy. Anat Rec. 1999;257(6):195-207.
14. Aversi-Ferreira TA, de Araújo MFP, Lopes DB, Nishijo H. History, citoarchitecture and neurophysiology of human and nonhuman primates' parietal lobe: A review. Dement Neuropsychol. 2010;4(3):173-180.
15. Bai J, Trinh TL, Chuang KH, Qiu A. Atlas-based automatic mouse brain image segmentation revisited: model complexity vs. image registration. Magn Reson Imaging. 2012;30(6):789-798.
16. Bajada CJ, Haroon HA, Azadbakht H, Parker GJM, Lambon Ralph MA, Cloutman LL. The tract terminations in the temporal lobe: Their location and associated functions. Cortex. 2017;97:277-290.
17. Bastianelli E. Distribution of calcium-binding proteins in the cerebellum. *Cerebellum*. 2003;2(4):242-262.
18. Becker EB, Oliver PL, Glitsch MD, et al. A point mutation in TRPC3 causes abnormal Purkinje cell development and cerebellar ataxia in moonwalker mice. Proc Natl Acad Sci U S A. 2009;106(16):6706-6711.

19. Becker L, Mito T, Takashima S, Onodera K. Growth and development of the brain in Down syndrome. Prog Clin Biol Res. 1991;373:133-152.
20. Belzung C, Lemoine M. Criteria of validity for animal models of psychiatric disorders: focus on anxiety disorders and depression. Biol Mood Anxiety Disord. 2011;1(1):9.
21. Benavides-Piccione R, Ballesteros-Yáñez I, de Lagrán MM, et al. On dendrites in Down syndrome and DS murine models: a spiny way to learn. Prog Neurobiol. 2004;74(2):111-126.
22. Bernstein H, Steiner J, Bogerts B. Glial cells in schizophrenia: pathophysiological significance and possible consequences for therapy. Journal Expert Review of Neurotherapeutics; Volume 9, 2009 - Issue 7.
23. Berret E, Kim SE, Lee SY, Kushmerick C, Kim JH. Functional and structural properties of ion channels at the nerve terminal depends on compact myelin. J Physiol. 2016;594(19):5593-5609.
24. Birken DL, Oldendorf WH. N-acetyl-L-aspartic acid: a literature review of a compound prominent in 1H-NMR spectroscopic studies of brain. *Neurosci Biobehav Rev*. 1989;13(1):23-31.
25. Brandt AS, Unschuld PG, Pradhan S, et al. Age-related changes in anterior cingulate cortex glutamate in schizophrenia: A (1)H MRS Study at 7 Tesla. *Schizophr Res*. 2016;172(1-3):101-105.
26. Bratt A, Wilson WJ, Troyanovsky B, et al. Angiomotin belongs to a novel protein family with conserved coiled-coil and PDZ binding domains [published correction appears in Gene. 2003 May 22;310;231. Meir, EG [corrected to Van Meir, EG]]. Gene. 2002;298(1):69-77.
27. Broadbelt K, Byne W, Jones LB. Evidence for a decrease in basilar dendrites of pyramidal cells in schizophrenic medial prefrontal cortex. Schizophr Res. 2002;58(1):75-81.
28. Broca PP. Loss of speech, chronic softening and partial destruction of the anterior left lobe of the brain. Bulletin de la Société Anthropologique. 1861;2:235–238
29. Buckner RL. The cerebellum and cognitive function: 25 years of insight from anatomy and neuroimaging. Neuron. 2013;80(3):807-815.
30. Buitrago MM, Schulz JB, Dichgans J, Luft AR. Short and long-term motor skill learning in an accelerated rotarod training paradigm. *Neurobiol Learn Mem*. 2004;81(3):211-216.
31. Campbell DB, D'Oronzio R, Garbett K, et al. Disruption of cerebral cortex MET signaling in autism spectrum disorder. Ann Neurol. 2007;62(3):243-250.
32. Campos Y, Qiu X, Gomero E, et al. Alix-mediated assembly of the actomyosin-tight junction polarity complex preserves epithelial polarity and epithelial barrier. Nat Commun. 2016;7:11876.
33. Capecchi MR. Targeted gene replacement. Sci Am. 1994;270(3):52-59.
34. Cappello S, Gray MJ, Badouel C, et al. Mutations in genes encoding the cadherin receptor-ligand pair DCHS1 and FAT4 disrupt cerebral cortical development. *Nat Genet*. 2013;45(11):1300-1308.
35. Cardinal RN, Parkinson JA, Hall J, Everitt BJ. Emotion and motivation: the role of the amygdala, ventral striatum, and prefrontal cortex. Neurosci Biobehav Rev. 2002;26(3):321-352.
36. Carreno-Munoz MI, Martins F, Medrano MC, et al. Potential Involvement of Impaired BK_{Ca} Channel Function in Sensory Defensiveness and Some Behavioral Disturbances Induced by Unfamiliar Environment in a Mouse Model of Fragile X Syndrome. *Neuropsychopharmacology*. 2018;43(3):492-502.
37. Chan SW, Lim CJ, Chong YF, Pobbati AV, Huang C, Hong W. Hippo pathway-independent restriction of TAZ and YAP by angiomotin. J Biol Chem. 2011;286(9):7018-7026.

38. Chan SW, Lim CJ, Guo F, Tan I, Leung T, Hong W. Actin-binding and cell proliferation activities of angiomotin family members are regulated by Hippo pathway-mediated phosphorylation. J Biol Chem. 2013;288(52):37296-37307.
39. Charych EI, Akum BF, Goldberg JS, et al. Activity-independent regulation of dendrite patterning by postsynaptic density protein PSD-95. J Neurosci. 2006;26(40):10164-10176.
40. Chenji Wang, Jian An, Pingzhao Zhang, Chen Xu, Kun Gao, Di Wu, Dejie Wang, Hongxiu Yu, Jun O. Liu, Long Yu; The Nedd4-like ubiquitin E3 ligases target angiomotin/p130 to ubiquitin-dependent degradation. Biochem J 1 June 2012; 444 (2): 279–289.
41. Cline HT. Dendritic arbor development and synaptogenesis. Curr Opin Neurobiol. 2001;11(1):118-126.
42. Collins A, Koechlin E. Reasoning, learning, and creativity: frontal lobe function and human decision-making. PLoS Biol. 2012;10(3):e1001293.
43. Cupolillo D, Hoxha E, Faralli A, et al. Autistic-Like Traits and Cerebellar Dysfunction in Purkinje Cell PTEN Knock-Out Mice. Neuropsychopharmacology. 2016;41(6):1457-1466.
44. Curzon G, Fernando JC, Lees AJ. Backward walking and circling: behavioural responses induced by drug treatments which cause simultaneous release of catecholamines and 5-hydroxytryptamine. Br J Pharmacol. 1979;66(4):573-579.
45. Cushing H, Goetsch E. Concerning the secretion of the infundibular lobe of the pituitary body and its presence in the cerebrospinal fluid. Amer J Physiol. 1910;27:60–86.
46. Daikhin Y, Yudkoff M. Compartmentation of brain glutamate metabolism in neurons and glia. J Nutr. 2000;130(4S Suppl):1026S-31S.
47. Dailey ME, Smith SJ. The dynamics of dendritic structure in developing hippocampal slices. J Neurosci. 1996;16(9):2983-2994.
48. Davis M, Whalen PJ. The amygdala: vigilance and emotion. Mol Psychiatry. 2001;6(1):13-34.
49. Davis WM, Bedford JA, Buelke JL, et al. Acute toxicity and gross behavioral effects of amphetamine, four methoxyamphetamines, and mescaline in rodents, dogs, and monkeys. Toxicol Appl Pharmacol. 1978;45(1):49-62.
50. Domínguez-Calderón A, Ávila-Flores A, Ponce A, et al. ZO-2 silencing induces renal hypertrophy through a cell cycle mechanism and the activation of YAP and the mTOR pathway. Mol Biol Cell. 2016;27(10):1581-1595.
51. Donald S, Humby T, Fyfe I, et al. P-Rex2 regulates Purkinje cell dendrite morphology and motor coordination. *PNAS*. 2008, 105 (11) 4483-4488.
52. Duarte JMN, Xin L. Magnetic Resonance Spectroscopy in Schizophrenia: Evidence for Glutamatergic Dysfunction and Impaired Energy Metabolism. Neurochem Res. 2019;44(1):102-116.
53. Edsbagge M, Tisell M, Jacobsson L, Wikkelso C. Spinal CSF absorption in healthy individuals. Am J Physiol Regul Integr Comp Physiol. 2004;287:R1450–1455.
54. Eiland L, McEwen BS. Early life stress followed by subsequent adult chronic stress potentiates anxiety and blunts hippocampal structural remodeling. Hippocampus. 2012;22(1):82-91.
55. Ernkvist M, Aase K, Ukomadu C, et al. p130-angiomotin associates to actin and controls endothelial cell shape. FEBS J. 2006;273(9):2000-2011.
56. Ernkvist M, Birot O, Sinha I, et al. Differential roles of p80- and p130-angiomotin in the switch between migration and stabilization of endothelial cells. Biochim Biophys Acta. 2008;1783(3):429-437.
57. Ernkvist M, Luna Persson N, Audebert S, et al. The Amot/Patj/Syx signaling complex spatially controls RhoA GTPase activity in migrating endothelial cells. Blood. 2009;113(1):244-253.
58. Evans MJ, Kaufman MH. Establishment in culture of pluripotential cells from mouse embryos. Nature. 1981;292(5819):154-156.

59. Fama R, Sullivan EV. Thalamic structures and associated cognitive functions: Relations with age and aging. Neurosci Biobehav Rev. 2015;54:29-37.
60. Fedorov A, Beichel R, Kalpathy-Cramer J, et al. 3D Slicer as an image computing platform for the Quantitative Imaging Network. Magn Reson Imaging. 2012;30(9):1323-1341.
61. Feldner A, Adam MG, Tetzlaff F, et al. Loss of Mpdz impairs ependymal cell integrity leading to perinatal-onset hydrocephalus in mice. *EMBO Mol Med*. 2017;9(7):890-905.
62. Fernandez-L A, Northcott PA, Dalton J, et al. YAP1 is amplified and up-regulated in hedgehog-associated medulloblastomas and mediates Sonic hedgehog-driven neural precursor proliferation. *Genes Dev*. 2009;23(23):2729-2741.
63. Frese CK, Mikhaylova M, Stucchi R, et al. Quantitative Map of Proteome Dynamics during Neuronal Differentiation. Cell Rep. 2017;18(6):1527-1542.
64. Fujita K, Mao Y, Uchida S, et al. Developmental YAPdeltaC determines adult pathology in a model of spinocerebellar ataxia type 1. Nat Commun. 2017;8(1):1864.
65. Gagné V, Moreau J, Plourde M, et al. Human angiomotin-like 1 associates with an angiomotin protein complex through its coiled-coil domain and induces the remodeling of the actin cytoskeleton. Cell Motil Cytoskeleton. 2009;66(9):754-768.
66. Gao FB. Molecular and cellular mechanisms of dendritic morphogenesis. Curr Opin Neurobiol. 2007;17(5):525-532.
67. Giacometti E, Luikenhuis S, Beard C, Jaenisch R. Partial rescue of MeCP2 deficiency by postnatal activation of MeCP2. Proc Natl Acad Sci U S A. 2007;104(6):1931-1936.
68. Gibson DA, Ma L. Mosaic analysis of gene function in postnatal mouse brain development by using virus-based Cre recombination. J Vis Exp. 2011;(54):2823.
69. Glantz LA, Lewis DA. Decreased dendritic spine density on prefrontal cortical pyramidal neurons in schizophrenia. Arch Gen Psychiatry. 2000;57(1):65-73.
70. Glantz LA, Lewis DA. Reduction of synaptophysin immunoreactivity in the prefrontal cortex of subjects with schizophrenia. Regional and diagnostic specificity. Arch Gen Psychiatry. 1997;54(10):943-952.
71. Golden JA, Hyman BT. Development of the superior temporal neocortex is anomalous in trisomy 21. J Neuropathol Exp Neurol. 1994;53(5):513-520.
72. Gonzales ML, LaSalle JM. The role of MeCP2 in brain development and neurodevelopmental disorders. Curr Psychiatry Rep. 2010;12(2):127-134.
73. Greene C, Kealy J, Humphries MM, et al. Dose-dependent expression of claudin-5 is a modifying factor in schizophrenia. Mol Psychiatry. 2018;23(11):2156-2166.
74. Gutierrez H, Dolcet X, Tolcos M, Davies A. HGF regulates the development of cortical pyramidal dendrites. Development. 2004;131(15):3717-3726.
75. Gutierrez H, Hale VA, Dolcet X, Davies A. NF-kappaB signalling regulates the growth of neural processes in the developing PNS and CNS. Development. 2005;132(7):1713-1726.
76. Hagiwara A, Sugiyama N, Ohtsuka T. Impaired experience-dependent maternal care in presynaptic active zone protein CAST-deficient dams. *Sci Rep*. 2020;10(1):5238.
77. Hammelrath L, Škokić S, Khmelinskii A, et al. Morphological maturation of the mouse brain: An in vivo MRI and histology investigation. Neuroimage. 2016;125:144-152.
78. Han H, Yang B, Wang W. Angiomotin-like 2 interacts with and negatively regulates AKT. Oncogene. 2017;36(32):4662-4669.
79. Han Z, Ruthel G, Dash S, et al. Angiomotin regulates budding and spread of ebola virus. J Biol Chem. 2020;jbc.AC120.013171.
80. Hand R, Bortone D, Mattar P, et al. Phosphorylation of Neurogenin2 specifies the migration properties and the dendritic morphology of pyramidal neurons in the neocortex. Neuron. 2005;48(1):45-62.

81. Harvey I, Ron MA, Du Boulay G, Wicks D, Lewis SW, Murray RM. Reduction of cortical volume in schizophrenia on magnetic resonance imaging. Psychol Med. 1993;23(3):591-604.
82. Hashimoto K, Engberg G, Shimizu E, Nordin C, Lindström LH, Iyo M. Elevated glutamine/glutamate ratio in cerebrospinal fluid of first episode and drug naive schizophrenic patients. *BMC Psychiatry*. 2005;5:6.
83. Heyes C. New thinking: the evolution of human cognition. Philos Trans R Soc Lond B Biol Sci. 2012;367(1599):2091-2096.
84. Hill JJ, Hashimoto T, Lewis DA. Molecular mechanisms contributing to dendritic spine alterations in the prefrontal cortex of subjects with schizophrenia. Mol Psychiatry. 2006;11(6):557-566.
85. Hirate Y, Hirahara S, Inoue K, et al. Polarity-dependent distribution of angiomotin localizes Hippo signaling in preimplantation embryos. Curr Biol. 2013;23(13):1181-1194.
86. Hirate Y, Sasaki H. The role of Angiomotin phosphorylation in the Hippo pathway during preimplantation mouse development. Tissue Barriers. 2014;2:1181–94.
87. Horch HW, Katz LC. BDNF release from single cells elicits local dendritic growth in nearby neurons. Nat Neurosci. 2002;5(11):1177-1184.
88. Hou C, Ding L, Zhang J, et al. Abnormal cerebellar development and Purkinje cell defects in Lgl1-Pax2 conditional knockout mice. *Dev Biol*. 2014;395(1):167-181.
89. Huang H, Lu FI, Jia S, et al. Amotl2 is essential for cell movements in zebrafish embryo and regulates c-Src translocation. Development. 2007;134(5):979-988.
90. Huang T, Zhou Y, Zhang J, et al. The physiological role of Motin family and its dysregulation in tumorigenesis. J Transl Med. 2018;16(1):98.
91. Huang Z, Hu J, Pan J, et al. YAP stabilizes SMAD1 and promotes BMP2-induced neocortical astrocytic differentiation. *Development*. 2016;143(13):2398-2409.
92. Hutsler JJ, Zhang H. Increased dendritic spine densities on cortical projection neurons in autism spectrum disorders. Brain Res. 2010;1309:83-94.
93. Jaworski J, Spangler S, Seeburg DP, Hoogenraad CC, Sheng M. Control of dendritic arborization by the phosphoinositide-3'-kinase-Akt-mammalian target of rapamycin pathway. J Neurosci. 2005;25(49):11300–12.
94. Jellinger K, Seitelberger F. Neuropathology of Rett syndrome. Am J Med Genet Suppl. 1986;1:259-288.
95. Jiang WG, Watkins G, Douglas-Jones A, Holmgren L, Mansel RE. Angiomotin and angiomotin like proteins, their expression and correlation with angiogenesis and clinical outcome in human breast cancer. BMC Cancer. 2006;6:16.
96. Kang PH, Schaffer DV, Kumar S. Angiomotin links ROCK and YAP signaling in mechanosensitive differentiation of neural stem cells. Mol Biol Cell. 2020;31(5):386-396.
97. Kaufmann WE, Moser HW. Dendritic anomalies in disorders associated with mental retardation. Cereb Cortex. 2000;10(10):981-991.
98. Kazdoba TM, Leach PT, Crawley JN. Behavioral phenotypes of genetic mouse models of autism. *Genes Brain Behav*. 2016;15(1):7-26.
99. Kazdoba TM, Leach PT, Silverman JL, Crawley JN. Modeling fragile X syndrome in the Fmr1 knockout mouse. *Intractable Rare Dis Res*. 2014;3(4):118-133.
100. Kedia S, Chattarji S. Marble burying as a test of the delayed anxiogenic effects of acute immobilisation stress in mice. *J Neurosci Methods*. 2014;233:150-154.
101. Kim E, Wang Y, Kim SJ, et al. Transient inhibition of the ERK pathway prevents cerebellar developmental defects and improves long-term motor functions in murine models of neurofibromatosis type 1. *Elife*. 2014;3:e05151.

102. Ichimaru Y, Egawa T, Sawa A. 5-HT1A-receptor subtype mediates the effect of fluvoxamine, a selective serotonin reuptake inhibitor, on marble-burying behavior in mice. *Jpn J Pharmacol*. 1995;68(1):65-70.
103. Isgrig K, McDougald DS, Zhu J, Wang HJ, Bennett J, Chien WW. AAV2.7m8 is a powerful viral vector for inner ear gene therapy. *Nat Commun*. 2019;10(1):427.
104. Itoh M, Ide S, Takashima S, et al. Methyl CpG-binding protein 2 (a mutation of which causes Rett syndrome) directly regulates insulin-like growth factor binding protein 3 in mouse and human brains. J Neuropathol Exp Neurol. 2007;66(2):117-123.
105. Jaaro-Peled H, Ayhan Y, Pletnikov MV, Sawa A. Review of pathological hallmarks of schizophrenia: comparison of genetic models with patients and nongenetic models. Schizophr Bull. 2010;36(2):301-313.
106. Jaarsma D, van den Berg R, Wulf PS, et al. A role for Bicaudal-D2 in radial cerebellar granule cell migration. *Nat Commun*. 2014;5:3411.
107. Jamain S, Quach H, Betancur C, et al. Mutations of the X-linked genes encoding neuroligins NLGN3 and NLGN4 are associated with autism. Nat Genet. 2003;34(1):27-29.
108. Jan YN, Jan LY. The control of dendrite development. Neuron. 2003;40(2):229-242.
109. Koeppen AH. The Purkinje cell and its afferents in human hereditary ataxia. J Neuropathol Exp Neurol. 1991;50(4):505-514.
110. Kolomeets NS, Orlovskaya DD, Uranova NA. Decreased numerical density of CA3 hippocampal mossy fiber synapses in schizophrenia. Synapse. 2007;61(8):615-621.
111. Kumar R, Hunt CR, Gupta A, et al. Purkinje cell-specific males absent on the first (mMof) gene deletion results in an ataxia-telangiectasia-like neurological phenotype and backward walking in mice. Proc Natl Acad Sci U S A. 2011;108(9):3636-3641.
112. Leemhuis J, Boutillier S, Barth H, et al. Rho GTPases and phosphoinositide 3-kinase organize formation of branched dendrites. J Biol Chem. 2004;279(1):585-596.
113. Li F, Ponissery-Saidu S, Yee KK, et al. Heterotrimeric G protein subunit Gγ13 is critical to olfaction. *J Neurosci*. 2013;33(18):7975-7984.
114. Li X, Morrow D, Witkin JM. Decreases in nestlet shredding of mice by serotonin uptake inhibitors: comparison with marble burying. *Life Sci*. 2006;78(17):1933-1939.
115. Li Y, Zhou H, Li F, et al. Angiomotin binding-induced activation of Merlin/NF2 in the Hippo pathway. Cell Res. 2015;25(7):801-817.
116. Li Z, Wang Y, Zhang M, Xu P, Huang H, Wu D, Meng A. The Amotl2 gene inhibits Wnt/β-catenin signaling and regulates embryonic development in zebrafish. J Biol Chem. 2012;287:13005–15.
117. Lisman J, Buzsáki G, Eichenbaum H, Nadel L, Ranganath C, Redish AD. Viewpoints: how the hippocampus contributes to memory, navigation and cognition. Nat Neurosci. 2017;20(11):1434-1447.
118. Liu P, Calvisi DF, Kiss A, et al. Central role of mTORC1 downstream of YAP/TAZ in hepatoblastoma development. *Oncotarget*. 2017;8(43):73433-73447.
119. Long C, Grueter CE, Song K, et al. Ataxia and Purkinje cell degeneration in mice lacking the CAMTA1 transcription factor. *Proc Natl Acad Sci U S A*. 2014;111(31):11521-11526.
120. Louis ED, Lee M, Babij R, et al. Reduced Purkinje cell dendritic arborization and loss of dendritic spines in essential tremor. Brain. 2014;137(Pt 12):3142-3148.
121. Luo L. Actin cytoskeleton regulation in neuronal morphogenesis and structural plasticity. Annu Rev Cell Dev Biol. 2002;18:601-635.
122. Lv M, Lv M, Chen L, et al. Angiomotin promotes breast cancer cell proliferation and invasion. Oncol Rep. 2015;33(4):1938-1946.

123. Ma L, Greenwood JA, Schachner M. CRP1, a protein localized in filopodia of growth cones, is involved in dendritic growth. J Neurosci. 2011;31(46):16781-16791.
124. MacLean EL. Unraveling the evolution of uniquely human cognition. Proc Natl Acad Sci U S A. 2016;113(23):6348-6354.
125. Madisen L, Zwingman TA, Sunkin SM, et al. A robust and high-throughput Cre reporting and characterization system for the whole mouse brain. *Nat Neurosci*. 2010;13(1):133-140.
126. Mana-Capelli S, Paramasivam M, Dutta S, McCollum D. Angiomotins link F-actin architecture to Hippo pathway signaling. Mol Biol Cell. 2014;25(10):1676-1685.
127. Manto M, Bower JM, Conforto AB, et al. Consensus paper: roles of the cerebellum in motor control--the diversity of ideas on cerebellar involvement in movement. Cerebellum. 2012;11(2):457-487.
128. Mao Y, Chen X, Xu M, et al. Targeting TEAD/YAP-transcription-dependent necrosis, TRIAD, ameliorates Huntington's disease pathology. *Hum Mol Genet*. 2016;25(21):4749-4770.
129. Matsuki T, Matthews RT, Cooper JA, et al. Reelin and stk25 have opposing roles in neuronal polarization and dendritic Golgi deployment. Cell. 2010;143(5):826-836.
130. McBride KL, Varga EA, Pastore MT, et al. Confirmation study of PTEN mutations among individuals with autism or developmental delays/mental retardation and macrocephaly. Autism Res. 2010;3(3):137-141.
131. Mehta MV, Gandal MJ, Siegel SJ. mGluR5-antagonist mediated reversal of elevated stereotyped, repetitive behaviors in the VPA model of autism. *PLoS One*. 2011;6(10):e26077.
132. Men Y, Zhang A, Li H, et al. LKB1 Regulates Cerebellar Development by Controlling Sonic Hedgehog-mediated Granule Cell Precursor Proliferation and Granule Cell Migration. *Sci Rep*. 2015;5:16232.
133. Mercenne G, Alam SL, Arii J, Lalonde MS, Sundquist WI. Angiomotin functions in HIV-1 assembly and budding. Elife. 2015;4:e03778.
134. Merritt K, Egerton A, Kempton MJ, Taylor MJ, McGuire PK. Nature of Glutamate Alterations in Schizophrenia: A Meta-analysis of Proton Magnetic Resonance Spectroscopy Studies. *JAMA Psychiatry*. 2016;73(7):665-674.
135. Mihajlović AI, Bruce AW. Rho-associated protein kinase regulates subcellular localisation of Angiomotin and Hippo-signalling during preimplantation mouse embryo development. Reprod BioMed Online. 2016;33:381–90.
136. Mitterauer Bernhard J. Pathophysiology of Schizophrenia Based on Impaired Glial-Neuronal Interactions. Open Journal of Medical Psychology. 2014; Vol.3 No.2.
137. Mohamoud HS, Ahmed S, Jelani M, et al. A missense mutation in TRAPPC6A leads to build-up of the protein, in patients with a neurodevelopmental syndrome and dysmorphic features. Sci Rep. 2018;8(1):2053.
138. Moleirinho S, Guerrant W, Kissil JL. The Angiomotins--from discovery to function. FEBS Lett. 2014;588(16):2693-2703.
139. Mueller KA, Glajch KE, Huizenga MN, et al. Hippo Signaling Pathway Dysregulation in Human Huntington's Disease Brain and Neuronal Stem Cells. *Sci Rep*. 2018;8(1):11355.
140. Muhle R, Trentacoste SV, Rapin I. The genetics of autism. Pediatrics. 2004;113(5):e472-e486.
141. Nakamura F, Ugajin K, Yamashita N, et al. Increased proximal bifurcation of CA1 pyramidal apical dendrites in sema3A mutant mice. J Comp Neurol. 2009;516(5):360-375.
142. Nestler EJ, Hyman SE. Animal models of neuropsychiatric disorders. Nat Neurosci. 2010;13(10):1161-1169.
143. Nicholson C. Signals that go with the flow. Trends Neurosci. 1999;22:143–145
144. Nieuwenhuys R, Voogd J, van Huijzen C. The Human Central Nervous System. 4. Berlin: Springer; 2008.

145. Nilsson C, Lindvall-Axelsson M, Owman C. Neuroendocrine regulatory mechanisms in the choroid plexus-cerebrospinal fluid system. Brain Res Brain Res Rev. 1992;17:109–138.
146. Nishimura M, Kakizaki M, Ono Y, et al. JEAP, a novel component of tight junctions in exocrine cells. J Biol Chem. 2002;277(7):5583-5587.
147. Nishioka N, Inoue K-I, Adachi K, Kiyonari H, Ota M, Ralston A, Yabuta N, Hirahara S, Stephenson RO, Ogonuki N. The Hippo signaling pathway components Lats and Yap pattern Tead4 activity to distinguish mouse trophectoderm from inner cell mass. Dev Cell. 2009;16:398–410.
148. Nitschke MF, Kleinschmidt A, Wessel K, Frahm J. Somatotopic motor representation in the human anterior cerebellum. A high-resolution functional MRI study. *Brain*. 1996;119 (Pt 3):1023-1029.
149. Njung'e K, Handley SL. Evaluation of marble-burying behavior as a model of anxiety. Pharmacol Biochem Behav. 1991;38(1):63-67.
150. Noguchi J, Hayama T, Watanabe S, et al. State-dependent diffusion of actin-depolymerizing factor/cofilin underlies the enlargement and shrinkage of dendritic spines. *Sci Rep*. 2016;6:32897.
151. Ogawa K, Ishikawa H, Suzuki Y, Oishi M, Kamei S. Clinical study of the visual field defects caused by occipital lobe lesions. Cerebrovasc Dis. 2014;37(2):102-108.
152. Oka T, Schmitt AP, Sudol M. Opposing roles of angiomotin-like-1 and zona occludens-2 on pro-apoptotic function of YAP. Oncogene. 2012;31(1):128-134.
153. Orr BA, Bai H, Odia Y, Jain D, Anders RA, Eberhart CG. Yes-associated protein 1 is widely expressed in human brain tumors and promotes glioblastoma growth. *J Neuropathol Exp Neurol*. 2011;70(7):568-577.
154. Ovsepian SV. The birth of the synapse. Brain Struct Funct. 2017;222(8):3369-3374.
155. Park SJ, Lee JY, Kim SJ, Choi SY, Yune TY, Ryu JH. Toll-like receptor-2 deficiency induces schizophrenia-like behaviors in mice. *Sci Rep*. 2015;5:8502.
156. Patrie KM. Identification and characterization of a novel tight junction-associated family of proteins that interacts with a WW domain of MAGI-1. Biochim Biophys Acta. 2005;1745(1):131-144.
157. Patterson PH. Modeling autistic features in animals. *Pediatr Res*. 2011;69(5 Pt 2):34R-40R.
158. Perez-Figares JM, Jimenez AJ, Rodriguez EM. Subcommissural organ, cerebrospinal fluid circulation, and hydrocephalus. Microsc Res Tech. 2001;52:591–607.
159. Pinyol, R., Haeckel, A., Ritter, A., Qualmann, B., and Kessels, M. M. (2007). Regulation of N-WASP and the Arp2/3 complex by Abp1 controls neuronal morphology. PLoS ONE 2:e400.
160. Priyanka A. Abhang, Bharti W. Gawali, and Suresh C. Mehrotra. 2016. Introduction to EEG- and Speech-Based Emotion Recognition (1st. ed.). Academic Press, Inc., USA.
161. Proszynski TJ, Sanes JR. Amotl2 interacts with LL5β, localizes to podosomes and regulates postsynaptic differentiation in muscle. J Cell Sci. 2013;126(Pt 10):2225-2235.
162. Provencher SW. Estimation of metabolite concentrations from localized in vivo proton NMR spectra. Magn Reson Med. 1993;30(6):672-679.
163. Puram SV, Kim AH, Ikeuchi Y, et al. A CaMKIIβ signaling pathway at the centrosome regulates dendrite patterning in the brain. Nat Neurosci. 2011;14(8):973-983.
164. Puścian A, Łęski S, Kasprowicz G, et al. Eco-HAB as a fully automated and ecologically relevant assessment of social impairments in mouse models of autism. Elife. 2016;5:e19532. Published 2016 Oct 12.
165. Quevedo C, Sauzeau V, Menacho-Márquez M, et al. Vav3-deficient Mice Exhibit a Transient Delay in Cerebellar Development. *Mol Biol of the Cell*. 2010; 21 (6).

166. Ragni CV, Diguet N, Le Garrec JF, et al. Amotl1 mediates sequestration of the Hippo effector Yap1 downstream of Fat4 to restrict heart growth. *Nat Commun*. 2017;8:14582.
167. Rapin I. Autism. N Engl J Med. 1997;337(2):97-104.
168. Ray G, Schmitt PT, Schmitt AP. Angiomotin-Like 1 Links Paramyxovirus M Proteins to NEDD4 Family Ubiquitin Ligases. Viruses. 2019;11(2):128.
169. Raymond GV, Bauman ML, Kemper TL. Hippocampus in autism: a Golgi analysis. Acta Neuropathol. 1996;91(1):117-119.
170. Raz N, Torres IJ, Briggs SD, et al. Selective neuroanatomic abnormalities in Down's syndrome and their cognitive correlates: evidence from MRI morphometry. Neurology. 1995;45(2):356-366.
171. Redmond L, Kashani AH, Ghosh A. Calcium regulation of dendritic growth via CaM kinase IV and CREB-mediated transcription. Neuron. 2002;34(6):999-1010.
172. Rojek KO, Krzemień J, Doleżyczek H, et al. Amot and Yap1 regulate neuronal dendritic tree complexity and locomotor coordination in mice. PLoS Biol. 2019;17(5):e3000253.
173. Rorden C, Davis B, George MS, Borckardt J, Fridriksson J. Broca's area is crucial for visual discrimination of speech but not non-speech oral movements. Brain Stimul. 2008;1(4):383-385.
174. Rosso SB, Sussman D, Wynshaw-Boris A, Salinas PC. Wnt signaling through Dishevelled, Rac and JNK regulates dendritic development. Nat Neurosci. 2005;8(1):34-42.
175. Roussos P, Guennewig B, Kaczorowski DC, Barry G, Brennand KJ. Activity-Dependent Changes in Gene Expression in Schizophrenia Human-Induced Pluripotent Stem Cell Neurons. JAMA Psychiatry. 2016;73(11):1180-1188.
176. Sakai Y, Kassai H, Nakayama H, et al. Hyperactivation of mTORC1 disrupts cellular homeostasis in cerebellar Purkinje cells. Sci Rep. 2019;9(1):2799.
177. Saugier-Veber P, Marguet F, Lecoquierre F, et al. Hydrocephalus due to multiple ependymal malformations is caused by mutations in the MPDZ gene. *Acta Neuropathol Commun*. 2017;5(1):36.
178. Schanzenbächer CT, Sambandan S, Langer JD, Schuman EM. Nascent Proteome Remodeling following Homeostatic Scaling at Hippocampal Synapses. Neuron. 2016;92(2):358-371.
179. Schneider C. Behavioural effects of some morphine antagonists and hallucinogens in the rat. Nature. 1968;220(5167):586-587.
180. Schumann CM, Hamstra J, Goodlin-Jones BL, et al. The amygdala is enlarged in children but not adolescents with autism; the hippocampus is enlarged at all ages. J Neurosci. 2004;24(28):6392-6401.
181. Seibenhener ML, Wooten MC. Use of the Open Field Maze to measure locomotor and anxiety-like behavior in mice. *J Vis Exp*. 2015;(96):e52434.
182. Sherman DL, Brophy PJ. Mechanisms of axon ensheathment and myelin growth. Nat Rev Neurosci. 2005;6(9):683-690.
183. Shimono A, Behringer RR. Angiomotin regulates visceral endoderm movements during mouse embryogenesis. Curr Biol. 2003;13(7):613-617.
184. Shintani T, Takeuchi Y, Fujikawa A, Noda M. Directional neuronal migration is impaired in mice lacking adenomatous polyposis coli 2. *J Neurosci*. 2012;32(19):6468-6484.
185. Simon P, Dupuis R, Costentin J. Thigmotaxis as an index of anxiety in mice. Influence of dopaminergic transmissions. *Behav Brain Res*. 1994;61(1):59-64.
186. Skipor J, Thiery JC. The choroid plexus--cerebrospinal fluid system: undervaluated pathway of neuroendocrine signaling into the brain. Acta Neurobiol Exp (Wars) 2008;68:414–428.
187. Skouloudaki K, Walz G. YAP1 recruits c-Abl to protect angiomotin-like 1 from Nedd4-mediated degradation. PLoS One. 2012;7(4):e35735.

188. Smithies O, Gregg RG, Boggs SS, Koralewski MA, Kucherlapati RS. Insertion of DNA sequences into the human chromosomal beta-globin locus by homologous recombination. Nature. 1985;317(6034):230-234.
189. Smythies JR, Johnston VS, Bradley RJ, Benington F, Morin RD, Clark LC. Some new behaviour-disrupting amphetamines and their significance. *Nature*. 1967;216(5111):128-129.
190. Snyder SH. Amphetamine psychosis: a "model" schizophrenia mediated by catecholamines. Am J Psychiatry. 1973;130(1):61-67.
191. Soetanto A, Wilson RS, Talbot K, et al. Association of anxiety and depression with microtubule-associated protein 2- and synaptopodin-immunolabeled dendrite and spine densities in hippocampal CA3 of older humans. Arch Gen Psychiatry. 2010;67(5):448-457.
192. Sotelo C, Dusart I. Intrinsic versus extrinsic determinants during the development of Purkinje cell dendrites. *Neuroscience*. 2009;162(3):589-600.
193. Steen RG, Hamer RM, Lieberman JA. Measurement of brain metabolites by 1H magnetic resonance spectroscopy in patients with schizophrenia: a systematic review and meta-analysis. *Neuropsychopharmacology*. 2005;30(11):1949-1962.
194. Stoodley CJ, Schmahmann JD. Evidence for topographic organization in the cerebellum of motor control versus cognitive and affective processing. *Cortex*. 2010;46(7):831-844.
195. Stoodley CJ, Valera EM, Schmahmann JD. Functional topography of the cerebellum for motor and cognitive tasks: an fMRI study. Neuroimage. 2012;59(2):1560-1570.
196. Suárez R, Gobius I, Richards LJ. Evolution and development of interhemispheric connections in the vertebrate forebrain. *Front Hum Neurosci*. 2014;8:497.
197. Südhof TC. Neuroligins and neurexins link synaptic function to cognitive disease. Nature. 2008;455(7215):903-911.
198. Sugihara-Mizuno Y, Adachi M, Kobayashi Y, et al. Molecular characterization of angiomotin/JEAP family proteins: interaction with MUPP1/Patj and their endogenous properties. Genes Cells. 2007;12(4):473-486.
199. Takashima S, Ieshima A, Nakamura H, Becker LE. Dendrites, dementia and the Down syndrome. Brain Dev. 1989;11(2):131-133.
200. Taylor GT, Lerch S, Chourbaji S. Marble burying as compulsive behaviors in male and female mice. *Acta Neurobiol Exp (Wars)*. 2017;77(3):254-260.
201. Thach WT, Goodkin HP, Keating JG. The cerebellum and the adaptive coordination of movement. Annu Rev Neurosci. 1992;15:403-442.
202. Thomanetz V, Angliker N, Cloëtta D, et al. Ablation of the mTORC2 component rictor in brain or Purkinje cells affects size and neuron morphology. J Cell Biol. 2013;201(2):293-308.
203. Thomas KR, Capecchi MR. Site-directed mutagenesis by gene targeting in mouse embryo-derived stem cells. Cell. 1987;51(3):503-512.
204. Tibbo P, Hanstock C, Valiakalayil A, Allen P. 3-T proton MRS investigation of glutamate and glutamine in adolescents at high genetic risk for schizophrenia. *Am J Psychiatry*. 2004;161(6):1116-1118.
205. Timmann D, Drepper J, Frings M, et al. The human cerebellum contributes to motor, emotional and cognitive associative learning. A review. Cortex. 2010;46(7):845-857.
206. Toga AW, Thompson PM. Mapping brain asymmetry. *Nat Rev Neurosci*. 2003;4(1):37-48.
207. Troyanovsky B, Levchenko T, Månsson G, Matvijenko O, Holmgren L. Angiomotin: an angiostatin binding protein that regulates endothelial cell migration and tube formation. J Cell Biol. 2001;152(6):1247-1254.
208. Tumaneng K, Schlegelmilch K, Russell RC, et al. YAP mediates crosstalk between the Hippo and PI(3)K–TOR pathways by suppressing PTEN via miR-29. Nat Cell Biol. 2012;14(12):1322-1329.

209. Turner AH, Greenspan KS, van Erp TGM. Pallidum and lateral ventricle volume enlargement in autism spectrum disorder. Psychiatry Res Neuroimaging. 2016;252:40-45.
210. Urbanska M, Gozdz A, Swiech LJ, Jaworski J. Mammalian target of rapamycin complex 1 (mTORC1) and 2 (mTORC2) control the dendritic arbor morphology of hippocampal neurons. J Biol Chem. 2012;287(36):30240–56. pmid:22810227.
211. van der Staay FJ, Arndt SS, Nordquist RE. Evaluation of animal models of neurobehavioral disorders. Behav Brain Funct. 2009;5:11.
212. Vassilev A, Kaneko KJ, Shu H, Zhao Y, DePamphilis ML. TEAD/TEF transcription factors utilize the activation domain of YAP65, a Src/Yes-associated protein localized in the cytoplasm. Genes Dev. 2001;15(10):1229-1241.
213. Vogel G. Nobel Prizes. A knockout award in medicine. Science. 2007;318(5848):178-179.
214. von Bartheld CS, Bahney J, Herculano-Houzel S. The search for true numbers of neurons and glial cells in the human brain: A review of 150 years of cell counting. J Comp Neurol. 2016;524(18):3865-3895.
215. Wang JY, Yu IS, Huang CC, et al. Sun1 deficiency leads to cerebellar ataxia in mice. *Dis Model Mech*. 2015;8(8):957-967.
216. Wang VY, Zoghbi HY. Genetic regulation of cerebellar development. Nat Rev Neurosci. 2001;2(7):484-491.
217. Wang W, Huang J, Chen J. Angiomotin-like proteins associate with and negatively regulate YAP1. J Biol Chem. 2011;286(6):4364-4370.
218. Watrin F, Manent JB, Cardoso C, Represa A. Causes and consequences of gray matter heterotopia. CNS Neurosci Ther. 2015;21(2):112-122.
219. Weickert CS, Fung SJ, Catts VS, et al. Molecular evidence of N-methyl-D-aspartate receptor hypofunction in schizophrenia. Mol Psychiatry. 2013;18(11):1185-1192.
220. Weller RO, Djuanda E, Yow HY, Carare RO. Lymphatic drainage of the brain and the pathophysiology of neurological disease. Acta Neuropathol. 2009;117:1–14.
221. Wells CD, Fawcett JP, Traweger A, et al. A Rich1/Amot complex regulates the Cdc42 GTPase and apical-polarity proteins in epithelial cells. Cell. 2006;125(3):535-548.
222. Welniak-Kaminska M, Fiedorowicz M, Orzel J, et al. Volumes of brain structures in captive wild-type and laboratory rats: 7T magnetic resonance in vivo automatic atlas-based study. PLoS One. 2019;14(4):e0215348.
223. Weyer A, Schilling K. Developmental and cell type-specific expression of the neuronal marker NeuN in the murine cerebellum. *J Neurosci Res*. 2003;73(3):400-409.
224. Wigerius M, Quinn D, Diab A, et al. The polarity protein Angiomotin p130 controls dendritic spine maturation. J Cell Biol. 2018;217(2):715-730.
225. Wischhof L, Maida S, Piazzesi A, et al. The SWI/SNF subunit Bcl7a contributes to motor coordination and Purkinje cell function. *Sci Rep*. 2017;7(1):17055.
226. Wright IC, Rabe-Hesketh S, Woodruff PW, David AS, Murray RM, Bullmore ET. Meta-analysis of regional brain volumes in schizophrenia. Am J Psychiatry. 2000;157(1):16-25.
227. Yang J, Simonneau C, Kilker R, et al. Murine *MPDZ*-linked hydrocephalus is caused by hyperpermeability of the choroid plexus. *EMBO Mol Med*. 2019;11(1):e9540.
228. Yang Y, Sun K, Liu W, et al. Disruption of Tmem30a results in cerebellar ataxia and degeneration of Purkinje cells. *Cell Death Dis*. 2018;9(9):899.
229. Yang Z, Joyner AL. YAP1 is involved in replenishment of granule cell precursors following injury to the neonatal cerebellum. Dev Biol. 2019;455(2):458-472.
230. Yi C, Troutman S, Fera D, Stemmer-Rachamimov A, Avila JL, Christian N, Persson NL, Shimono A, Speicher DW, Marmorstein R, Holmgren L, Kissil JL. A tight junction-associated Merlin-

angiomotin complex mediates Merlin's regulation of mitogenic signaling and tumor suppressive functions. Cancer Cell. 2011;19:527–540.
231. Zaltsman Y, Masuko S, Bensen JJ, Kiessling LL. Angiomotin Regulates YAP Localization during Neural Differentiation of Human Pluripotent Stem Cells. Stem Cell Reports. 2019;12(5):869-877.
232. Zhang C, Milunsky JM, Newton S, et al. A neuroligin-4 missense mutation associated with autism impairs neuroligin-4 folding and endoplasmic reticulum export. J Neurosci. 2009;29(35):10843-10854.
233. Zhang N, Bai H, David KK, et al. The Merlin/NF2 tumor suppressor functions through the YAP oncoprotein to regulate tissue homeostasis in mammals. Dev Cell. 2010;19(1):27-38.
234. Zhao B, Li L, Lei Q, Guan KL. The Hippo-YAP pathway in organ size control and tumorigenesis: an updated version. Genes Dev. 2010;24(9):862–74. pmid:20439427.
235. Zhao B, Li L, Lu Q, et al. Angiomotin is a novel Hippo pathway component that inhibits YAP oncoprotein. Genes Dev. 2011;25(1):51-63.
236. Zhao B, Tumaneng K, Guan K-L. The Hippo pathway in organ size control, tissue regeneration and stem cell self-renewal. Nat Cell Biol. 2011;13:877–83.
237. Zhao B, Wei X, Li W, Udan RS, Yang Q, Kim J, et al. Inactivation of YAP oncoprotein by the Hippo pathway is involved in cell contact inhibition and tissue growth control. Genes Dev. 2007;21(21):2747–61. pmid:17974916.
238. Zhao B, Ye X, Yu J, et al. TEAD mediates YAP-dependent gene induction and growth control. Genes Dev. 2008;22(14):1962-1971.
239. Zheng Y, Vertuani S, Nyström S, et al. Angiomotin-like protein 1 controls endothelial polarity and junction stability during sprouting angiogenesis. Circ Res. 2009;105(3):260-270.
240. Zheng Y, Zhang Y, Barutello G, et al. Angiomotin like-1 is a novel component of the N-cadherin complex affecting endothelial/pericyte interaction in normal and tumor angiogenesis. *Sci Rep*. 2016;6:30622.
241. Zhou Y, Zhang J, Li H, et al. AMOTL1 enhances YAP1 stability and promotes YAP1-driven gastric oncogenesis. Oncogene. 2020;10.1038/s41388-020-1293-5.
242. Zhou Z, Hong EJ, Cohen S, et al. Brain-specific phosphorylation of MeCP2 regulates activity-dependent Bdnf transcription, dendritic growth, and spine maturation. Neuron. 2006;52(2):255-269.
243. Zhu Y, Romero MI, Ghosh P, et al. Ablation of NF1 function in neurons induces abnormal development of cerebral cortex and reactive gliosis in the brain. *Genes Dev*. 2001;15(7):859-876.
244. Zipursky RB, Lim KO, Sullivan EV, Brown BW, Pfefferbaum A. Widespread cerebral gray matter volume deficits in schizophrenia. Arch Gen Psychiatry. 1992;49(3):19